Jagiellonian University

Faculty of Physics, Astronomy and Applied Computer Science

Maciej Majka

Microscopic models for spatially correlated phenomena in soft matter and bio-molecular systems

A thesis submitted for the degree of

Doctor of Philosophy

supervised by dr hab. Paweł F. Góra

Kraków 2015

Wydział Fizyki Astronomii i Informatyki Stosowanej
Uniwersytet Jagielloński

Oświadczenie

Ja niżej podpisany, *Maciej Majka* (nr indeksu: 470) doktorant Wydziału Fizyki, Astronomii i Informatyki Stosowanej Uniwersytetu Jagiellońskiego oświadczam, że przedłożona przeze mnie rozprawa doktorska pt. *„Microscopic models for spatially correlated phenomena in soft matter and bio-molecular systems"* jest oryginalna i przedstawia wyniki badań wykonanych przeze mnie osobiście, pod kierunkiem dr hab. Pawła F. Góry. Pracę napisałem samodzielnie. Oświadczam, że moja rozprawa doktorska została opracowana zgodnie z Ustawą o prawie autorskim i prawach pokrewnych z dnia 4 lutego 1994 r. (Dziennik Ustaw 1994 nr 24 poz. 83 wraz z późniejszymi zmianami). Jestem świadomy, że niezgodność niniejszego oświadczenia z prawdą ujawniona w dowolnym czasie, niezależnie od skutków prawnych wynikających z ww. ustawy, może spowodować unieważnienie stopnia nabytego na podstawie tej rozprawy.

Kraków, dnia ....

podpis doktoranta

Streszczenie

Zrozumienie samoorganizacji w układach biologicznych wciąż stanowi wyzwanie dla współczesnej nauki. Rozwój eksperymentalnych technik biofizyki oraz postęp w dziedzinie miękkiej materii skondensowanej dostarczył szeregu nowych narzędzi umożliwiających głębszą analizę tego zagadnienia. W niniejszej pracy zostanie przedyskutowane zarówno pochodzenie przestrzennie skorelowanej dynamiki układów modelowych, jak i efekty będące konsekwencją takich korelacji. Skorelowanie przestrzenne napotyka się w mikro-przepływach cytoplazmy, w pobliżu przejść fazowych oraz w fazie szklistej, a także w samoorganizujących się mieszaninach dwuskładnikowych. Ten ostatni przypadek został wybrany jako archetypiczny model pochodzenia korelacji przestrzennych, w którym jeden typ cząstek kontroluje samoorganizację drugiego typu cząstek. Obecność cząstek otoczenia wprowadza tzw. efektywne oddziaływania między samoorganizującymi się cząstkami. Równocześnie samoorganizacja może być rozumiana jako efekt wynikający z kolektywnego zachowania cząstek otoczenia.

W niniejszej pracy wprowadzam nową teorię efektywnych oddziaływań, przechodząc z klasycznego opisu w zmiennych położenia i pędów do formalizmu funkcjonału liczby obsadzeń. Istniejące teorie dla układów koloidalnych były jak dotąd nakierowane na uzyskiwanie dokładnych wyników numerycznych. W odróżnieniu od nich, nowa teoria pozwala otrzymywać wyniki analityczne dla szerokiej gamy modeli. W pracy przedstawiam szczegółowe wyprowadzenie nowego formalizmu, jak i dyskutuję jego ograniczenia. Przedstawiony jest również szereg zastosowań, które obejmują: cząstki naładowane w obecności jonów, mieszaniny cząstek oddziałujących potencjałami Yukawy, mieszaniny polimerów oraz mieszaniny dużych i małych cząstek opisanych odpychającym rdzeniem oraz przyciągającym lub odpychającym oddziaływaniem długo-zasięgowym. W tym ostatnim modelu analitycznie odtwarzam efekty „przyciągania

przez odpychanie" oraz „odpychania przez przyciąganie". Efekty te przewidywano jak dotąd jedyni na podstawie symulacji. Zaproponowany formalizm pozwala także wyprowadzić ścisły związek między efektywnymi oddziaływaniami a korelacjami przestrzennymi w szumie termicznym.

Kolejna grupa wyników prezentuje wpływ szumu skorelowanego przestrzennie na dynamikę modelowego łańcuch polimerowego. Jako wprowadzenie omawiam metody numerycznego rozwiązywania równań Langevina oraz generacji skorelowanych zmiennych Gaussowskich. Model polimeru oparty jest o oddziaływania harmoniczne między kolejnymi węzłami oraz globalny potencjał Lennarda-Jonesa przypisany każdemu węzłowi, aby zapewnić efekty wykluczonej objętości. Wprowadzone są również harmoniczne oddziaływanie między co drugim węzłem, co wymusza preferencję dla konformacji o kształcie piły. Wpływ korelacji przestrzennych w szumie na dynamikę jest znaczący i objawia się synchronizacją ruchu węzłów oraz ogólnym usztywnieniem struktury, widocznym w funkcjach korelacji długości segmentów i kątów między nimi. Widoczny jest również efekt „spontanicznego rozprostowywania", tzn. polimer preferuje konformacje zlinearyzowane. Efekt ten tłumaczony jest akumulacją lokalnie rozciągniętych fragmentów, których relaksacja jest utrudniona w obecności przestrzennych korelacji.

Ostatni problem analizowany w tej pracy dotyczy nie-Gaussowskich łańcuchów polimerowych, opisywanych rozkładami alfa-stabilnymi. Taka nietypowa statystyka w zachowaniu łańcucha może być wywołana opisanym powyżej efektem spontanicznego rozprostowywania. Inne przykłady to także częściowo nieuporządkowane białka oraz polimery zaadsorbowane do powierzchni. W tym ostatnim przypadku skalowanie promienia żyracji w kierunku równoległym do powierzchni zmienia się od przypadku Gaussowskiego dla silnej adsorpcji do przypadku ciężko-ogonowego dla słabej adsorpcji. Dla omawianego modelu możliwe jest obliczenie rozkładu położeń końców łańcucha, rozkładu węzłów w funkcji odległości od środka masy łańcucha oraz potencjału oddziaływania między dwoma łańcuchami. Wyniki te są analityczne i przyjmują zamkniętą postać w przestrzeni Fouriera. Używając wprowadzonej w tej pracy metody

obliczania efektywnych oddziaływań możliwe jest również przeanalizowanie zachowania mieszanin dwuskładnikowych, złożonych z łańcuchów alfa-stabilnych. Jako główny wynik otrzymujemy tu uogólnienie warunku na rozkład spinodalny mieszaniny, znanego dotąd jedynie dla cząstek Gaussowskich. W szczególności możliwe jest zastosowanie tego wyniku do przewidywania warunków na separację powierzchniową w trakcie adsorpcji z jednorodnego lub niejednorodnego roztworu.

Abstract

The understanding of self-organization in biological systems imposes a long lasting challenge. The development of biophysical experimental techniques and the progress in the field of soft matter has provided new tools and theories to address this problem. In this thesis the origin and consequences of spatially correlated dynamics in molecular systems are discussed. The spatially correlated dynamics is encountered in cytoplasmic micro-flows, in the near-phase transition and glassy systems and in the self-organizing binary mixtures. This last case is chosen as the archetypical model for the spatially correlated phenomena, in which one species of particles is utilized to control the behavior of the second species. The presence of the second species introduces the additional 'effective interactions' between the particles of the first species, but it is also a manifestation of collective dynamics in the motion of the second species.

In this thesis a new theory of effective interactions is introduced, which is based on translating the classical momentum-position representation of partition function into the occupation number functional formalism. While the existing methods for binary systems provide excellent numerical results, the new theory is versatile and robust in delivering analytical results. We provide a detailed derivation of the new method as well as a discussion of its validity. Several applications are proposed, which are: mixtures of charged spheres and ions, mixtures of Yukawa particles and binary mixtures of particles described with repulsive core and attractive or repulsive Yukawa tail. For this last type of particles the new method analytically reproduces the 'attraction-through-repulsion' and 'repulsion-through-attraction' effects, which have been previously observed in simulations. The formalism of occupation number functional can be also conveniently applied to establish the relation between effective interactions and the spatial correlations in the thermal noise.

Another part of our research is focused on the influence of spatially correlated disturbances on the dynamics of a model polymeric chain. The methods for simulating the Langevin equations with spatially correlated Gaussian noise are discussed first. The polymeric chain is based on the bead-spring model with the global Lennard-Jones potential for every bead providing the excluded volume effects and the second-nearest neighbor harmonic interaction stimulating saw-like conformations. The influence of spatial correlations in the noise on the chain dynamics is significant. The beads motion synchronizes and the chain structure is more persistent. However, we also observe the spontaneous unfolding effect, i. e. the chain prefers linearized conformations. This effect is explained as the accumulation of local frustrations, stimulated by random driving but conserved by the presence of spatial correlations.

In the last part of our research we propose the model of non-Gaussian polymeric chains, described by the alpha-stable distributions. This model is inspired by the aforementioned unfolding effect, but such heavy tailed distributions are also encountered in disordered proteins and for adsorbed polymers. In this last case, the gyration radius parallel to the surface obeys the statistics, which depends on the adsorption strength and varies from the Gaussian distribution for strong adsorption to the heavy-tailed distribution for weak adsorption. In our model we derive the analytical expressions for the end-to-end distance, the distribution of nodes around the mass center and the coarse-grained interaction potential between two chains. These results are closed-form in the Fourier space. Finally, using our theory of effective interactions, we analyze the stability of binary mixtures composed of alpha-stable chains, which leads to the generalization of spinodal decomposition condition previously known for the Gaussian particles. In particular, we address the problem of on-surface versus in the bulk separation.

Contents

Content and reading

This thesis consists of the present introductory article as well as four published papers, which contain a selection of problems related to the origin and consequences of spatially correlated behavior. These papers read:

- [A1]: *Analytical theory of effective interactions in binary colloidal systems of soft particles*, M. Majka, P.F. Góra, Phys. Rev. E, 90, 3, 032303 (2014)
- [A2]: *Polymer unfolding and motion synchronization induced by spatially correlated noise*, M. Majka, P.F. Góra, Phys. Rev. E, 86, 5, 051122 (2012)
- [A3]: *Reinterpreting polymer unfolding effect induced by spatially correlated noise*, Acta Phys. Pol. B, 44, 5, 1099 (2013)
- [A4]: *Non-Gaussian polymers described by alpha-stable chain statistics: model, effective interactions in binary mixtures and application to on-surface separation*, Phys. Rev. E, 91, 5, 052602 (2015)

The detailed discussion and summary of these publications is included in Section 5 of this introductory article. They are presented according to their logical succession, rather than in chronological order. The main part of this introduction is designed to motivate our research, to show the explicit links between its different aspects and to put it in the broader perspective of biological self-organization. A significant part of our research is focused on the dynamics of a system driven by the stochastic but spatially correlated force. In this introduction we also present a few physical realizations of such system. This includes cytoplasmic micro-flows, glassy and near-phase transition systems and multicomponent mixtures.

The introduction is organized as follows. In Section 1 we discuss the general importance of soft matter physics for molecular biophysics. In Section 2 the concept of spatial correlations for one-component systems is formalized and presented in the context of systems exhibiting strong spatial correlations, such as near-phase transition and glassy systems. Further, in Section 3, we proceed to

the multicomponent systems and examine the effective interactions as a source of spatial organization. In this section we also discuss the biological meaning of effective interaction. In Section 4 we provide unpublished results formally linking the effective interactions and spatial correlations in the multicomponent systems. As mentioned before, in Section 5 we summarize the papers [A1]-[A4]. Once again, we would like to emphasize that these articles are the integral part of this thesis and they include the main body of results.

1 Introduction

1.1 Challenges of molecular biophysics

Although the extremely fine spatio-temporal organization is the essence of biological life, both order and disorder are its necessary ingredients. At the molecular level, chaos is inevitable, which became evident at the advent of atomistic hypothesis and the arrival of statistical physics. Observation of what is now known as the Brownian motion provided the first insight into the world of molecular unrest, in which the energy of every particle fluctuates and the magnitude of these fluctuations grows with the temperature in the system. However, this molecular chaos is not merely a destructive factor, which has to be overcome for the purpose of organization. It is a manifestation of subtle statistical laws, on the flip side of which there exist such phenomena as phase transitions, interactions of entropic origin and collective dynamics. All of them can substantially promote or prevent the spatial organization and provide numerous control mechanisms over a system.

The question of how the complex behavior of a living system arise from the low-level physical laws is the fundamental problem for biophysics. From this perspective, biophysics is a branch of science which fits into the conceptual framework presented in the famous article 'More is different' [1], i.e. the fairly complete understanding of physical laws on the molecular level gives little intuition about the many-particle system as a whole. Unfortunately, the variety of processes and dependencies in a real biological system is so enormous that addressing its unique physics is particularly difficult. Typically, many processes are based on the 'specific interactions', i.e. a certain particle can chemically bind only to a specific place. While the understanding of a specific binding mechanisms is challenging on its own, it is not solely their chemistry that matters. The biological system also depends on the fine tuning of time scales, local availability of substrates and the efficiency of their transport. All of these aspects are intimately related to the environment in which the process occurs and

might be regulated in, both, the specific and non-specific way. The latter case is especially interesting for physicists, since this is where the general principles characteristic of molecular biological systems manifest. However, the dependence on environment is also what makes this unique physics so challenging, since it cannot be easily separated from the properties of the entire system.

1.2 Experimental perspective

From this perspective, two strategies are adequate to address the challenges of molecular biophysics. One strategy is to focus on the *in vivo* experiments. Indeed, it was not until the arrival of fluorescent microscopy [2] and optical tweezers technology [3] that physicists gained tools for the quantitative and qualitative analysis of molecular organization in biological systems. A rapid development of the imaging techniques has led to important advances. One is a discovery that the passive diffusion in cells has often the anomalous character, e.g. the mean square displacement grows sub-linearly in time [4]. The evidence for this behavior is abundant e.g. for cytoplasm [5, 6, 7], membranes [8, 9], chromatin [10] and even at the protein domain level [11]. On the other hand, some researchers point to the fact that the viscosity of a crowded environment 'perceived' by a diffusing particle is strongly dependent on the size of this particle [12, 13], thus the character of diffusion changes over the growing length-scale.

Another group of recent results focuses on the visualization of cytoplasm flows in the entire cell. It has been shown that the long-term ('deterministic') component of theses flows is correlated with the cytoskeleton structure and mainly caused by the collective activity of molecular motors [14]. However, it has been recently established that not only are motors responsible for long-term flows, but also for the most of the random disturbances [15]. I.e. the cytoplasm, at least at the length scale of 50 nm (the probe size applied in [15]), is constantly stirred as the side effect of the active transport and this influence is much stronger than the thermal noise, which can induce sub-diffusion only. Since the random micro-flows are spatially extensive entities, one can conclude

that the noise in the intracellular environment is essentially characterized by distinct spatial correlations, i.e. a group of particles within certain correlation length experience the same random forcing. These findings are particularly interesting for this thesis, because they suggest that in the bio-molecular context a stochastic force in the Langevin dynamics should be enriched with spatial correlations. Indeed, as we show in [A2], this modification can lead to some non-trivial consequences.

1.3 Soft matter perspective

The other strategy to address the challenges of molecular biophysics stems from the soft matter physics and it is focused on designing and understanding more and more complicated model systems. Soft matter physics deals with the class of systems which, in room temperature ($\approx 300K$), is characterized by the interactions of a magnitude comparable to the energy of thermal fluctuations [19]. This means that such systems can be easily deformed by shear stress. However, this also results in a rich phase behavior, since a minor change to thermodynamical parameters or interactions is usually enough to establish a new thermodynamical state. The research on the self-organization in colloidal systems is a significant sub-discipline of soft matter, with multiple applications. These include industry and medicine, but it is also important for e.g. protein crystallization [16, 17] and wet nano-technology [18].

Soft matter physics provides the theoretical and experimental framework to analyze the behavior of complex fluids. One of the most significant breakthroughs in this context is the idea of effective interactions [19, 20]. These interactions arise on the statistical basis in multicomponent systems and they result from the presence of more than one type of particles. In fact, in their simplest realizations they are a straightforward manifestation that 'more is different'. The first theory of effective interactions has been formulated in 50' by Asakura and Oosawa [21, 22] and in the context of polymers by Vrij [23], who considered the excluded volume effects in the hard sphere systems. Several other

analytically solvable systems has been identified since then (e.g. Derjaguin-Landau-Verwey-Overbeek (DLVO) theory of ionic fluids [24], polymer mixtures or polymer-wall interactions [20]), but this problem is usually addressed numerically via specialized methods originating from Mayer bond expansion [25, 26], Density Functional Theory and closure relation techniques [27]. Presently, all of these approaches constitute a well-developed theoretical framework, which is highly successful in predicting the characteristics of various systems, e.g. phase behavior in hard spheres mixtures [26], freezing in the systems of Yukawa particles [28], effective interactions in the mixtures of hard spheres interacting via Yukawa potentials [29] or in the polymer blends [30] and many more. However, this theoretical framework is primarily designed for numerical calculations and, usually, it gives little insight into how and why certain microscopic potentials lead to the predicted behavior. Another problem is that one has to choose a particular closure relation and the choice between its different variants is to some extent arbitrary. Finally, its computational implementation is technically demanding, so it is difficult to apply it as a part of high-level modeling. For these reasons, an analytical yet versatile theory, which could reproduce the sought phenomena in at least qualitative way is of considerable interest.

Effective interactions are directly responsible for the behavior of binary mixtures, which ranges from 'stabilized colloids', in which both phases are well-dispersed, to self-organization, in which two phases separate [20]. Since effective interactions are sensitive to minor changes in the composition of a mixture, they provide a very flexible mechanism of control over self-organization. In the biological context, their significance has been recognized relatively recently, e.g. in the excluded volume effects as a factor promoting ordering and aggregation of intracellular structures [31], as a factor affecting the organization of chromatin in nuclei [31, 32] (especially in the chromosome formation [33]) or as a driving force behind local phase separation in cytoplasm [34]. In fact, one can expect that effective interactions are ubiquitous in the intracellular environment and should be involved in much of the 'nonspecific' physics regulating the efficiency

of many processes. This makes their better analytical understanding even more desired.

1.4 Spatial correlations: deterministic vs. stochastic picture

In qualitative terms, the self-organization phenomena in a multicomponent system can be understood both deterministically and stochastically. In the deterministic picture, one focuses solely on the self-organizing particles and eliminates the environment particles by replacing their influence with the effective interactions. This is deterministic in the sense that the evolution of the system obeys the principles of the one-component case, but with modified potentials. The change in the interaction is responsible for any qualitatively new behavior of the system.

From the microscopic perspective the self-organizing particles undergo a diffusive motion driven by collisions with environment particles. These collisions, the thermal noise, are stochastic in their nature. When there is no microscopic attraction between self-organizing particles (e.g. the hard-sphere case), the sole reason why two particles do not diffuse away from each other is that they experience the same random forcing. This means that in the self-organizing systems the thermal noise is expected to be characterized by spatial correlations i.e. it should act in a similar manner over a certain length-scale. This constitutes the stochastic picture of spatial organization.

This deterministic vs. stochastic picture allows us to divide the interpretation of spatially correlated phenomena into two categories. On the one hand, it is related to the spatial ordering itself, i.e. one species of particles distributes itself in a volume in some correlated manner. On the other hand, these are the spatial correlations in the influence of environment on some subsystem. Since these interpretations are two facets of the same phenomenon, one might expect that it should be possible to link them formally. Indeed, in the later part of this introduction we will argue that this two ideas are intimately related.

1.5 What is this thesis about?

The complete theoretical description of the biological spatio-temporal organization in its entire complexity is still a hopeless task. Most often, we are limited to either very general ideas, which are non-productive in the quantitative sense or to partial, specific results for highly simplified models. For this reason, it is of utmost importance to systematically develop the microscopic theories and extend the range of their applicability. Indeed, in this thesis we attempt to establish a formalism which is derived from the first principles and which can be conveniently applied to model the spatially correlated phenomena. In the preceding sections we have signalized the two fields in which certain development is desired. One problem is the inclusion of spatial correlations in the stochastic dynamics and the other is the versatile analytical tool to predict the effective interactions. Throughout this thesis we propose solutions to both of these challenges and show the relation between them. Our ideas are included in the four papers:

- *Analytical theory of effective interactions in binary colloidal system of soft particles* [A1] This is the main article, which introduces a new theory of effective interactions based on path-integral approach, in which we are able to identify the single, closed-form formula relating microscopic interactions to the effective potential. In [A1] we provide the derivation as well as the selection of applications. This includes a comparison to well-known systems (polymer blends, DLVO theory) and the systems previously unsolved (the mixtures of Yukawa particles with repulsive cores).

- *Polymer unfolding and motion synchronization induced by spatially correlated noise* [A2] In this article we analyze the effects of spatially correlated noise on the model polymer chain. The results are numerical and indicate that spatial correlations in noise can substantially affect the system at many levels, including the preference for non-equilibrium conformations.

- *Reinterpreting polymer unfolding effect induced by spatially correlated noise* [A3] This paper provides additional insight into to effect of unfolding presented in [A2].

- *Non-Gaussian polymers described by alpha-stable chain statistics: model, effective interactions in binary mixtures and application to on-surface separation* [A4] This article presents the application of our theoretical tools to a new model of polymers based on the non-Gaussian statistics. Such statistics can result from the presence of spatial correlations in the environment, presence of domains in the chain or adsorption to a surface. Applying the methods developed in the previous articles we are able to address the problem of the on-surface separation in adsorption from a binary mixture.

These results cover a wide spectrum of phenomena related to the spatial correlations and their application. Additionally, in Section 4 we provide the unpublished result on the correspondence between spatial correlations and effective interactions to emphasize the link between our research included in papers [A1] and [A2].

2 Spatial correlations in one component systems

2.1 Correlation function

In this section the formal definition of the spatial correlation function is provided. Let us consider a system consisting of N particles, which have a mass m and interact via a pair potential $U(|\mathbf{r}_i - \mathbf{r}_j|)$. The volume of the system reads Ω and the temperature is T. We denote $\beta = (k_B T)^{-1}$, where k_B is the Boltzmann constant. We are interested in the spatial correlations of a certain quantity $\phi(\mathbf{r}_i)$ which is dependent on the position of particles $\mathbf{r}_i$. We expect that the spatial correlation function of $\phi(\mathbf{r}_i)$ reads:

$$\langle \phi(\mathbf{r}_i)\phi(\mathbf{r}_j)\rangle = f(|\mathbf{r}_i - \mathbf{r}_j|) \tag{1}$$

where $\langle . \rangle$ denotes the average over the ensemble. Limiting our considerations to the equilibrium case, we can interpret the average as taken with respect to the probability function arising from the partition function. For this system, the partition function in the standard position-momentum variables and with momenta integrated out, reads:

$$\Xi = \frac{z^N}{N!} \int_\Omega \{d\mathbf{r}\} \exp\left(-\beta \left(\frac{1}{2} \sum_{\substack{k,l \\ k \neq l}}^{N} U(|\mathbf{r}_k - \mathbf{r}_l|)\right)\right) \tag{2}$$

where $\{d\mathbf{r}\}$ denotes the integration with respect to every $\mathbf{r}_k$ and:

$$z = \left(\frac{2\pi m}{\beta h^2}\right)^{D/2} \tag{3}$$

From Ξ it follows that the marginal probability distribution for a pair i-j is given by:

$$P(\mathbf{r}_i, \mathbf{r}_j) = \frac{z^N}{N! \Xi} \int_\Omega \{d\mathbf{r}\}_{i,j} \exp\left(-\beta \left(\frac{1}{2} \sum_{\substack{k,l \\ k \neq l}}^{N} U(|\mathbf{r}_k - \mathbf{r}_l|)\right)\right) \tag{4}$$

where $\{d\mathbf{r}\}_{i,j}$ denotes the integration with respect to every $\mathbf{r}_k$ except for $k = i, j$. Then, the correlation function can be expressed as:

$$\langle \phi(\mathbf{r}_i)\phi(\mathbf{r}_i + \Delta\mathbf{r}) \rangle = \int_\Omega d\mathbf{r}_i \phi(\mathbf{r}_i)\phi(\mathbf{r}_i + \Delta\mathbf{r}) P(\mathbf{r}_i, \mathbf{r}_i + \Delta\mathbf{r}) \tag{5}$$

From (4) and (5) it is clear that the shape of potential U has a strong influence on the spatial correlation function. However, the exact form of the correlation function might be highly non-intuitive and look considerably different in various regimes of thermodynamical parameters. A main reason for that is the possibility of phase transitions, embedded in the partition function.

2.2 Phase transitions and glassy state

The higher organization in one component system can be obtained via globally changing thermodynamical parameters such as temperature, volume or pressure.

This can lead to the phase transition in which the scale-free behavior occurs [35], manifested by the power-law type correlation function:

$$\langle \phi(0)\phi(\Delta\mathbf{r})\rangle \propto \frac{1}{\Delta r^{D-2+\eta}} \tag{6}$$

where $\phi(\mathbf{r})$ is the order parameter, D is the system dimension and η is the critical exponent. Whenever the physics of the system can be formulated in terms of the Ginzburg-Landau meta-model, the methods of renormalization group techniques can be applied to obtain the analytical results. While fascinating on its own, the physics of phase transitions is not in the main scope of this thesis. A comprehensive introduction to the topic can be found in [35]. For the discussion of fluid oriented techniques such as half-analytical methods based on the Meyer bond expansion, Density Functional Theory and integral equations techniques see [27].

In the context of paper [A2], we are interested in the systems in which the spatially correlated noise can be identified. We have already mentioned the micro-flows as a possible realization of such 'noise' and the near-phase transition systems are another example. However, while for phase transitions the long range-correlations are available in the relatively narrow range of parameters, there exists another state of matter which is less elusive, but exhibits equally interesting properties. This is the glassy state, which, among many surprising features, is characterized by the strong spatial correlations in its dynamics. Since the theoretical description of glasses is still not complete, we will discuss them here in a greater detail.

The glassy state occurs in the supercooled fluids or in the highly packed systems and exhibits a behavior known as 'jammed mechanics' [36]. In contrast to the crystallization, which occurs at the volume fraction of packing equal to 0.494 and results in the increased molecular order, the glassy state requires the volume fraction of at least 0.58 [37, 38] and it is highly disordered. The glassy state is characterized by an extreme rise in viscosity (e.g. by 14 orders of magnitude) and a dramatic slow down of dynamics, with typical relaxation timescale of the order of 100 s [36]. From the molecular perspective, there appear a rise in

the number of collectively rearranging particles. This parameter increases from approximately 1 in the liquid state to the 4-10 in the glassy state [39], which has been measured via impedance spectroscopy. Another characteristic is the correlation length. While it is possible to measure it indirectly via calorimetry or NMR techniques [41], the relatively recent application of confocal microscopy allowed a direct measurement, resulting in the correlation length equal to 2-4 diameters of particles.

Although the correlation length can be determined on its own, its response to the variation of thermodynamical parameters does not match the phase transition picture [36]. The problem of what is the order parameter for the glassy transition and whether it exists is open, but an interesting proposition has been recently given by Mosayebi et all. in [40]. In their approach, based on the technique known as affine structure analysis, a random configuration of particles X^q at certain volume packing is generated and then refined by the energy minimization algorithm to obtain a configuration X. Another step is to disturb the configuration X with the affine transformation to obtain a structure X^d. Finally, the structure X^{dq} is determined, such that the energy minimization of X^{dq} results in X^d. Analyzing the statistical differences between non-minimized structures X^q and X^{dq} it is possible to determine a 'static correlation' length which has a scale-free behavior and diverges in a finite critical temperature.

As we have already mentioned, the glassy state is characterized by the well-pronounced spatial correlation function. Most knowledge regarding this function comes from simulations. In particular, Doliwa and Heuer report that the correlation function has an exponential form [42]:

$$\langle \phi(0)\phi(\Delta\mathbf{r})\rangle \propto \exp\left(-\frac{\Delta r}{\xi_\phi}\right) \tag{7}$$

where ϕ can be assigned to velocity or the direction of motion and ξ_ϕ is the correlation length. The exponential prediction for correlation functions is confirmed by confocal microscopy experiments [38], especially when a long relaxation time of a sample is applied. Interestingly, both simulations [42] and experiment [38] indicate the oscillating behavior in the correlation functions, which is not well

understood. The cooperative rearrangement and persistent spatial correlations indicate the cluster formation, which has been also studied numerically e.g. in references [43] and [44].

Summarizing this section, it should be clear now that both in the near-crystallization conditions and in the glassy state, the system acts in a spatially correlated manner. This means that any finite-size sub-system submerged in such environment is affected by the spatially correlated disturbance. In many model systems the correlations in noise can transfer into the behavior of the system [45]. Our results from [A2] indicate that, indeed, in the glassy state the dynamics of a subsystem can be strongly modified by the collective behavior.

3 Spatial correlations in multicomponent systems

3.1 Effective interactions in binary systems

Let us now get back to the relation between interactions and the spatial correlation function and focus our attention on the binary systems, i.e. systems which consist of two types of particles. The multicomponent systems are of primary interest for this thesis, because they provide a flexible mechanism of spatial organization different from the phase transitions. The central concept for this mechanism are the interactions of statistical origin, known as effective interactions.

We consider the system in which there are two species of particles. The positions for the first species (also called 'distinguished' or 'observed') are denoted with $\mathbf{R}_i$ and for the second species (referred to as 'depletant' or 'environment') with $\mathbf{r}_i$. Assuming that there are microscopic interactions between particles of the same type as well as the cross-species interactions, the total partition

function of the system reads:

$$\Xi_{tot} = \frac{z_1^{N_1}}{N_1!} \int_\Omega \{d\mathbf{R}\} \exp\left(-\beta \left(\frac{1}{2} \sum_{\substack{k,l \\ k \neq l}}^{N_1} U_{RR}(|\mathbf{R}_k - \mathbf{R}_l| - \frac{1}{\beta} \ln \Xi) \right) \right) \tag{8}$$

where U_{RR} is the interaction between the particles of the first species and Ξ is the partition function containing the second species and cross interactions:

$$\Xi = \frac{z_2^{N_2}}{N_2!} \int_\Omega \{d\mathbf{r}\} \exp\left(-\beta \left(\sum_k^{N_1} \sum_i^{N_2} U(|\mathbf{R}_k - \mathbf{r}_i| + \frac{1}{2} \sum_{\substack{i,j \\ i \neq j}}^{N_2} V(|\mathbf{r}_j - \mathbf{r}_i|) \right) \right) \tag{9}$$

Here, V denotes the interaction between the particles of the second species and U denotes the cross-interaction between species. As previously:

$$z_i = \left(\frac{2\pi m_i}{\beta h^2} \right)^{D/2} \tag{10}$$

From (8) one can notice that the expression:

$$U_{eff} = -\frac{1}{\beta} \ln \Xi \tag{11}$$

acts as an additional potential. Indeed, this is the formal definition of effective interactions [19], which is the force of entropic origin arising from the presence of additional particle species.

In the one component system the only way to control the spatial organization requires the variation of thermodynamical parameters in order to induce a phase transition. This also imposes a demand that the system is abundant enough so the statistical mechanics applies and collective phenomena can occur. Obviously, the multicomponent systems can also undergo phase transition, leading to a possibly more complex phases than in the one-component case. However, in a multicomponent system the effective interactions provide a control mechanism over spatial organization, which does not resort to the variation of thermodynamical parameters.

The effective interactions depend on the microscopic potentials U and V, and these potentials are determined by the physical characteristic of particles,

be it their elasticity, charge, polarity etc. Therefore, replacing or modifying particles belonging to the second species results in the effective interactions being altered and this affects the behavior of the first species. In particular, this means there is no need to modify the global thermodynamical parameters such as temperature or pressure in order to increase or decrease organization. Another advantage of this mechanism is that the first species does not have to be abundant anymore. For example, in the system which consists of only two particles of the first kind, one can obtain the exact result for the correlation function of their positions, which reads:

$$\langle \mathbf{R}(\mathbf{R}+\Delta\mathbf{R})\rangle = \exp\left(-\beta(U_{RR}(\Delta R)+U_{eff}(\Delta R))\right)\left(\int_{\Omega} d\mathbf{R}\mathbf{R}(\mathbf{R}+\Delta\mathbf{R})\right) \tag{12}$$

Indeed, this shows that a properly designed effective potential can drive the self assembly of even low-abundant particles. This is especially interesting in the biological context.

3.2 Biological meaning

In *in vivo* experiments one deals with effective dynamics almost exclusively. The reason is that one cannot dye every particle in the biological system, let alone register its trajectory. This makes the effective interactions important *in principle*. However, the equilibrium theory of effective interaction by no means can be directly applied to the highly non-equilibrium intracellular environment. Nevertheless, basing on certain field-theoretical formulations of non-equilibrium thermodynamics (e.g. [46]), one might expect that it applies at least locally. For this reason let us speculate on several processes in which the effective interactions can affect the biological systems.

As we have already mentioned, obtaining a higher organization by the means of phase transitions requires both the abundance of particles and the ability to globally vary thermodynamical parameters. None of these is readily available for a cell. While the overall packing in the cellular environment is high, the concentrations of specific compounds are not. As pointed out by Bustamante

[47], in bacteria they are usually as low as single molecules. Another issue is that the requirement to maintain the physiological conditions makes the significant variation of temperature, pressure or volume unfavorable. On the other hand, a cell is well equipped to modify its chemical composition. As we have discussed, changing the composition affects the effective interactions and provide a valuable mechanism of self-organization.

The typical problem of molecular biology is the formation of complexes and aggregates. Let us consider two particles which can bind chemically. To form a bond, these particles has to position in a specific spatial configuration. Incorporating the effective interaction into this picture has some dire consequences. First of all, effective interactions introduce an additional potential which can be attractive. This means that whenever two parts of a complex exploring randomly the available volume come close enough to feel the effective potential, their diffusion is no longer that of the free particles. Effective interaction can bind them non-specifically, sometimes with energy higher than thermal fluctuations. This means that particles can be trapped in the vicinity of each other for a significantly longer time than the overall characteristic timescale of diffusion. Finally, the non-specific binding due to the effective interactions provides the additional time for the rotational diffusion to find configuration required for chemical binding.

Another aspect of complex formation is the time required to find the other particle. The binding by effective interactions means that it is not necessary to exactly find the surface of the other particle, but it is enough to get in the range of this interaction. While for the hard sphere model this additional range is as small as the size of depletant particles, for the electrostatic interactions this can be significantly larger. In [A1], we show that the range of interaction can be larger than the radius of a particle. This means that in many situations two parts of a complex seek for an object which is considerably bigger that the molecule itself. Although this effect strongly depends on the interaction type, the described mechanism can potentially enhance the search process.

Yet another influence is that the effective interactions provide not only the particle-particle interactions, but it may also result in the affinity to the surfaces. This can also affect the complex formation, since the bigger particles might tend to reach a surface first (be it cell membrane or the surface of an organelle) and then seek each other diffusively taking the advantage of the reduced dimensionality and the mechanisms described in the two previous paragraphs. However, it should be mentioned that the surfaces in the cellular environment are highly functionalized with proteins and receptors and this can seriously affect the particle-surface affinity of entropic origin.

Finally, the effective interactions might contribute to the sub-diffusive behavior. The sub-diffusion appears for particles which combine free diffusion and trapping. When the effective interaction can bind a particle with the energy comparable to the fluctuation magnitude, this satisfies the aforementioned situation. From this perspective, the effective interactions can enhance the sub-diffusive character of the transport in cytoplasm.

4 Spatial correlations in the thermal noise

4.1 Effective interactions from the stochastic perspective

We have discussed the effective interactions from the perspective of observed species, in the spirit of 'deterministic' interpretation. However, while the effective interactions enter the partition function like a regular potential, their origin is purely stochastic. This means that they should not be perceived as a direct force between two distinguished particles, but rather as an effect of collective and spatially correlated motion of the environment particles. This is what we have called the 'stochastic' picture and in this section we will make the relation between the spatial correlations in thermal noise and effective interactions explicit. However, since the thermal noise is closely related to the concept of Langevin equation, let us briefly discuss its nuances.

In its standard form (altough including the inertial terms), the Langevin-type equation for a set of N_1 particles reads:

$$m_1\ddot{\mathbf{R}}_i + \gamma\dot{\mathbf{R}}_i + \sum_{j\neq i}^{N_1}\mathbf{F}_i(\mathbf{R}_i - \mathbf{R}_j) = \boldsymbol{\xi}_i(t) \tag{13}$$

In this notation $\mathbf{F}_i(\mathbf{R}_i - \mathbf{R}_j)$ denotes all inter-particle forces which we would like to include in the dynamics. $\boldsymbol{\xi}_i$ is the stochastic force experienced by the i-th particle and in the standard approach it is assumed that:

$$\left\langle \boldsymbol{\xi}_i(t)\cdot\boldsymbol{\xi}_j(t')\right\rangle \propto \delta_{ij}\delta(t-t') \tag{14}$$

so there are no temporal nor spatial correlations in this force. The friction term $\gamma\dot{\boldsymbol{R}}_i$ is determined by the Stokes law. The attempts to justify Langevin equations on the microscopic basis has led to the discovery of Generalized Langevin Equations (GLE), in which the temporal correlations in stochastic force are accompanied by the memory kernel in the friction term [24, 11]. Since GLE are capable of describing sub-diffusion [11], enormous effort has been put into understanding the relation between GLE and other formalisms leading to sub-diffusion, e.g. Continuous Time Random Walks and fractional Fokker-Planck equations [4]. On the other hand, relatively little work has been devoted to the presence of spatial correlations in the noise. This problem occurred in the context of the diffusion in plasma [48, 49] and for the problem of spatial confinement [50], yet it has been addressed only from the perspective of a single particle. No systematic treatment of multi-particle systems is known to the present author. While the spatial correlations in the noise could possibly demand some currently unknown form of friction, which would account for collectivity and self-organization, in this thesis (and especially in paper [A2]) we restrict ourself to the Stokes law. Nevertheless, we are aware that the friction which should accompany the spatially correlated noise is an open problem.

Let us focus now on the equilibrium systems, in which the temporal correlation is negligible because the probability distribution for any physical value has achieved a steady state. $\boldsymbol{\xi}_i$ mimics the interaction with environment, so it can

be interpreted as the sum of forces acting on the particle in a given moment:

$$\boldsymbol{\xi}_i = \sum_j^{N_2} \nabla_{\mathbf{R}_i} U(|\mathbf{R}_i - \mathbf{r}_j|) = \boldsymbol{\xi}(\mathbf{R}_i) \tag{15}$$

It is possible now to interpret the noise correlation function $\left\langle \boldsymbol{\xi}(\mathbf{R}_i)\boldsymbol{\xi}_j(\mathbf{R}_j)\right\rangle$ as the average with respect to the probability distribution derived from Ξ_{tot} as in (8). This reads:

$$\begin{aligned}\langle \boldsymbol{\xi}(\mathbf{R}_i)\cdot\boldsymbol{\xi}(\mathbf{R}_i+\Delta\mathbf{R})\rangle = \int_\Omega d\mathbf{R}_i \int_\Omega \{d\mathbf{r}\} P(\mathbf{R}_i, \mathbf{R}_i+\Delta\mathbf{R}, \mathbf{r}_1,\ldots,\mathbf{r}_{N_2})\times \\ \times \left(\sum_j^{N_2} \nabla_{\mathbf{R}_i} U(|\mathbf{R}_i-\mathbf{r}_j|)\right)\cdot\left(\sum_{j'}^{N_2} \nabla_{\mathbf{R}_i} U(|\mathbf{R}_i+\Delta\mathbf{R}-\mathbf{r}_{j'}|)\right)\end{aligned} \tag{16}$$

where:

$$\begin{aligned}P(\mathbf{R}_i,\mathbf{R}_j,\mathbf{r}_1,\ldots,\mathbf{r}_{N_2}) = \frac{z_1^{N_1} z_2^{N_2}}{\Xi_{tot} N_1! N_2!}\int_\Omega \{d\mathbf{R}\}_{i,j}\times \\ \exp\left(-\beta\left(\frac{1}{2}\sum_{\substack{k,k'\\k\neq k'}}^{N_1} U_{RR}(|\mathbf{R}_k-\mathbf{R}_{k'}|) + \sum_{k,l}^{N_1,N_2} U(|\mathbf{R}_k-\mathbf{r}_l|) + \frac{1}{2}\sum_{\substack{l,l'\\l\neq l'}}^{N_2} V(|\mathbf{r}_l-\mathbf{r}_{l'}|)\right)\right)\end{aligned} \tag{17}$$

The equations (16) and (17) constitute the formal definition of noise correlation function. Unfortunately, it is not possible to proceed with calculations for the current form of this equation. Its structure is complicated by the fact that we express the partition function in terms of space-momentum coordinates. However, there exists a much more convenient representation, which allows us to calculate the desired correlation function.

4.2 Occupation number functional formalism

We will now use the occupation number functional, the formalism which we meticulously introduce in paper [A1]. While in this section we restrict our considerations to the canonical ensemble, in [A1] we use the grand canonical ensemble. For the current derivation, the differences are irrelevant.

We introduce a field $\alpha(\mathbf{r})$ which provides the number of environment particles in a certain position $\mathbf{r}$. Let us remind that the total number of environment particles reads N_2, and the total number of distinguished particles reads N_1. What follows:

$$N_2 = \int_\Omega d\mathbf{r}\alpha(\mathbf{r}) \tag{18}$$

The environment-environment interaction and cross-species interaction can be translated in the following way:

$$\sum_{i,j}^{N_2} V(|\mathbf{r}_i - \mathbf{r}_j|) = \iint_\Omega d\mathbf{r}d\mathbf{r}'\alpha(\mathbf{r})\alpha(\mathbf{r}')V(|\mathbf{r} - \mathbf{r}'|) \tag{19}$$

$$\sum_{i}^{N_1}\sum_{j}^{N_2} U(|\mathbf{R}_i - \mathbf{r}_j|) = \int_\Omega d\mathbf{r}\alpha(\mathbf{r})U(|\mathbf{R}_i - \mathbf{r}|) \tag{20}$$

Now, we propose to treat the partition function of environment particles as the path integral with respect to the every physically meaningful field $\alpha(\mathbf{r})$, namely:

$$\begin{aligned}\Xi = \frac{\tilde{z}_2^{N_2}}{N_2!}\int \mathcal{D}[\alpha]\exp\left(-\beta\mathcal{H}\right) = \frac{\tilde{z}_2^{N_2}}{N_2!}\int \mathcal{D}[\alpha]\times \\ \times\exp\left(-\beta\left(\sum_k^{N_1}\int_\Omega d\mathbf{r}\alpha(\mathbf{r})U(|\mathbf{R}_k - \mathbf{r}|) + \frac{1}{2}\iint_\Omega d\mathbf{r}d\mathbf{r}'\alpha(\mathbf{r})\alpha(\mathbf{r}')V(|\mathbf{r} - \mathbf{r}'|)\right)\right)\end{aligned} \tag{21}$$

Here $\int \mathcal{D}[\alpha]$ stands for the path integral measure. In [A1] we discuss the subtleties of $\int \mathcal{D}[\alpha]$ in detail. In (21) we modify z_2 in the following way:

$$\tilde{z}_2 = \left(\frac{2\pi m_2}{\beta h^2}\right)^{D/2} e^{\beta V(0)} \tag{22}$$

This compensates for abandoning the $i \neq j$ restriction in (19). Further, we can apply $\alpha(\mathbf{r})$ to translate $\boldsymbol{\xi}(\mathbf{R}_i)$:

$$\boldsymbol{\xi}(\mathbf{R}_i) = \int_\Omega d\mathbf{r}\alpha(\mathbf{r})\nabla_{\mathbf{R}_i}U(|\mathbf{R}_i - \mathbf{r}|) \tag{23}$$

In the light of (23), one can notice that:

$$\begin{aligned}\nabla_{\mathbf{R}_i}\exp\left(-\beta\left(\sum_k^{N_1}\int_\Omega d\mathbf{r}\alpha(\mathbf{r})U(|\mathbf{R}_k - \mathbf{r}|)\right)\right) = \\ = -\beta\boldsymbol{\xi}(\mathbf{R}_i)\exp\left(-\beta\left(\sum_k^{N_1}\int_\Omega d\mathbf{r}\alpha(\mathbf{r})U(|\mathbf{R}_k - \mathbf{r}|)\right)\right)\end{aligned} \tag{24}$$

For shorter notation we will use:

$$\mathcal{H}_{RR} = \frac{1}{2} \sum_{\substack{k,k' \\ k \neq k'}}^{N_1} U_{RR}(|\mathbf{R}_k - \mathbf{R}_{k'}|) \tag{25}$$

From the path integral formulation (21) and identity (24), it follows that the noise correlation function reads:

$$\begin{aligned} \langle \boldsymbol{\xi}(\mathbf{R}_i) \cdot \boldsymbol{\xi}(\mathbf{R}_j) \rangle &= \frac{z_1^{N_1} z_2^{N_2}}{N_1! N_2! \Xi_{tot}} \int_\Omega \{d\mathbf{R}\}_j e^{-\beta \mathcal{H}_{RR}} \int \mathcal{D}[\alpha] \boldsymbol{\xi}(\mathbf{R}_i) \cdot \boldsymbol{\xi}(\mathbf{R}_j) e^{-\beta \mathcal{H}} \\ &= \frac{z_1^{N_1} z_2^{N_2}}{N_1! N_2! \Xi_{tot} \beta^2} \int_\Omega \{d\mathbf{R}\}_j e^{-\beta \mathcal{H}_{RR}} \nabla_{\mathbf{R}_i} \cdot \nabla_{\mathbf{R}_j} \Xi \end{aligned} \tag{26}$$

Knowing the relation (11) between Ξ and the effective potential U_{eff}, one can write:

$$\langle \boldsymbol{\xi}(\mathbf{R}_i) \cdot \boldsymbol{\xi}(\mathbf{R}_j) \rangle = \frac{z_1^{N_1} z_2^{N_2}}{N_1! N_2! \Xi_{tot} \beta^2} \int_\Omega \{d\mathbf{R}\}_j e^{-\beta \mathcal{H}_{RR}} \nabla_{\mathbf{R}_i} \cdot \nabla_{\mathbf{R}_j} e^{-\beta U_{eff}} \tag{27}$$

Further, in this integral we can move ∇_{R_i} from the second factor to the first, so:

$$\langle \boldsymbol{\xi}(\mathbf{R}_i) \cdot \boldsymbol{\xi}(\mathbf{R}_j) \rangle = -\frac{z_1^{N_1} z_2^{N_2}}{N_1! N_2! \Xi_{tot} \beta^2} \int_\Omega \{d\mathbf{R}\}_j \nabla_{\mathbf{R}_i} e^{-\beta \mathcal{H}_{RR}} \cdot \nabla_{\mathbf{R}_j} e^{-\beta U_{eff}} \tag{28}$$

This result can be finally rewritten in a more compact form:

$$\langle \boldsymbol{\xi}(\mathbf{R}_i) \cdot \boldsymbol{\xi}(\mathbf{R}_j) \rangle = - \langle \mathbf{F}_{RR,i}(\mathbf{R}_i) \cdot \mathbf{F}_{eff,j}(\mathbf{R}_j) \rangle \tag{29}$$

where $\mathbf{F}_{RR,i}(\mathbf{R}_i) = -\nabla_{\mathbf{R}_i} \mathcal{H}_{RR}$ and $\mathbf{F}_{eff,j}(\mathbf{R}_j) = -\nabla_{\mathbf{R}_j} U_{eff}$. This establishes the formal relation between effective interactions and spatial correlations in thermal noise.

5 Included papers: summary and comments

5.1 Analytical theory of effective interactions in binary colloidal systems of soft particles

Up to now, it should be clear that the understanding of effective interactions in binary mixtures is a crucial problem. Although the general expression for

effective interactions is given by (11), it is ineffective. In [A1] we introduce a new analytical method of calculating the effective interactions, which is alternative to standard techniques. The entire approach is based on translating the Hamiltonian of the system from the momentum-position variables into the occupation field $\alpha(\mathbf{r})$. The interactions are translated according to equations (18)-(20). Similarly to (21), one can translate the grand partition function of the system from the space-momentum problem into the path integral over every possible field $\alpha(\mathbf{r})$. Replacing the problem of space-momentum integrals with path integral is similar to the approach of Density Functional Theory. However, we do not resort to the functional differentials and Mayer bond expansion in order to calculate the correlation function, as the standard approach goes. Instead, we employ the phonon-theory methods expanding $\alpha(\mathbf{r})$ into its Fourier modes and interpreting the path integrals as an integral over these mods. This approach allows us to identify the following expression for effective interactions:

$$U_{eff}(\mathbf{R}_i - \mathbf{R}_j) = -\frac{1}{(2\pi)^D} \int_{\tilde{\Omega}} d\mathbf{k} e^{i\mathbf{k}\cdot(\mathbf{R_i}-\mathbf{R_j})} \frac{|\mathcal{U}(k)|^2}{\mathcal{V}(k)} \tag{30}$$

where:

$$\mathcal{U}(k) = \int_{\Omega} d\mathbf{r} e^{i\mathbf{k}\cdot\mathbf{r}} U(r)$$
$$\mathcal{V}(k) = \int_{\Omega} d\mathbf{r} e^{i\mathbf{k}\cdot\mathbf{r}} V(r)$$

are Fourier transforms of the microscopic potentials. The formula (30) is the most significant outcome from the proposed formalism and it is central for this thesis.

The status of formula (30) requires a comment. The path integrals should be performed over all physically meaningful fields $\alpha(\mathbf{r})$, but it is difficult to express a non-negative field in terms of its Fourier modes. While our approach simplifies the integrands, it comes at the cost of complicated integration limits. Nevertheless, the formula (30) is factored out before any approximation to calculate the integrals is applied, so we expect (30) to act as an zeroth-order theory. In fact, one can see that some important modifications are embedded in

the neglected part, since the shape of (30) does not depend on the temperature nor concentrations and these parameters appear in our estimates of corrections. On the other hand, (30) leads to some non-trivial potential shapes, and, as we show, despite all its downsides, it is surprisingly robust in producing meaningful results.

Once the formula (30) is established, we employ it to predict the effective interactions in several systems. The first system is a classical problem of charged hard spheres in the presence of ions. We model this situation using Coulomb potentials for electrostatic interactions and step function for the excluded regions. Applying the formula (30) we predict that effective interactions counterbalance Coulomb repulsion, so the total interaction between two spheres is described by the Yukawa potential. This result fully agrees with the standard model for this problem, which is known as Derjaguin-Landau-Verwey-Overbeek theory and predicts the effect of charge screening.

Another class of systems is the binary mixture of particles described solely by Yukawa potentials. Also in this case it is possible to predict the effective interactions analytically. Our results indicate that it is possible to obtain a variety of effective interactions ranging from attractive to repulsive. Although this model is too simplified to describe particles in the solution, we draw a connection with the phase separation in plasma research.

Yet another model is aimed at describing a binary system of particles which consist of a hard sphere core and the Yukawa interaction tail. As discussed earlier, this type of particles is a reliable model of charged particles in the screening ionic solution. In this case we consider a binary mixture of particles which differ in their size and the sign of interaction. In [29] such binary systems have been simulated allowing either attractive, repulsive or no interaction tail. In general, nine possible combinations of interactions are possible and a variety of possible effective interactions is revealed. In particular, the repulsive big-small interaction induces attractive effective interaction, while the attractive big-small potential results in the effective repulsion. For big-small interaction reduced to the hard sphere case, the effective interaction depends on the sign of small-small in-

teraction tail. Applying (30), we analytically predict the expression for effective interactions, albeit using two Yukawa potentials, one for the core of a particle and the other one for the interaction tail. Despite this modification, we succeed in qualitatively reproducing the effective interactions in terms of their sign and range for almost every case. The best agreement is achieved for the 'attraction-through-repulsion' case, while for the 'repulsion-through-attraction' our model does not reproduce a higher order oscillatory structure. It is not clear whether this discrepancy is the result of approximations in (30) or replacing the hard sphere potential with its soft substitute. Nevertheless, it should be emphasized that this model has not been solved analytically before and our results are in satisfying qualitative agreement with simulations.

Finally, we discuss the systems of Gaussian particles, which are a well established model for polymers in the semi-dilute regime. We predict the effective interaction to be also a rescaled Gaussian potential, although always attractive. Using this result we examine the condition for polymer separation in binary mixture, assuming that the separation occurs when the total interaction between bigger particles is also attractive. This happens whenever the effective interaction prevails over the microscopic repulsion, which is dependent on the system parameters, most notably on the ratio of gyration radii. Finally, we are able to obtain an analytical prediction for the phase separation condition.

The formula given in the article is comparable to the spinodal decomposition condition for Gaussian particles [51, 52]. However, the result included in [A1] contains a mistake due to an inconsistent choice of 2π factor in the Fourier transform of potentials. In fact, after refinement, the obtained result turns out to be exactly the same as the spinodal decomposition condition from [51, 52] and [A4].

Summarizing the analyzed examples, our model provides a sufficient and unified approach to analytically reproduce the specific features of systems as different as polymers and charged particle mixtures. The results are generally comparable to the mean-field approach. However, it should be pointed out that the mean-field nature is already embedded e.g. in the Gaussian and Yukawa

microscopic potentials, since they are derived from a lower-level theories. On the other hand, the 'renormalized' nature of these microscopic potentials means that they already include thermodynamical parameters. This is the advantage which remedies the fact that (30) lacks a dependence on these parameters. Having this in mind, the presented theory could be applied in the high-level modeling, since its analyticity makes it possible to avoid extensive numerical calculations usually necessary to determine effective interactions.

5.2 Polymer unfolding and motion synchronization induced by spatially correlated noise

In the second article we explore the possibility of enhancing the molecular modeling by the inclusion of spatially correlated effects from the environment. As we have already discussed, the spatial correlations in thermal noise appear in the multicomponent systems, as well as in the cytoplasmic micro-flows and in the glassy state. The formula (27) relates effective interaction and the noise correlation function.

Langevin equations, in which a stochastic force mimics the collisions with environment particles, is a convenient tool in the molecular dynamics simulations. In the standard approach, this stochastic term is non-correlated, either spatially or temporally. While there is an ongoing interest in the generalized Langevin equations, in which the temporally correlated noise is accompanied by the friction memory kernel [11], little work has been done to understand the effects of spatial correlations in the thermal noise. In this paper, we propose to model the collective, spatially correlated behavior of environment via the application of spatially correlated noise in the Langevin dynamics. The equations of motion for observed particles has the general form of (13), but the noise term $\boldsymbol{\xi}$ is a random correlated Gaussian variable. However, for the purpose of this article we limit our considerations to the two dimensional systems and the

following correlation function:

$$\begin{aligned}&\langle \xi_x(\mathbf{r}_i(t))\xi_x(\mathbf{r}_j(t'))\rangle = \langle \xi_y(\mathbf{r}_i(t))\xi_y(\mathbf{r}_j(t')\rangle = \\ &= \frac{2k_BT\gamma}{m}\exp\left(-\frac{|\mathbf{r}_i-\mathbf{r}_j|}{\lambda}\right)\delta(t-t')\end{aligned} \tag{31}$$

For the simplicity of the generation procedure, we assume no correlations between different directions, so $\langle \xi_x(\mathbf{r}_i(t))\xi_y(\mathbf{r}_j(t'))\rangle = 0$. The generated noise tends to form clusters of vectors characterized by a similar length and direction within the range of λ, but their pattern changes with every iteration.

The system that becomes a subject to the spatially correlated disturbance is a 2D polymeric chain. The chain model is based on the bead-spring approach (harmonic potential between nearest neighbors), but with two significant modification. One difference is the inclusion of a global Lennard-Jones potential for each bead, which introduces the excluded volumes effects. The other modification is the harmonic potential between second nearest neighbors, which results in the saw-like conformations minimizing the energy of the chain. In the introductory part of the article we analyze the energy landscape for a single bead in the relation to the position of its four nearest neighbors. This allows us to conveniently represent the conformational space both for the relaxed and the locally stretched geometry.

The presence of spatial correlations in the noise leads to a remarkable change in the system dynamics. First, we introduce a measure of synchronization to show that the spatial correlations induce the synchronization of beads motion, i.e. the velocity vectors of beads within the correlation length are similar. This is further confirmed by the investigation of time correlation functions for angles between segments (ψ) and for the length of the segments. There is a significant rise in these time correlation functions, which indicates that the shape of chain is more persistent than in the presence of non-correlated noise.

In the thermodynamical perspective, the spatially correlated noise attenuates the effect of increased temperature. Generally, as the magnitude of the noise grows, the angular degrees of freedom are released and the distribution of angles $\Phi(\psi)$ evolves from a double-peaked shape to the mono-peaked. How-

ever, in the presence of non-zero spatial correlations, this transition requires remarkably higher temperature, once again making the chain geometry more persistent.

All these observations are somewhat expected, since the spatially correlated noise provides a fairly uniform forcing over the correlation length. However, the distribution $\Phi(\psi)$ allows us to observe one more effect. This is the spontaneous unfolding, manifested by the narrowing of $\Phi(\psi)$, as the noise correlation length grows. This means that in the presence of non-zero spatial correlations more elongated conformations are preferred. This is an interesting result, since linearized structures are neither energetically optimal nor they minimize the polymer entropy. This means that the spatially correlated noise can induce and support the non-equilibrium state of the system. In [A2] we attempt to explain the unfolding effect from the perspective of beads mobility. However, our additional studies over the distribution of linearized fragments suggested a different explanation, and this is included in the paper [A3].

Although limited to the specific case, our results show that the spatial correlations in the behavior of environment can effectively transfer into the dynamics of the observed subsystem. As such, they provide another tool of system control at the molecular level. While introducing the spatial correlations via the noise term requires more computational effort than the standard Langevin dynamics, it can be applied instead of full-scale molecular simulations. This approach is especially tempting whenever the correlation function is already known, e.g. from experiments.

5.3 Reinterpreting polymer unfolding effect induced by spatially correlated noise

This paper compliments the publication [A2] and it is focused on analyzing the spontaneous unfolding effect more thoroughly. The narrowing of the distribution $\Phi(\psi)$ indicates that a significant number of segments tend to form a linearized structure. Comparing the angles between subsequent segments we

introduce a measure indicating whether this pair of segments can be treated as linearized. Further, we gather the data regarding the average abundance of linearized fragments containing different numbers of segments, for a range of temperatures and correlation lengths in the noise. These data indicate that the spontaneous unfolding effect is mainly based on the short, 2-3 segment long linearized fragments.

This fact suggests the following interpretation. Let us consider a single instance of time. The spatially correlated noise provides little relative forcing below correlation length λ, i.e. it can move the beads within the range of λ as a one group. Nevertheless, on the length-scale greater than λ these groups move in an uncorrelated manner, so at several sites the chain becomes stretched (at least three beads in line). In the following moment, the spatially correlated noise imposes a new pattern of forces and it is probable that the stretched fragments are now moved as a one entity, while the new frustrated sites are generated. This process leads to the accumulation of linearized fragments and, globally, to the chain unfolding. One can also notice that the reduction in the relative forcing at the length-scale below λ hinders the relaxation processes.

The methodology applied in this paper provides us insight into the statistics describing the chain. This will become important in the context of next paper in which we are interested in the statistics of long fragments.

5.4 Non-Gaussian polymers described by alpha-stable chain statistics: model, applications and effective interactions in binary mixtures

In the last paper included in this thesis we apply the tools developed in the previous articles to introduce the model of non-Gaussian polymeric chain and its applications to the on-surface separation.

The Gaussian chain is the elementary model of a polymer, in which the geometry of a chain is equivalent to the trajectory of a Brownian particle. This model is based on the Gaussian statistics, which makes it possible to calculate an

entire hierarchy of analytical results. In particular, this includes the distribution of segments around the mass center of the chain, the coarse-grained interaction potential between two chains and the condition for spinodal separation in binary mixtures. Most of these results are obtained thanks to the fact that the Gaussian distribution is stable.

In this paper we propose to extend the approach known from the Gaussian chain theory to the wider class of alpha-stable distributions. In this case, the geometry of a chain can be interpreted as a result of diffusion including Levy flights and the relevant statistics have the asymptotic form of a power-law. Thanks to the alpha-stability we are able to recreate the results listed in the previous paragraph, obtaining the analytical formulas which are closed-form in the Fourier space. Most notably, we predict the generalized spinodal decomposition condition:

$$\tilde{\epsilon} > \left(\frac{4g^{\alpha}}{(1+g^{\alpha})^2} \right)^{D/(2\alpha)} \tag{32}$$

where α is the characteristic exponent of the distribution, D is the system dimensionality, g is the ratio of gyration radii and $\tilde{\epsilon}$ is the common energy scale of particle interactions. This result is calculated with the aid of formula (30), which is particularly suitable to handle interactions characterized by a well-defined Fourier transform. For $\alpha = 2$ and $D = 3$ the generalized condition becomes the spinodal decomposition condition for Gaussian particles, which can be found in literature [51, 52].

While the idea of alpha-stable polymeric chains might seem impractical, a few physical situations in which this model is relevant, are discussed in the article. In particular, we provide our simulations of polymeric chain under the spatially correlated noise, as one example. The simulations are performed in the same manner as in [A2], but we replace the exponential correlation function with the power-law function. Using the methodology from [A3], we analyze the distribution of n-segment long linearized fragments to show the effect of spatial correlations on the chain. However, in this case we are explicitly interested in the very long (up to 50 segments) linearized fragments. The distribution widens

due to the unfolding effect [A2] and gradually approaches a shape that can be modeled with a heavy-tailed alpha-stable distributions.

Another context is provided by the process of polymer adsorption. As discussed by Bouchad and Daoud [53], the radius of polymeric chain in the direction parallel to the surface can be modeled with random walk and it is dependent on the strength of adsorption. In the strong adsorption limit this radius is governed by the Gaussian statistics. However, in the weak adsorption limit, this distribution becomes of a power-law type, with characteristic exponent $\alpha = 1$. This behavior can be conveniently modeled by an alpha-stable distribution.

In the final part of our article, we analyze the separation in binary mixture of polymers, considering 'on surface' versus 'in the bulk' separation. The two species of particles can differ both in the number of segments and in their persistence length. Knowing that the statistical characteristics of adsorbed polymers ($D = 2$, $\alpha = 1$ or $\alpha = 2$) are different from the case of freely floating particles (purely Gaussian case, $D = 3$, $\alpha = 2$), we compare the generalized spinodal decomposition condition for both situations. In the case of strong adsorption limit, three scenarios are possible. These are: (a) homogeneous mixing in both phases, (b) simultaneous separation in the bulk and on the surface and (c) separation on the surface coexisting with homogeneous solution. In the weak adsorption limit these three scenarios occur for slightly different parameters, but there is also one additional scenario. Namely, it is possible that there occurs (d) demixing in the bulk, while the coverage on the surface is still homogeneous.

In summary, the theoretical concept of non-Gaussian polymers leads to the practical problem of surface coverage. This issue is important from both experimental and industrial point of view. Our model provides an insight into the entropic aspect of phase separation. One should remember, however, that this picture can be strongly modified by the properties of a surface and the inclusion of an adsorption mechanism.

6 Final remarks

In this thesis, the spatially correlated phenomena have been discussed, with emphasis on their formal origin and their impact on the behavior of a system. Spatial correlations are related to the multicomponent mixtures and to the problem of effective interactions. The new, analytical theory of effective interactions is proposed and a formal link between spatial correlations and effective interactions is established. The proposed theory proves itself as a versatile tool, efficient in the modeling of both ionic and polymeric systems. It also provides a convenient framework for the analysis of molecular systems with new interaction types, such as non-Gaussian polymers, and provides an insight into the spinodal decomposition of their mixtures. The influence of spatial correlations on the dynamics of a polymeric chain is also investigated in this thesis. Although restricted to a single model system, our results indicate that spatial correlations can significantly affect the system, leading to a quantitatively new behavior, e.g. spontaneous unfolding. While the presented approach is still not directly applicable to the highly non-equilibrium systems, it forms a foundation for further development. In particular, the analytical theory of effective interactions could be further applied to the high level modeling of complex bio-molecular systems such as membranes, chromatin etc., provided that adequate models of microscopic interactions could be established.

A few unexplored areas open in the context of this thesis. One problem is the more precise treatment of effective interactions, in order to include temperature and density effects. While the presented theory seems to be a reasonable starting point, some vital modifications are still necessary to obtain even wider applicability and firmer foundation for our results. Especially, the mechanism of phase transitions should be incorporated into our approach. Another interesting problem is the formal derivation of Generalized Langeving Equations with spatially correlated noise. While the link between statistical mechanics and the spatial correlations in the stochastic force has been signalized, the problem of friction in such systems is an open challenge. In the light of our findings,

the theory of such Langevin equations appears as an attractive field of future research, providing a further insight into the dynamics of self-organization.

References

[A1] M. Majka, P.F. Góra, Phys. Rev. E, 90, 3, 032303 (2014)

[A2] M. Majka, P.F. Góra, Phys. Rev. E, 86, 5, 051122 (2012)

[A3] M. Majka, P.F. Góra Acta Phys. Pol. B, 44, 5, 1099 (2013)

[A4] M. Majka, P.F. Góra, Phys. Rev. E, 91, 5, 052602 (2015)

[1] P. W. Anderson, Science, 177, 4047, 393 (1972)

[2] B. Huang, M. Bates, X. Zhuang, Annu. Rev. Biochem., 78, 993 (2009)

[3] D. G. Grier, Nature (London) 424, 810 (2003)

[4] R. Metzler, J. Klafter, Phys. Rep., 339, 1, 1 (2000)

[5] I. M. Tolić-Nørrelykke, E. L. Munteanu, G. Thon, Lene Oddershede and Kirstine Berg-Sørensen, Phys. Rev. Lett., 93, 7, 078102 (2004)

[6] M. Weiss, M. Elsner, F. Kartberg, T. Nilsson, Biophys. J, 87, 5, 3518 (2004)

[7] J. H. Jeon, V. Tejedor, S. Burov, E. Barkai, C. Selhuber-Unkel, K. Berg-Sørensen, L. Oddershede and R. Metzler, Phys. Rev. Lett., 106, 4, 048103 (2011)

[8] M. Weiss, H. Hashimoto, T. Nilsson, Biophys. J., 84, 6, 4043 (2003)

[9] M. J. Skaug, R. Faller and M. L. Longo, J. Phys. Chem., 134, 215101 (2011)

[10] K. Burnecki, E. Kepten, J. Janczura, I. Bronshtein, Y. Garini, A. Weron, Biophys. J., 103, 9, 1839 (2012)

[11] S. C. Kou, Ann. Appl. Stat. 2, 501 (2008)

[12] T. Kalwarczyk, N. Ziębacz, A. Bielejewska, E. Zaboklicka, K. Koynov, J. Szymański, A. Wilk, A. Patkowski, J. Gapiński, H. J. Butt and R. Hołyst, Nano Lett., 11, 5, 2157 (2011)

[13] J. Szymański, A. Patkowski, A. Wilk, P. Garstecki and R. Hołyst , J. Phys. Chem. B, 110, 51, 25593 (2006)

[14] S. Ganguly, L. S. Williams, I. M. Palacios and R. E. Goldstein, PNAS, 109, 38, 15109 (2012)

[15] M. Guo, A. J. Ehrlicher, M. H. Jensen, M. Renz, J. R. Moore, R. D. Goldman, J. Lippincott-Schwartz, F. C. Mackintosh and D. A. Weitz, Cell, 158, 4, 822 (2014)

[16] R. Piazza, J. Cryst. Growth, 196, 2, 415 (1999)

[17] G. Foffi, G. D. McCullagh, A. Lawlor, E. Zaccarelli, and K. A. Dawson, Phys. Rev. E, 65, 3, 031407 (2002)

[18] H. Dietsch, V. Malik, M. Reufer, C. Dagallier, A. Shalkevich, M. Saric, T. Gibaud, F. Cardinaux, F. Scheffold, A. Stradner, P. Schurtenberger, Chimia, 62, 805 (2008)

[19] C. N. Likos, Phys. Rep., 348, 267 (2001)

[20] H. N. W. Lekkerkerker, R. Tuinier, *Colloids and the Depletion Interaction* (Springer, London, 2011)

[21] S. Asakura, F. Oosawa, J. Polym. Sci., 33, 183 (1958)

[22] S. Asakura, F. Oosawa, J. Polym. Sci., 22, 1255 (1954)

[23] A. Vrij, Pure Appl. Chem., 48, 471 (1976)

[24] R. Kubo, M. Toda, and N. Hashitsume, *Statistical Mechanics I* (Springer, Berlin, 1985).

[25] M. Dijkstra, R. van Roij, R. Evans, Phys. Rev. E, 59, 5744 (1999)

[26] M. Dijkstra, J. M. Brader, J. Phys.: Condens. Matter, 11, 10079 (1999)

[27] J.P. Hansen, I.R. McDonald, *Theory of Simple Liquids*(Elsevier Academic Press, London,2006)

[28] V. Heinonen, A. Mijailovi, C. V. Achim, T. Ala-Nissila, R. E. Rozas, J. Horbach, and H. Löwen, J. Chem. Phys. 138, 044705 (2013)

[29] A. A. Louis, E. Allahyarov, H. Löwen, R. Roth, Phys. Rev. E, 65, 061407 (2002)

[30] P. G. Bolhuis, A. A. Louis, J. P. Hansen, and E. J. Meijer, J. Chem. Phys. 114, 4296 (2001)

[31] D. Marenduzzo, K. Finan, P. R. Cook, J. Cell. Biol., 175, 5 (2006)

[32] K. Richter, M. Nessling, P. Lichter, BBA-Mol. Cell Res., 11, 1783, 2100 (2008)

[33] R. Hancock, Semin. Cell Dev. Biol., 18, 5, 668 (2007)

[34] C. F. Lee, C. P. Brangwynne, J. Gharakhani, A. A. Hyman and F. Jülicher, Phys. Rev. Lett., 111, 8, 088101 (2013)

[35] J. J. Binney et al., *The Theory of Critical Phenomena* (Oxford University Press, Oxford, 1992).

[36] L. Berthier, G. Biroli, Rev. Mod. Phys., 83, 2, 587 (2011)

[37] P. N. Pusey, W. van Megen, Phys. Rev. Lett. 59, 18, 2083 (1987)

[38] E. R. Weeks, J. C. Crocker, D. A. Weitz *J. Phys.: Condens. Matter*, 19, 205131 (2007)

[39] C. Dalle-Ferrier, C. Thibierge, C. Alba-Simionesco, L. Berthier, G. Biroli, J. P. Bouchaud, F. Ladieu, D. L'Hôte, G. Tarjus, *Phys. Rev. E*, 76, 041510 (2007)

[40] M. Mosayebi, E. Del Gado, P. Ilg, H. C. Öttinger *Phys. Rev. Lett.*, 104, 205704 (2010)

[41] E. Donth, H. Huth, M. Beiner, *J. Phys.: Condens. Matter*, 13, L451 (2001)

[42] B. Doliwa, A. Heuer, *Phys. Rev. E*, vol. 61, 6 (2000)

[43] C. Donati, S. C. Glotzer, P. H. Poole, W. Kob, S. J. Plimpton, *Phys. Rev. E*, vol. 60, **3**, 3107 (1999)

[44] A. C. Mitus, A. Z. Patashinski, A. Patrykiejew, A. Sokolowski, *Phys. Rev. B*, **66**, 184202 (2002)

[45] F. Sagués, J. M. Sancho, J. García-Ojalvo, *Rev. Mod. Phys.*, **79**, 829 (2007)

[46] D. N. Zubariew, *Termodynamika statystyczna*, PWN, Warszawa (1974)

[47] A. Zweil et all., *Physical Biology: From Atoms to Medicine*(Imperial College Press, London, 2008)

[48] R. Balescu, Chaos Soliton. Fract., 34, 1, 62 (2007)

[49] V. V. Belyi, J. Phys.: Conf. Ser. 11, 61 (2005)

[50] P. S. Burada, G. Schmid, D. Reguera, J. M. Rubi, and P. Hänggi, Phys. Rev. E, 75, 5, 051111 (2007)

[51] A. A. Louis, P. G. Bolhuis, J. P. Hansen, Phys. Rev. E, 62, 6, 7961 (2000)

[52] R. Finken, J. P. Hansen, A. A. Louis, J. Stat. Phys., 110, 3, 1015 (2003)

[53] E. Bouchaud, M. Daoud, J. Phys. A: Math. Gen., 20, 6, 1463 (1987)

Publications

dr hab. P.F.Góra
Wydział Fizyki, Astronomii i Informatyki
Stosowanej UJ
tel. (12) 664 4566
e-mail pawel.gora@uj.edu.pl

Kraków, 18 czerwca 2015

UNIWERSYTET
JAGIELLOŃSKI
W KRAKOWIE

Wydział
Fizyki
Astronomii
i Informatyki
Stosowanej

Oświadczenie o współautorstwie

M. Majka, P.F. Góra, *Analytical theory of effective interactions in binary colloidal systems of soft particles*, Phys. Rev. E, 90, 3, 032303 (2014)

Majka – 90%, Góra – 10%

M. Majka, P.F. Góra, *Polymer unfolding and motion synchronization induced by spatially correlated noise*, Phys. Rev. E, 86, 5, 051122 (2012)

Majka – 85%, Góra – 15%

M. Majka, P.F. Góra, *Reinterpreting polymer unfolding effect induced by spatially correlated noise*, Acta Phys. Pol. B, 44, 5, 1099 (2013)

Majka – 90%, Góra – 10%

M. Majka, P.F. Góra, *Non-Gaussian polymers described by alpha-stable chain statistics: model, effective interactions in binary mixtures and application to onsurface separation*, Phys. Rev. E, 91, 5, 052602 (2015)

Majka – 85%, Góra – 15%

W przypadku wszystkich prac mój (P.F.Góra) udział ograniczał się do sformułowania pierwotnego pomysłu, który potem bywał modyfikowany w trakcie postępu prac, krytycznej analizy kolejnych etapów pracy i współudziału w redakcji ostatecznej wersji publikacji. Wszystkie uzyskane w tych publikacjach wyniki są osiągnięciem pana Macieja Majki.

ul. prof. Stanisława
Łojasiewicza 11
PL 30-348 Kraków
tel. +48(12) 664-48-90
fax +48(12) 664-49-05
e-mail:
wydzial.fais@uj.edu.pl

Analytical theory of effective interactions in binary colloidal systems of soft particles

M. Majka* and P. F. Góra
Marian Smoluchowski Institute of Physics, Jagiellonian University, Reymonta 4, 30-059 Kraków, Poland
(Received 24 July 2013; revised manuscript received 19 May 2014; published 16 September 2014)

While density functional theory with integral equations techniques are very efficient tools in the numerical analysis of complex fluids, analytical insight into the phenomenon of effective interactions is still limited. In this paper, we propose a theory of binary systems that results in a relatively simple analytical expression combining arbitrary microscopic potentials into effective interaction. The derivation is based on translating a many-particle Hamiltonian including particle-depletant and depletant-depletant interactions into the occupation field language, which turns the partition function into multiple Gaussian integrals, regardless of what microscopic potentials are chosen. As a result, we calculate the effective Hamiltonian and discuss when our formula is a dominant contribution to the effective interactions. Our theory allows us to analytically reproduce several important characteristics of systems under scrutiny. In particular, we analyze the following: the effective attraction as a demixing factor in the binary systems of Gaussian particles, the screening of charged spheres by ions, which proves equivalent to Derjaguin-Landau-Verwey-Overbeek (DLVO) theory, effective interactions in the binary mixtures of Yukawa particles, and the system of particles consisting of both a repulsive core and an attractive/repulsive Yukawa interaction tail. For this last case, we reproduce the "attraction-through-repulsion" and "repulsion-through-attraction" effects previously observed in simulations.

DOI: 10.1103/PhysRevE.90.032303 PACS number(s): 82.70.Dd, 89.75.Fb, 61.20.−p

I. INTRODUCTION

Effective interactions are of fundamental interest in the field of soft matter physics [1], especially in colloid studies. Their significance is enormous because they are essential for spontaneous self-organization, and they play a key role in polymer studies [1] as well as gel- and glass-forming research [2,3]. They are also important for molecular biophysics [4] and find multiple applications in nanotechnology [5]. Qualitatively similar phenomena of size separation are also encountered in vibrated granular matter research [6,7].

A comprehensive introduction to the contemporary theories of effective interactions can be found in [1,8,9]. The first successful description of effective interactions dates back to the research of Asakura and Oosawa [10,11], and later on to the work of Vrij [12]. Their approach, which was based on the consideration of excluded volume, is still used today, especially for nonspherical particles (e.g., [13,14]). At the advent of optical tweezers technology [15], effective interactions became accessible for direct measurements [16], which sparked a new interest in the systems for which the Asakura-Oosawa model proved insufficient.

One reason for violating the predictions of the Asakura-Oosawa model is that at high volume fraction packing, the system approaches a glassy transition, experiencing jammed dynamics. This is observed both experimentally [3,17,18] and via simulations [19–21]. On the other hand, systems with nontrivial or long-range interactions can be constructed. This includes charged particles [22], polymer-coated particles interacting via mushroom-like potentials [23], or polymer coils, which behave like soft, Gaussian-profiled particles [24]. The molecular-dynamics simulations for various combinations of repulsions and attractions have also shown that unexpected effects can be encountered, e.g., effective repulsion arising from attractive microscopic potentials or effective attraction induced by repulsive microscopic potentials [25].

A general theory capable of handling these phenomena has been proposed by Dijkstra *et al.* [26]. In their approach, a partition function for the system with arbitrarily chosen particle-depletant and depletant-depletant interaction is systematically expanded in terms of Mayer bond functions [1,8]. While this expansion is exact in principle, it is usually challenging to include high-order terms due to their mathematical form and nonperturbative character. Approximated techniques also exist based on integral equations, closure relations, and utilizing various density correlation functions [1,8]. Both tools have become a standard in the field, allowing the efficient numerical analysis of various systems, e.g., [24,27,28]. However, the analytical form of effective interactions is known only for several model systems (see [9] for review), and similar results for complex fluids are rather scarce (e.g., [29,30]).

While it is notoriously challenging to predict the effective interactions from arbitrary microscopic potentials, a simplified, tough analytical theory could find multiple applications in colloid research, e.g., in high-level solution design or in the context of Langevin dynamics simulation (e.g., [31–34]). In this paper, we propose such a theory, which offers both generality and comprehensible analytical form.

We consider a binary system of spherically symmetric particles with arbitrarily chosen microscopic potentials. In our approach, we introduce the so-called occupation functional (representing a number of particles at every position) and translate the semi-grand-canonical ensemble into the path-integral problem related to this functional. Regardless of microscopic potentials, this method turns the partition function into multiple Gaussian integrals. There are two major advantages of this transformation. On the one hand, we are able to identify and factorize a closed-form formula contributing to

*maciej.majka@uj.edu.pl

effective interactions, which is exact. On the other hand, we can approximate the effective Hamiltonian in order to identify further contributions and propose the criteria under which the exact part is dominant.

In our model, similar to [1] and [26], we consider two distinct species of particles in the D-dimensional volume $\Omega = L^D$. The system has temperature T, and we will denote $\beta = (k_B T)^{-1}$, where k_B is the Boltzmann constant. We will also use h to denote the Planck constant. In the system, there are N_1 particles of the first kind, and we denote the position and momentum of the ith particle with $\mathbf{R}_i$ and $\mathbf{P}_i$, respectively. The microscopic potential between these particles reads $U_{RR}(|\mathbf{R}_i - \mathbf{R}_j|)$, and effective interaction will be derived for this species. The second species, identified as depletant, consists of N_2 particles, which interact via potential $V(|\mathbf{r}_i - \mathbf{r}_j|)$, and their positions and momenta are denoted by $\mathbf{r}_i$ and $\mathbf{p}_i$. We will use the grand-canonical ensemble for depletant particles, so we associate a chemical potential μ with this species. Both types of particles cross-interact via the potential $U(|\mathbf{R}_i - \mathbf{r}_j|)$. The masses of colloid and depletant particles are m_1 and m_2, respectively. The total Hamiltonian of the system in its initial form has three contributions:

$$H_{\text{tot}} = H_{RR} + H_{rR} + H_{rr}, \tag{1}$$

where

$$H_{RR} = \sum_i^{N_1} \frac{\mathbf{P}_i^2}{2m_1} + \frac{1}{2} \sum_{\substack{i,j \\ i \neq j}}^{N_1} U_{RR}(|\mathbf{R}_i - \mathbf{R}_j|), \tag{2}$$

$$H_{rR} = \sum_i^{N_1} \sum_j^{N_2} U(|\mathbf{R}_i - \mathbf{r}_j|), \tag{3}$$

$$H_{rr} = \sum_i^{N_2} \frac{\mathbf{p}_i^2}{2m_2} + \frac{1}{2} \sum_{\substack{i,j \\ i \neq j}}^{N_2} V(|\mathbf{r}_i - \mathbf{r}_j|). \tag{4}$$

Let us introduce a pair of Fourier transforms:

$$\mathcal{U}(k) = \int_\Omega d\mathbf{r}\, e^{i\mathbf{k}\cdot\mathbf{r}} U(r),$$

$$\mathcal{V}(k) = \int_\Omega d\mathbf{r}\, e^{i\mathbf{k}\cdot\mathbf{r}} V(r).$$

We will show that effective interaction between a pair of colloid particles positioned at $\mathbf{R}_i$ and $\mathbf{R}_j$ has the following contribution:

$$U_{\text{eff}}(\mathbf{R}_i - \mathbf{R}_j) = -\frac{1}{(2\pi)^D} \int_{\tilde{\Omega}} d\mathbf{k}\, e^{i\mathbf{k}\cdot(\mathbf{R}_i - \mathbf{R}_j)} \frac{|\mathcal{U}(k)|^2}{\mathcal{V}(k)}. \tag{5}$$

This result is exact and sufficient to analytically reproduce many important characteristics of binary mixtures. This includes demixing of Gaussian particles, screening of charge in the system of charged spheres and ions, and "attraction-through-repulsion"/"repulsion-through-attraction" effects for particles characterized by a Yukawa interaction tail and a repulsive core. All of these effects were observed previously in simulations or described with various theories, but our approach provides a common framework for all of them, and our predictions are at least in qualitative agreement with existing results. By calculating the approximated form of the effective Hamiltonian, we will also show that there are other sources of effective interactions, and we will propose a criterion under which $U_{\text{eff}}(\mathbf{R}_i - \mathbf{R}_j)$ is dominant.

The paper is organized as follows: In Secs. II A–II C, we introduce our framework of occupation functional, in Sec. II D the formula for $U_{\text{eff}}(\mathbf{R}_i - \mathbf{R}_j)$ is derived, in Sec. II E the approximated partition functions is calculated, and Sec. II F concludes with the effective Hamiltonian and the accuracy of our model. The assumptions and caveats regarding the derivation are summarized in Sec. II G. Section III contains examples of applications for our theory. These includes the binary mixtures of Gaussian particles (Sec. III B), charged spheres in the presence of ions (Sec. III C), mixtures of Yukawa particles (Sec. III D), and mixtures of Yukawa particles with impenetrable cores (Sec. III E).

II. MODEL DERIVATION

A. System partition function

To begin the derivation of our model, we have to specify the partition function of the system. Our aim is to apply a new way to integrate out the depletant degrees of freedom. As a result, the effective Hamiltonian will be derived from the remaining expression. The initial Hamiltonian H_{tot} is defined by Eqs. (1)–(4). For this Hamiltonian, we introduce the mixed ensemble Ξ_{tot}, which is the grand-canonical ensemble for the depletant and the canonical ensemble for colloid particles. Written in standard space-momentum coordinates $\{\mathbf{P}_i, \mathbf{R}_i\}_{N_1}$ and $\{\mathbf{p}_i, \mathbf{r}_i\}_{N_2}$, the mixed ensemble can be regrouped in the following manner:

$$\Xi_{\text{tot}} = \prod_i^{N_1} \int d\mathbf{P}_i d\mathbf{R}_i \frac{\exp\left(-\beta(H_{RR} - \frac{1}{\beta}\ln \Xi)\right)}{N_1! h^{DN_1}}, \tag{6}$$

where

$$H_{\text{eff}} = H_{RR} - \frac{1}{\beta} \ln \Xi \tag{7}$$

is the effective Hamiltonian for the first species of particles, and

$$\Xi = \sum_{N_2=0}^{+\infty} \int d\mathbf{p}_i d\mathbf{r}_i \frac{\exp[-\beta(H_{rR} + H_{rr} - \mu N_2)]}{N_2! h^{DN_2}}. \tag{8}$$

According to [1], the term

$$U_{\text{eff}}^{\text{tot}} = -\frac{1}{\beta} \ln \Xi \tag{9}$$

acts as an additional potential, and this is the source of effective interactions. Therefore, calculating Ξ is of central interest for us.

First, it is feasible to rewrite H_{rr} in the following manner:

$$H_{rr} = \sum_i^{N_2} \frac{\mathbf{p}_i^2}{2m_2} + \frac{1}{2} \sum_{i,j}^{N_2} V(|\mathbf{r}_i - \mathbf{r}_j|) - \frac{N_2}{2} V(0), \tag{10}$$

which explicitly introduces $V(0)$. Another step is to integrate out depletant momenta $\mathbf{p}_j$, which allows us to rearrange Ξ into

the form

$$\Xi = \sum_{N_2} \frac{1}{L^{DN_2}} \prod_{j}^{N_2} \int d\mathbf{r}_j \frac{\exp[-\beta(\mathcal{H} - \tilde{\mu}N_2)]}{\Gamma(N_2+1)}, \tag{11}$$

where $\Gamma(\cdots)$ is the Euler Gamma function replacing the factorial, and

$$\mathcal{H} = \frac{1}{2}\sum_{i,j}^{N_2} V(|\mathbf{r}_i - \mathbf{r}_j|) + \sum_{i}^{N_1}\sum_{j}^{N_2} U(|\mathbf{R}_i - \mathbf{r}_j|), \tag{12}$$

$$\tilde{\mu} = \mu + \frac{1}{2}V(0) + \frac{D}{2\beta}\ln\frac{2\pi L^2 m_2}{\beta h^2}. \tag{13}$$

The partition function Ξ given in the form (11) is ready to be translated into the occupation field representation.

B. Occupation field representation

Let us consider a scalar field that assigns the number of depletant particles $\alpha(\mathbf{r})$ at certain position $\mathbf{r}$ to this position. The total number of depletant particles in the system reads

$$N_2 = \int_\Omega d\mathbf{r}\alpha(\mathbf{r}). \tag{14}$$

If $\alpha(\mathbf{r})$ particles occupy a position $\mathbf{r}$ and $\alpha(\mathbf{r}')$ particles occupy position $\mathbf{r}'$, then the energy of interaction between the sites $\mathbf{r}$ and $\mathbf{r}'$ is equal to $\alpha(\mathbf{r})\alpha(\mathbf{r}')V(|\mathbf{r}-\mathbf{r}'|)$. Therefore, we can use $\alpha(\mathbf{r})$ to translate interaction terms in the following manner:

$$\sum_{i,j}^{N_2} V(|\mathbf{r}_i - \mathbf{r}_j|) = \iint_\Omega d\mathbf{r}\, d\mathbf{r}'\alpha(\mathbf{r})\alpha(\mathbf{r}')V(|\mathbf{r}-\mathbf{r}'|), \tag{15}$$

$$\sum_{i}^{N_1}\sum_{j}^{N_2} U(|\mathbf{R}_i - \mathbf{r}_j|) = \sum_{i}^{N_1}\int_\Omega d\mathbf{r}\,\alpha(\mathbf{r})U(|\mathbf{R}_i - \mathbf{r}|). \tag{16}$$

In principle, $\alpha(\mathbf{r})$ takes only discrete values $0,1,2,\ldots$, but we will allow it to vary continuously.

The formulas (14)–(16) suggest that we can understand $\mathcal{H}$ and N_2 as the functionals of $\alpha(\mathbf{r})$. In turn, we could replace the multiple integrations in (11) with a functional integral with respect to $\alpha(\mathbf{r})$, namely

$$\Xi \to \int \mathcal{D}[\alpha]\frac{\exp[-\beta(\mathcal{H} - \tilde{\mu}N_2)]}{\Gamma(N_2+1)}. \tag{17}$$

The path integral can be specified as the integral with respect to the Fourier series coefficients of $\alpha(\mathbf{r})$ [35]:

$$\alpha(\mathbf{r}) = \frac{1}{\Omega}\sum_{\mathbf{n}\in Z^D} a_n e^{i\frac{2\pi}{L}\mathbf{n}\cdot\mathbf{r}}. \tag{18}$$

Here $\mathbf{n}$ is a D-dimensional vector, whose components vary discretely from $-\infty$ to $+\infty$. Therefore, we shall denote the set of index vectors $\mathbf{n}$ with Z^D. The Fourier series expansion of $\alpha(\mathbf{r})$ requires us to assume periodic boundary conditions. Since the field $\alpha(\mathbf{r})$ is real, the symmetry $a_{-\mathbf{n}} = a_{\mathbf{n}}^*$ is also required. The a_0 coefficient has a special interpretation:

$$a_0 = \int_\Omega d\mathbf{r}\,\alpha(\mathbf{r}) = N_2. \tag{19}$$

Additionally, we have to assume that potentials $U(\mathbf{r})$ and $V(\mathbf{r})$ are also periodic over length L, which should be of little influence if the range of those potentials is much shorter than L. If so, then the Fourier series expansion (18) simplifies the interaction terms:

$$\iint_\Omega d\mathbf{r}\, d\mathbf{r}'\alpha(\mathbf{r})\alpha(\mathbf{r}')V(|\mathbf{r}-\mathbf{r}'|) = \frac{1}{\Omega}\sum_{\mathbf{n}\in Z^D}|a_\mathbf{n}|^2\mathcal{V}_\mathbf{n}, \tag{20}$$

$$\sum_{i}^{N_1}\int_\Omega d\mathbf{r}\,\alpha(\mathbf{r})U(|\mathbf{R}_i - \mathbf{r}|) = \frac{1}{\Omega}\sum_{\mathbf{n}\in Z^D} a_\mathbf{n}\sum_i \mathcal{U}_\mathbf{n}^{(i)}, \tag{21}$$

where

$$\mathcal{V}_\mathbf{n} = \int_\Omega d\mathbf{r}\, e^{i\frac{2\pi}{L}\mathbf{n}\cdot\mathbf{r}}V(r), \tag{22}$$

$$\mathcal{U}_\mathbf{n}^{(i)} = \int_\Omega d\mathbf{r}\, e^{i\frac{2\pi}{L}\mathbf{n}\cdot\mathbf{r}}U(|\mathbf{R}_i - \mathbf{r}|). \tag{23}$$

From these formulas, it follows that

$$\mathcal{H} - \tilde{\mu}N_2 = \frac{1}{2\Omega}\sum_{\mathbf{n}\in Z^D}|a_\mathbf{n}|^2\mathcal{V}_\mathbf{n} + \frac{1}{\Omega}\sum_{\mathbf{n}\in Z^D} a_\mathbf{n}\left(\sum_i \mathcal{U}_\mathbf{n}^{(i)} - \tilde{\mu}\Omega\delta_{\mathbf{n},0}\right), \tag{24}$$

which can be further rearranged into

$$\mathcal{H} - \tilde{\mu}N_2 = \sum_{\mathbf{n}\in Z^D}\frac{\mathcal{V}_\mathbf{n}}{2\Omega}\left|a_\mathbf{n} + \frac{\sum_i \mathcal{U}_{-\mathbf{n}}^{(i)} - \tilde{\mu}\Omega\delta_{\mathbf{n},0}}{\mathcal{V}_\mathbf{n}}\right|^2 - \sum_{\mathbf{n}\in Z^D}\frac{\left|\sum_i \mathcal{U}_\mathbf{n}^{(i)} - \tilde{\mu}\Omega\delta_{\mathbf{n},0}\right|^2}{2\Omega\mathcal{V}_\mathbf{n}}, \tag{25}$$

and finally the path integral is specified as

$$\Xi = \prod_{\mathbf{n}\in Z^D}\int da_\mathbf{n}\frac{\exp[-\beta(\mathcal{H} - \tilde{\mu}N_2)]}{\Gamma(a_0+1)}. \tag{26}$$

In the above formula, we intentionally omit writing the limits of integration since they need to be discussed in greater detail in the following section.

C. Non-negative fields from Fourier modes

In principle, the occupation field $\alpha(\mathbf{r})$ should be non-negative. Unfortunately, a field constructed according to (18) from the arbitrarily chosen values of $a_\mathbf{n}$ does not necessarily meet this requirement. However, it is always true that $a_0 \geqslant 0$, since it is the number of depletant particles. Therefore, for any values of $a_{\mathbf{n}\neq 0}$ we can choose a_0 such that $\alpha(\mathbf{r})$ is non-negative. More precisely, we can write

$$\tilde{\alpha}(\mathbf{r}) = \sum_{\mathbf{n}\in Z^D\setminus 0} a_\mathbf{n} e^{i\frac{2\pi}{L}\mathbf{n}\cdot\mathbf{r}}, \tag{27}$$

where $\setminus 0$ indicates the exclusion of a_0. $\tilde{\alpha}(\mathbf{r})$ is a real function and, necessarily,

$$\int_\Omega d\mathbf{r}\,\tilde{\alpha}(\mathbf{r}) = 0. \tag{28}$$

This property means that $\tilde{\alpha}(\mathbf{r})$ has to take both negative and non-negative values for different $\mathbf{r}$, so integral (28) is 0. Therefore, there must exist a global minimum of $\tilde{\alpha}(\mathbf{r})$, and $\tilde{\alpha}(\mathbf{r})$ is negative in this minimum. Finally, for

$$a_0 \geqslant M = -\min_{\mathbf{r}}[\tilde{\alpha}(\mathbf{r})], \tag{29}$$

the occupation field $\alpha(\mathbf{r})$ is non-negative. Here, we denote the global minimum of $\tilde{\alpha}(\mathbf{r})$ with respect to $\mathbf{r}$ by $\min_{\mathbf{r}}[\tilde{\alpha}(\mathbf{r})]$. The limit M can be also rewritten in the following form:

$$M = -\sum_{\mathbf{n}\in Z^D\setminus 0} a_{\mathbf{n}} e^{i\frac{2\pi}{L}\mathbf{n}\cdot\mathbf{r}(a_{\mathbf{n}})}, \tag{30}$$

where $\mathbf{r}(a_{\mathbf{n}})$ is the position of the global minimum as a function of $a_{\mathbf{n}}$. Formally, $\mathbf{r}(a_{\mathbf{n}})$ can be determined from the equation

$$\nabla_{\mathbf{r}} \sum_{\mathbf{n}\in Z^D\setminus 0} a_{\mathbf{n}} e^{i\frac{2\pi}{L}\mathbf{n}\cdot\mathbf{r}} = 0. \tag{31}$$

Concluding this section, we can choose the limits of integration for $a_{\mathbf{n}\neq 0}$ as $\pm\infty$ and the limits for a_0 as $[M, +\infty)$. However, M is now a function of $a_{\mathbf{n}\neq 0}$, which fixes the order of integrals in (26). Let us combine (25) and (26) to write Ξ in the following form:

$$\Xi = e^{-\beta\Phi} \prod_{\mathbf{n}\in Z^D\setminus 0} I_{\mathbf{n}} I_0(M), \tag{32}$$

in which

$$\Phi = -\sum_{\mathbf{n}\in Z^D} \frac{\left|\sum_i \mathcal{U}_{\mathbf{n}}^{(i)} - \tilde{\mu}\Omega\delta_{\mathbf{n},0}\right|^2}{2\Omega\mathcal{V}_{\mathbf{n}}} \tag{33}$$

and

$$I_{\mathbf{n}\neq 0} = \int_{-\infty}^{+\infty} da_{\mathbf{n}} \exp\left(-\frac{\beta\mathcal{V}_{\mathbf{n}}}{2\Omega}\left|a_{\mathbf{n}} + \frac{\sum_i \mathcal{U}_{-\mathbf{n}}^{(i)}}{\mathcal{V}_{\mathbf{n}}}\right|^2\right), \tag{34}$$

$$I_0(M) = \int_M^{+\infty} da_0 \frac{\exp\left(-\frac{\beta\mathcal{V}_0}{2\Omega}\left|a_0 + \frac{\sum_i \mathcal{U}_0^{(i)} - \tilde{\mu}\Omega}{\mathcal{V}_0}\right|^2\right)}{\Gamma(a_0+1)}. \tag{35}$$

For the sake of more compact notation, we will denote

$$c_{\mathbf{n}} = \frac{\sum_i \mathcal{U}_{-\mathbf{n}}^{(i)} - \tilde{\mu}\Omega\delta_{0\mathbf{n}}}{\mathcal{V}_{\mathbf{n}}}, \quad \gamma_{\mathbf{n}} = \frac{\beta\mathcal{V}_{\mathbf{n}}}{2\Omega}. \tag{36}$$

D. The effective interaction

In this section, we will identify the exact part of effective interactions. We substitute now (32) into the formula for $U_{\text{eff}}^{\text{tot}}$, namely

$$U_{\text{eff}}^{\text{tot}} = -\frac{1}{\beta}\ln\Xi = \Phi - \frac{1}{\beta}\ln\left(\prod_{\mathbf{n}\in Z^D\setminus 0} I_{\mathbf{n}} I_0(M)\right). \tag{37}$$

We will show that Φ gives rise to the effective interaction $U_{\text{eff}}(|\mathbf{R}_i - \mathbf{R}_j|)$. Expanding (33) and taking advantage of the Kronecker δ, we arrive at

$$\Phi = -\sum_{i\neq j}\sum_{\mathbf{n}\in Z^D} \frac{\mathcal{U}_{\mathbf{n}}^{(i)}\mathcal{U}_{-\mathbf{n}}^{(j)}}{2\Omega\mathcal{V}_{\mathbf{n}}} - \sum_i \sum_{\mathbf{n}\in Z^D} \frac{\left|\mathcal{U}_{\mathbf{n}}^{(i)}\right|^2}{2\Omega\mathcal{V}_{\mathbf{n}}} + \frac{2\tilde{\mu}\sum_i \mathcal{U}_0^{(i)} - \tilde{\mu}^2\Omega}{2\mathcal{V}_0}. \tag{38}$$

To process the three terms in Φ, one can notice that

$$\begin{aligned}\mathcal{U}_{\mathbf{n}}^{(i)} &= \int_\Omega d\mathbf{r}\, e^{i\frac{2\pi}{L}\mathbf{n}\cdot\mathbf{r}} U(|\mathbf{R}_i - \mathbf{r}|) \\ &= e^{i\frac{2\pi}{L}\mathbf{n}\cdot\mathbf{R}_i} \int_{\Omega_i} d\mathbf{r}\, e^{i\frac{2\pi}{L}\mathbf{n}\cdot\mathbf{r}} U(r) \\ &= e^{i\frac{2\pi}{L}\mathbf{n}\cdot\mathbf{R}_i} \mathcal{U}\left(\frac{2\pi}{L}\mathbf{n}\right).\end{aligned} \tag{39}$$

Here Ω_i is a volume shifted by $\mathbf{R}_i$. In the continuous limit of huge volume $L \to +\infty$, we can substitute $\mathbf{k} = \frac{2\pi}{L}\mathbf{n}$, so

$$\mathcal{U}_{\mathbf{n}}^{(i)} \to e^{i\mathbf{k}\cdot\mathbf{R}_i}\mathcal{U}(\mathbf{k}). \tag{40}$$

Further, $\sum_{\mathbf{n}} \to \frac{\Omega}{(2\pi)^D}\int_{\tilde{\Omega}}$ and $\Omega_i \to \Omega$, so $\mathcal{U}(\mathbf{k})$ becomes a Fourier transform of $U(r)$. Similar considerations allow us to transform $\mathcal{V}_{\mathbf{n}}$ into $\mathcal{V}(\mathbf{k})$. Finally, in the continuous limit,

$$\begin{aligned}-\sum_{\mathbf{n}\in Z^D} \frac{\mathcal{U}_{\mathbf{n}}^{(i)}\mathcal{U}_{-\mathbf{n}}^{(j)}}{\Omega\mathcal{V}_{\mathbf{n}}} &\to -\frac{1}{(2\pi)^D}\int_{\tilde{\Omega}} d\mathbf{k}\, e^{i\mathbf{k}\cdot(\mathbf{R}_i - \mathbf{R}_j)} \frac{|\mathcal{U}(\mathbf{k})|^2}{\mathcal{V}(\mathbf{k})} \\ &= U_{\text{eff}}(\mathbf{R}_i - \mathbf{R}_i).\end{aligned} \tag{41}$$

Formula (41) constitutes the main result of this paper, which is the expression for the effective interaction between two particles. Having established this result, it follows that

$$-\sum_i \sum_{\mathbf{n}\in Z^D} \frac{\left|\mathcal{U}_{\mathbf{n}}^{(i)}\right|^2}{\Omega\mathcal{V}_{\mathbf{n}}} \to \sum_i U_{\text{eff}}(0) = N_1 U_{\text{eff}}(0) \tag{42}$$

and

$$\frac{2\tilde{\mu}\sum_i \mathcal{U}_0^{(i)} - \tilde{\mu}^2\Omega}{2\mathcal{V}_0} \to \frac{2\tilde{\mu}N_1\mathcal{U}(0) - \Omega\tilde{\mu}^2}{2\mathcal{V}(0)}. \tag{43}$$

In summary, we conclude that the general form of Φ reads

$$\Phi = \frac{1}{2}\sum_{i\neq j}^{N_1} U_{\text{eff}}(\mathbf{R}_i - \mathbf{R}_j) + \frac{N_1}{2}U_{\text{eff}}(0) + \frac{2\tilde{\mu}N_1\mathcal{U}(0) - \Omega\tilde{\mu}^2}{2\mathcal{V}(0)}. \tag{44}$$

Immediately one can recognize that we have obtained the effective interaction between every pair of particles, which is expected for the multiparticle system. This result is exact up to the approximations required to introduce the occupation number functional.

E. Approximated calculation of $\ln\prod I_{\mathbf{n}} I_0(M)$

Having found Φ, we would also like to calculate the $\prod I_{\mathbf{n}} I_0(M)$ to obtain the effective Hamiltonian. However, this can be completed only via certain approximations.

First of all, let us recall that, according to (35), $I_0(M)$ reads

$$I_0(M) = \int_M^{+\infty} da_0 \frac{e^{-\gamma_0(a_0+c_0)^2}}{\Gamma(a_0+1)}.$$

In principle M is non-negative, and for such an argument $I_0(M)$ is a decreasing function, reaching asymptotically 0 in the limit of $M \to +\infty$. $I_0(M)$ can have a well-defined kink at $M = -c_0$, provided that $c_0 < 0$ and $\gamma_0 \gg 1$. We will

approximate now $I_0(M)$ up to first order in the logarithmic derivative, namely

$$I_0(M) = \exp\left(\ln I_0(0) + \frac{I_0'(0)}{I_0(0)}M + \cdots\right) \simeq I_0(0)e^{\frac{I_0'(0)}{I_0(0)}M}. \tag{45}$$

This is accurate provided that there is no kink for $M \in [0, +\infty)$, which requires that $c_0 > 0$. For more compact notation, we denote

$$\mathcal{I}_0 = \frac{I_0'(0)}{I_0(0)}. \tag{46}$$

Under approximation (45) and using expansion (30) for M, we can write

$$\prod_{\mathbf{n}\in Z^D\setminus 0} I_{\mathbf{n}} I_0(M) \approx \prod_{\mathbf{n}\in Z^D\setminus 0} \int_{-\infty}^{+\infty} da_{\mathbf{n}} I_0(0) \times \exp\left(-\gamma_{\mathbf{n}}|a_{\mathbf{n}} + c_{\mathbf{n}}|^2 - \mathcal{I}_0 a_{\mathbf{n}} e^{i\frac{2\pi}{L}\mathbf{n}\cdot\mathbf{r}(a_{\mathbf{n}})}\right). \tag{47}$$

This expression is still dependent on $\mathbf{r}(a_{\mathbf{n}})$, which is an implicit function of $a_{\mathbf{n}}$. To proceed, we will approximate $\mathbf{r}(a_{\mathbf{n}})$ by a constant value. One can notice that the quadratic term in (47) has the extreme value for $a_{\mathbf{n}} = -c_{\mathbf{n}}$, and we expect that the integral (47) is dominated by the contribution from $a_{\mathbf{n}} \approx -c_{\mathbf{n}}$. Let us transform the integration variables,

$$\Delta a_{\mathbf{n}} = a_{\mathbf{n}} + c_{\mathbf{n}}, \tag{48}$$

and approximate M in the vicinity of $c_{\mathbf{n}}$ up to first order in $\Delta a_{\mathbf{n}}$:

$$-\sum_{\mathbf{n}\in Z^D\setminus 0} a_{\mathbf{n}} e^{i\frac{2\pi}{L}\mathbf{n}\cdot\mathbf{r}(a_{\mathbf{n}})} \simeq \sum_{\mathbf{n}\in Z^D\setminus 0} (c_{\mathbf{n}} - \Delta a_{\mathbf{n}}) e^{i\frac{2\pi}{L}\mathbf{n}\cdot\mathbf{r}(c_{\mathbf{n}})}. \tag{49}$$

Now, (47) turns into

$$\prod_{\mathbf{n}\in Z^D\setminus 0} I_{\mathbf{n}} I_0(M) \approx \prod_{\mathbf{n}\in Z^D\setminus 0} \exp\left(\mathcal{I}_0 c_{\mathbf{n}} e^{i\frac{2\pi}{L}\mathbf{n}\cdot\mathbf{r}(c_{\mathbf{n}})}\right) I_0(0) \times \int_{-\infty}^{+\infty} d\Delta a_{\mathbf{n}} \exp\left(-\gamma_{\mathbf{n}}|\Delta a_{\mathbf{n}}|^2 - \mathcal{I}_0 \Delta a_{\mathbf{n}} e^{i\frac{2\pi}{L}\mathbf{n}\cdot\mathbf{r}(c_{\mathbf{n}})}\right). \tag{50}$$

We can rearrange the quadratic expression in the exponent of (50),

$$\sum_{\mathbf{n}\in Z^D\setminus 0} \gamma_{\mathbf{n}}|\Delta a_{\mathbf{n}}|^2 + \mathcal{I}_0 \sum_{\mathbf{n}\in Z^D\setminus 0} \Delta a_{\mathbf{n}} e^{i\frac{2\pi}{L}\mathbf{n}\cdot\mathbf{r}(c_{\mathbf{n}})} = \sum_{\mathbf{n}\in Z^D\setminus 0} \gamma_{\mathbf{n}} \left|\Delta a_{\mathbf{n}} + \mathcal{I}_0 \frac{e^{-i\frac{2\pi}{L}\mathbf{n}\cdot\mathbf{r}(c_{\mathbf{n}})}}{2\gamma_{\mathbf{n}}}\right|^2 - \sum_{\mathbf{n}\in Z^D\setminus 0} \frac{\mathcal{I}_0^2}{4\gamma_{\mathbf{n}}}. \tag{51}$$

Finally, since the integration variable $\Delta a_{\mathbf{n}}$ is complex, we introduce its polar parametrization:

$$\rho_{\mathbf{n}} e^{\pm\imath\phi_{\mathbf{n}}} = \Delta a_{\pm\mathbf{n}} + \mathcal{I}_0 \frac{e^{\mp i\frac{2\pi}{L}\mathbf{n}\cdot\mathbf{r}(c_{\mathbf{n}})}}{2\gamma_{\pm\mathbf{n}}}. \tag{52}$$

Once (51) and (52) are applied to (50), the integrations can be performed, provided that all $\mathrm{Re}(\gamma_{\mathbf{n}}) > 0$. The result reads

$$\ln \prod_{\mathbf{n}\in Z^D\setminus 0} I_{\mathbf{n}} I_0(M) \approx \ln I_0(0) + \sum_{\mathbf{n}\in Z^D\setminus 0} \ln\frac{\pi}{\gamma_{\mathbf{n}}} + \mathcal{I}_0 \sum_{\mathbf{n}\in Z^D\setminus 0} c_{\mathbf{n}} e^{i\frac{2\pi}{L}\mathbf{n}\cdot\mathbf{r}(c_{\mathbf{n}})} + \sum_{\mathbf{n}\in Z^D\setminus 0} \frac{\mathcal{I}_0^2}{4\gamma_{\mathbf{n}}}. \tag{53}$$

F. Effective Hamiltonian and model accuracy

Let us summarize the two preceding sections. Getting back to the formula (7), the effective Hamiltonian of the entire system reads

$$H_{\mathrm{eff}} = H_{RR} + \Phi - \frac{1}{\beta}\ln \prod_{\mathbf{n}\in Z^D\setminus 0} I_{\mathbf{n}} I_0(M).$$

Turning (53) into its continuous form, we obtain the final expression for the effective Hamiltonian:

$$H_{\mathrm{eff}} \approx H_{RR} + \Phi - \frac{1}{\beta}\left(\frac{\Omega}{(2\pi)^D}\int_{\tilde{\Omega}} d\mathbf{k}\ln\frac{\pi}{\gamma(\mathbf{k})} + \frac{\mathcal{I}_0\Omega}{(2\pi)^D}\sum_i^{N_1}\int_{\tilde{\Omega}} d\mathbf{k}\, e^{i\mathbf{k}\cdot(\mathbf{r}_{\min}-\mathbf{R}_i)}\frac{\mathcal{U}(\mathbf{k})}{\mathcal{V}(\mathbf{k})} - \frac{N_1\mathcal{I}_0\mathcal{U}(0)}{\mathcal{V}(0)} + \frac{\mathcal{I}_0^2\Omega}{4(2\pi)^D}\int_{\tilde{\Omega}} d\mathbf{k}\frac{1}{\gamma(\mathbf{k})} - \frac{\mathcal{I}_0^2}{4\gamma(0)} + \ln\frac{\gamma(0)I_0(0)}{\pi}\right), \tag{54}$$

where $r_{\min}$ is the global minimum, found from the equation

$$\nabla_{\mathbf{r}}\sum_i^{N_1}\int_{\tilde{\Omega}} d\mathbf{k} e^{i\mathbf{k}\cdot(\mathbf{r}-\mathbf{R}_i)}\frac{\mathcal{U}(\mathbf{k})}{\mathcal{V}(\mathbf{k})} = 0. \tag{55}$$

Furthermore, according to (44), the exact part of H_{eff} reads

$$\Phi = \frac{1}{2}\sum_{i\neq j}^{N_1} U_{\mathrm{eff}}(\mathbf{R}_i - \mathbf{R}_j) + \frac{N_1}{2}U_{\mathrm{eff}}(0) + \frac{2\tilde{\mu}N_1\mathcal{U}(0) - \Omega\tilde{\mu}^2}{2\mathcal{V}(0)},$$

where the effective interaction $U_{\mathrm{eff}}(\mathbf{R}_i - \mathbf{R}_j)$ is defined by (41).

Let us scrutinize the following term from H_{eff}:

$$\Delta U_{\mathrm{eff}} = \frac{1}{\beta}\frac{\mathcal{I}_0\Omega}{(2\pi)^D}\sum_i^{N_1}\int_{\tilde{\Omega}} d\mathbf{k}\, e^{i\mathbf{k}\cdot(\mathbf{r}_{\min}-\mathbf{R}_i)}\frac{\mathcal{U}(\mathbf{k})}{\mathcal{V}(\mathbf{k})}. \tag{56}$$

First of all, this term is an explicit function of $\mathbf{R}_i$, which is in stark contrast to the Mayer bond expansion, in which such terms are excluded. This exclusion is motivated by the conservation of energy when the entire system is translated [1]. However, in our case, the global translation $\mathbf{R}_i \to \mathbf{R}_i + \delta$ yields $\mathbf{r}_{\min} \to \mathbf{r}_{\min} + \delta$, thus (56) is, in fact, translationally invariant.

Secondly, one can notice that since $\mathbf{r}_{\min}$ is a function of $\mathbf{R}_i$ itself, there is possibly an additional effective interaction embedded in ΔU_{eff}. Therefore, $U_{\mathrm{eff}}(\mathbf{R}_i - \mathbf{R}_j)$ is the dominant source of effective interactions provided that

$$U_{\mathrm{eff}}(\mathbf{R}_i - \mathbf{R}_j) \gg \Delta U_{\mathrm{eff}}. \tag{57}$$

Whether this relation is satisfied depends on both thermodynamic parameters and the choice of microscopic potentials, which makes it difficult to analyze in a general case. However,

if this relation is seriously violated, one might attempt to estimate the influence of ΔU_{eff} on effective interactions from the following reasoning:

$$\begin{aligned}|\Delta U_{\text{eff}}| &< \frac{1}{\beta}\frac{\mathcal{I}_0\Omega}{(2\pi)^D}\int_{\tilde{\Omega}} d\mathbf{k}\sqrt{\left|\sum_i^{N_1} e^{i\mathbf{k}\cdot(\mathbf{r}_{\min}-\mathbf{R}_i)}\frac{\mathcal{U}(\mathbf{k})}{\mathcal{V}(\mathbf{k})}\right|^2}\\ &= \frac{N_1^{1/2}}{\beta}\frac{\mathcal{I}_0\Omega}{(2\pi)^D}\int_{\tilde{\Omega}} d\mathbf{k}\left|\frac{\mathcal{U}(\mathbf{k})}{\mathcal{V}(\mathbf{k})}\right|\sqrt{1+\sum_{i\neq j}^{N_1}\frac{e^{i\mathbf{k}\cdot(\mathbf{R}_j-\mathbf{R}_i)}}{N_1}}\\ &\simeq \frac{1}{\beta}\frac{\mathcal{I}_0\Omega}{(2\pi)^D}\left(N_1^{1/2}\int_{\tilde{\Omega}} d\mathbf{k}\left|\frac{\mathcal{U}(\mathbf{k})}{\mathcal{V}(\mathbf{k})}\right|\right.\\ &\quad\left.+\frac{1}{2N_1^{1/2}}\sum_{i\neq j}^{N_1}\int_{\tilde{\Omega}} d\mathbf{k}\, e^{i\mathbf{k}\cdot(\mathbf{R}_j-\mathbf{R}_i)}\left|\frac{\mathcal{U}(\mathbf{k})}{\mathcal{V}(\mathbf{k})}\right|\right). \quad (58)\end{aligned}$$

This formula also predicts the effective interactions, though we expect it to be overestimated in this case.

G. Caveats

Throughout the derivation section, we introduced numerous concepts, assumptions, and approximations. We would like to list these now and discuss their validity.

One general concern is related to path integrals. We allow $\alpha(\mathbf{r})$ to vary continuously, while the number of particles at every position should be integer. This means that the discretely varying trajectories, which are physically meaningful, are given infinitesimally small statistical weights. This might result in losing some important characteristics, similarly to the Bose-Einstein condensation, which is lost if the discrete partition function is replaced with the continuous one without proper care [40]. This problem has yet to be investigated.

Further, let us explicitly recall that the total effective potential has two parts, Φ and $-\frac{1}{\beta}\ln\prod_{\mathbf{n}\in Z^D\setminus 0} I_{\mathbf{n}} I_0(M)$. While we show in Sec. III that Φ is enough to reproduce many desired characteristics of effective interactions, there is no guarantee that the other part can be neglected in particular conditions. This is caused by the approximations applied in Sec. II E. The logarithmic expansion (45) in M is accurate provided that $c_0 > 0$, or, explicitly,

$$N_1\mathcal{U}(0) > \tilde{\mu}\Omega. \quad (59)$$

Satisfying this relation requires a high N_1 in a small volume Ω, but there is a risk of falling into the range of thermodynamic parameters relevant for a crystal or glassy state. Alternatively, the concentration of depletant might be low, which should entail low $\tilde{\mu}$, but the exact dependence of $\tilde{\mu}$ on average N_2 is as difficult to establish as H_{eff}. If (59) is not satisfied (so $c_0 < 0$), then (45) works well for $M < -c_0$, but it loses accuracy for $M > -c_0$. Another issue is the expansion (49), linearizing M in the vicinity of $c_{\mathbf{n}}$. Since each $I_{\mathbf{n}\neq 0}$ is the integral of a Gaussian centered at $c_{\mathbf{n}}$, this expansion is justified, but the control over its accuracy is lost as the width of the Gaussian grows. Unfortunately, this is exactly the case for high-order $I_{\mathbf{n}}$, since we expect $\gamma_{\mathbf{n}} \to 0$ for large n.

Yet another concern is whether the depletant-depletant potential can have a negative or partially negative Fourier transform. Since each $I_{\mathbf{n}\neq 0}$ is the Gaussian integral, it would be divergent for $\mathcal{V}_{\mathbf{n}} < 0$, hence $\prod I_{\mathbf{n}} I_0(M) \to +\infty$. In this case, H_{eff} given by (54) is meaningless, but we will argue that Φ might still provide some useful information. In general, it is true that

$$\ln I_{\mathbf{n}} I_0(M) \leqslant \ln I_{\mathbf{n}} I_0(0) = \sum_{\mathbf{n}\in Z^D\setminus 0}\ln I_{\mathbf{n}} + \ln I_0(0). \quad (60)$$

Now, let us consider an observable $O(\mathbf{R}_i,\mathbf{P}_i)$ and its average,

$$\bar{O} = \frac{\int d\mathbf{P}_i d\mathbf{R}_i\, O(\mathbf{R}_i,\mathbf{P}_i)\exp(-\beta H_{\text{eff}})}{\int d\mathbf{P}_i d\mathbf{R}_i \exp(-\beta H_{\text{eff}})}. \quad (61)$$

We can use (60) to approximate H_{eff}, namely

$$H_{\text{eff}} \approx H_{RR} + \Phi - \frac{1}{\beta}\sum_{\mathbf{n}\in Z^D\setminus 0}\ln I_{\mathbf{n}} - \frac{1}{\beta}\ln I_0(0). \quad (62)$$

From (34) it follows that $I_{\mathbf{n}}$ is independent from $\mathbf{R}_i$ for the properly shifted integration variable. Applying (62) to (61), one can see that

$$\bar{O} = \frac{\int d\mathbf{P}_i d\mathbf{R}_i\, O(\mathbf{R}_i,\mathbf{P}_i)\exp[-\beta(H_{RR}+\Phi)]}{\int d\mathbf{P}_i d\mathbf{R}_i \exp[-\beta(H_{RR}+\Phi)]}, \quad (63)$$

which is independent from divergent $I_{\mathbf{n}}$. This reasoning, although not very rigorous, suggests that Φ and $U_{\text{eff}}(\mathbf{R}_i-\mathbf{R}_j)$ might work for potentials with partially negative $\mathcal{V}(\mathbf{k})$ and can be useful in determining the mean values.

Finally, there are several concerns related to Φ itself. One thing is that we resort to the continuous representation of discrete expressions, though we expect Ω to be finite. This is physically reasonable provided that the range of microscopic potentials is much smaller than the system size L. Another issue is that we require microscopic potentials $V(r)$ and $U(r)$ to possess their Fourier transforms. This rules out such useful potentials as Lennard-Jones or polynomial potentials. Moreover, since (41) has the form of an inverse Fourier transform, the integrand must be "well-behaving," i.e., convergent for $k \to +\infty$ and without any essential singularities. Although in particular situations certain mathematical tricks and approximations can be applied to circumvent such problems, these are the reasons why (41) is not a directly applicable "silver bullet" formula.

III. APPLICATIONS

A. Systems under scrutiny

In this section, we apply $U_{\text{eff}}(\mathbf{R}_i-\mathbf{R}_j)$ given by (41) to analyze effective interactions in various systems. First, we analyze the mixtures of Gaussian particles, predicting effective interactions and analyzing effective attraction as a driving force behind demixing (Sec. III B). Another example are screening effects in the system of charged hard spheres and ions which agree with the Derjaguin-Landau-Verwey-Overbeek (DLVO) potential (Sec. III C). Yet another example is the effective interaction in a binary mixture of Yukawa particles (Sec. III D). Finally, we scrutinize the mixture of particles that have both a Yukawa interaction tail and a repulsive core, in which case we qualitatively reproduce the effects of "attraction-through-repulsion"/"repulsion-through-attraction" and compare our results to simulations (Sec. III E).

B. Gaussian particles and demixing of binary mixtures

Particles interacting via the Gaussian potential are a typical example of soft particles, and they can be analyzed within our framework. We will take advantage of the fact that the Fourier transform of the Gaussian potential is also a Gaussian function:

$$G(r) = \epsilon e^{-\frac{1}{2}\frac{r^2}{\sigma^2}}, \quad \mathcal{G}(k) = \epsilon(2\pi)^{D/2}\sigma^D e^{-\frac{1}{2}k^2\sigma^2}. \tag{64}$$

The Gaussian potential has been identified as the accurate approximation of the interaction between two isolated polymers in a good solvent, both for identical [24] and nonidentical [36] chains. Therefore, the Gaussian-core model is a well established coarse-grained description of polymer solutions [1] both in the homogeneous and the nonhomogeneous case [37]. In particular, it has been found that the binary mixtures of Gaussian particles can undergo size separation transition [37,38], similarly to polymer blends.

In our model, we assume the binary mixture of different-sized Gaussian particles and assign index 1 to big-small interaction and 2 to small-small interaction. Then, the effective interaction, according to (41), reads

$$\begin{aligned} U_{\text{eff}}(\Delta R) &= -\frac{1}{(2\pi)^D}\int_{\tilde{\Omega}} d\mathbf{k}\, e^{i\mathbf{k}\cdot\Delta\mathbf{R}}\frac{|\mathcal{G}_1(k)|^2}{\mathcal{G}_2(k)} \\ &= -\frac{\epsilon_1^2}{\epsilon_2}\frac{\sigma_1^{2D}}{(2\pi)^{D/2}\sigma_2^D}\frac{e^{-\Delta R^2/(4\sigma_1^2-2\sigma_2^2)}}{\left(2\sigma_1^2-\sigma_2^2\right)^{D/2}}. \end{aligned} \tag{65}$$

$U_{\text{eff}}(\Delta R)$ proves to be a renormalized Gaussian, but, since $\epsilon_i > 0$, it is always negative. Examples of this interaction are presented in Fig. 1.

Result (65) suggests that the total interaction between bigger particles [i.e., $U_{RR}(\Delta R) + U_{\text{eff}}(\Delta R)$] can include an attractive tail, provided that for a certain choice of parameters there exist such ΔR that the effective interaction prevails over $U_{RR}(\Delta R)$. It is possible that such a tail could drive the separation process. Let the interaction between bigger particles read

$$U_{RR}(\Delta R) = G_0(\Delta R) = \epsilon_0 e^{-\frac{1}{2}\frac{\Delta R^2}{\sigma_0^2}}. \tag{66}$$

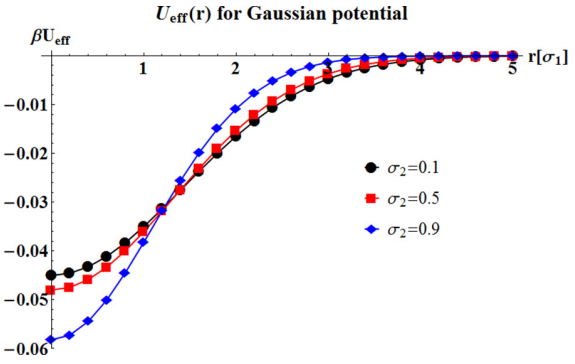

FIG. 1. (Color online) Effective interaction between Gaussian particles, according to formula (65). σ_1 is the unit length, and the scaling reads $\beta\epsilon_1^2/\epsilon_2 = 1$. U_{eff} is a negative Gaussian function for every σ_2.

The attractive tail will be present if the following inequality has a solution in ΔR:

$$G_0(\Delta R) + U_{\text{eff}}(\Delta R) < 0, \tag{67}$$

which can be reduced to

$$\begin{aligned} &\Delta R^2\left(\frac{1}{4\sigma_1^2-2\sigma_2^2}-\frac{1}{2\sigma_0^2}\right) \\ &< \ln\left(\frac{\epsilon_1^2}{\epsilon_0\epsilon_2}\frac{\sigma_1^{2D}}{(2\pi)^{D/2}\sigma_2^D}\frac{1}{\left(2\sigma_1^2-\sigma_2^2\right)^{D/2}}\right). \end{aligned} \tag{68}$$

This relation can be simplified further by assuming that $\sigma_1^2 = (\sigma_0^2+\sigma_2^2)/2$ and $\sigma_2 = c\sigma_0$, where c is the proportionality constant. Under such a choice of parameters, the right-hand side of (68) becomes identically 0, so the inequality reads

$$0 < \ln\left(\tilde{\epsilon}^2\frac{(1+c^2)^D}{(2\pi)^{D/2}c^D}\right), \tag{69}$$

where $\tilde{\epsilon} = \epsilon_1/\sqrt{\epsilon_0\epsilon_2}$ is a common energy scale. In Fig. 2, we have presented a region on the $\tilde{\epsilon}$-c plane where (69) is satisfied for $D = 3$. For comparison, in Fig. 2 we also plot the classical mean-field condition for spinodal separation of Gaussian particles, which reads [37,38]

$$\tilde{\epsilon} > \left(\frac{2c}{1+c^2}\right)^{3/2}. \tag{70}$$

Figure 2 illustrates a general qualitative agreement between the mean-field condition (70) and our condition (69), especially in terms of shape and the asymptotic behavior ($c \to 0$ and $c \gg 1$) of the mixing region. However, our

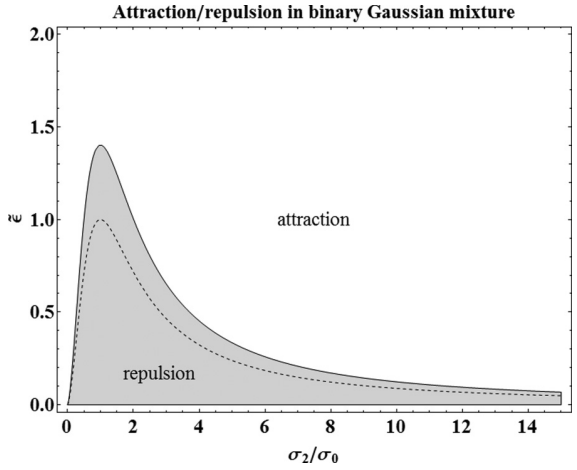

FIG. 2. Effective attraction in binary mixtures of Gaussian particles as a driving force behind phase separation. This plot visualizes inequality (69) for $D = 3$, where $\tilde{\epsilon} = \epsilon_1/\sqrt{\epsilon_0\epsilon_2}$ and $c = \sigma_2/\sigma_0$. Shaded region—total interaction is purely repulsive, no driving force for de-mixing. Plain region—total interaction has an attractive tail stimulating demixing. The dashed line illustrates mean-field condition (70) for spinodal decomposition in the Gaussian mixture.

theory systematically overshoots the mean-field behavior, with the highest discrepancy at $c \approx 1$. This means that the condition of attractive tail in total interaction leads to a broader region of mixing than the mean-field approach, which requires a higher sized ratio c or energy scale $\tilde{\epsilon}$ to obtain the separation.

C. Coulomb potential and charged sphere screening effects

In this example, we will examine the effective interaction between two charged hard spheres in the presence of ions. The dimensionality of the system is $D = 3$. Assigning index $i = 1$ for sphere-ion interaction and $i = 2$ for ion-ion interaction, we assume that every microscopic potential in this system consists of the hard-sphere (HS) potential and the Coulomb long-range interaction:

$$U_i(r) = U_{\mathrm{HS},i}(r) + V_{C,i}(r), \tag{71}$$

where

$$U_{\mathrm{HS},i}(r) = c_i \Theta(r - 2\sigma_i), \quad V_{C,i}(r) = \frac{\epsilon_i}{r}. \tag{72}$$

$\Theta(r - 2\sigma_i)$ is the Heaviside step function, the radius of the sphere reads σ_0, the ionic radius is denoted by σ_2 and $\sigma_1 = (\sigma_0 + \sigma_2)/2$, and c_i and ϵ_i are scaling constants.

The Fourier transform of the Coulomb potential can be calculated from its relation to the Yukawa potential:

$$V_{C,i}(r) = \frac{\epsilon_i}{r} = \lim_{\lambda \to 0} \frac{\epsilon_i e^{-\lambda r}}{r}. \tag{73}$$

Since the Fourier transform of the Yukawa potential is $4\pi/(k^2 + \lambda^2)$, then the sought-after Fourier transform reads

$$\mathcal{V}_{C,i}(k) = \frac{4\pi\epsilon_i}{k^2}. \tag{74}$$

The Fourier transform of $U_{\mathrm{HS},i}(r)$ can be calculated directly,

$$\mathcal{U}_{\mathrm{HS},i}(k) = 4\pi c_i \frac{\sin 2\sigma_i k - 2\sigma_i k \cos 2\sigma_i k}{k^3}. \tag{75}$$

This representation is adequate for sphere-ion interaction, but for ion-ion interaction we can simplify it significantly. Since σ_2 is the lowest length scale in the system, only k up to the order of $1/\sigma_2$ carries physically important information. In this range, we can approximate $\sin 2k\sigma_2 \simeq 2k\sigma_2$ and $\cos 2k\sigma_2 \simeq 1 - 2k^2\sigma_2^2$, so

$$\mathcal{U}_{\mathrm{HS},2}(k) \simeq 16\pi c_2 \sigma_2^3. \tag{76}$$

We would obtain a similar result by modeling the ion core with the Dirac-$\delta(\mathbf{r})$ potential, which indicates that (76) is, in fact, the pointlike approximation of $U_{\mathrm{HS},2}(r)$.

Having established both transforms, (41) can be applied and, after careful calculations, we obtain

$$\begin{aligned} U_{\mathrm{eff}}(\Delta R) &= -\frac{1}{(2\pi)^3} \int_{\Omega} d\mathbf{k}\, e^{i\mathbf{k}\cdot\Delta\mathbf{R}} \frac{|\mathcal{U}_{\mathrm{HS},1}(k) + \mathcal{V}_{C,1}(k)|^2}{\mathcal{U}_{\mathrm{HS},2}(k) + \mathcal{V}_{C,2}(k)} \\ &= -\frac{\epsilon_1^2}{\epsilon_2} \frac{1}{\Delta R} + C_0 \frac{e^{-\frac{\kappa_{\mathrm{eff}}}{2}\Delta R}}{\Delta R}. \end{aligned} \tag{77}$$

This result consists of Coulomb-like and Yukawa-like terms, and it is valid for $\Delta R > 4\sigma_1$. The constants read

$$\kappa_{\mathrm{eff}} = \sqrt{\frac{\epsilon_2}{c_2\sigma_2^3}}, \tag{78}$$

$$C_0 = \frac{c_2\sigma_2^3}{\epsilon_2^2}(\epsilon_1\kappa_{\mathrm{eff}} - 2c_1\sigma_1\kappa_{\mathrm{eff}} \cosh\sigma_1\kappa_{\mathrm{eff}} + 2c_1 \sinh\sigma_1\kappa_{\mathrm{eff}})^2. \tag{79}$$

Let us further specify our system by assuming that the charge of a single sphere reads Q and the charge of an ion is q. Then

$$\epsilon_1 = \frac{qQ}{4\pi\varepsilon}, \quad \epsilon_2 = \frac{q^2}{4\pi\varepsilon}, \quad \frac{\epsilon_1^2}{\epsilon_2} = \frac{Q^2}{4\pi\varepsilon}, \tag{80}$$

where ε is the electrostatic permittivity of the system. Since all spheres have the same charge, there is also a microscopic repulsion present, which, for $\Delta R \gg 2\sigma_0$, can be treated as a Coulomb potential:

$$U_{RR}(\Delta R) = \frac{Q^2}{4\pi\varepsilon\Delta R}. \tag{81}$$

Calculating the total sphere-sphere interaction, we obtain

$$U_{\mathrm{tot}}(\Delta R) = U_{RR}(\Delta R) + U_{\mathrm{eff}}(\Delta R) = C_0 \frac{e^{-\frac{\kappa_{\mathrm{eff}}}{2}\Delta R}}{\Delta R}. \tag{82}$$

One can immediately see that the Coulomb term from (77) cancels the long-range repulsion $U_{RR}(\Delta R)$, thus the total interaction consists solely of the Yukawa term. This term has the same functional form as the DLVO potential [9] in the Debye-Hückel (DH) approximation, which reads [22,39]

$$U_{\mathrm{DLVO}}(\Delta R) = C_{\mathrm{DLVO}} \frac{e^{-\kappa_{\mathrm{DH}}\Delta R}}{\Delta R}, \tag{83}$$

where

$$\kappa_{\mathrm{DH}}^2 = \beta\frac{4\pi}{\varepsilon}(n_1 Q^2 + n_2 q^2), \quad C_{\mathrm{DLVO}} = \frac{Q^2 e^{2\sigma_0\kappa_{\mathrm{DH}}}}{\varepsilon(1 + 2\sigma_0\kappa_{\mathrm{DH}})^2},$$

with n_1, n_2 the number densities of spheres and ions, respectively.

In our model, we expect that $c_i \gg k_B T$, so $U_{\mathrm{HS},i}(r)$ acts as an impenetrable core, but these core constants are not defined otherwise. However, by comparing (82) and (83),

$$\begin{aligned} 2\kappa_{\mathrm{DH}} &= \kappa_{\mathrm{eff}}, \\ C_0 &= C_{\mathrm{DLVO}}, \end{aligned} \tag{84}$$

we can relate c_i to the DLVO parameters:

$$\begin{aligned} c_2 &= \frac{\epsilon_2}{4\kappa_{\mathrm{DH}}^2\sigma_2^3}, \\ c_1 &= \frac{\kappa_{\mathrm{DH}}(\epsilon_1 \pm \sqrt{\epsilon_2|C_{\mathrm{DLVO}}|})}{2\sigma_1\kappa_{\mathrm{DH}}\cosh 2\sigma_1\kappa_{\mathrm{DH}} - \sinh 2\sigma_1\kappa_{\mathrm{DH}}}, \end{aligned} \tag{85}$$

where the sign is chosen so $c_1 > 0$. This choice of c_1 and c_2 tunes (82) to become exactly the DLVO interaction (83). In [22], Crocker and Grier have measured $\kappa_{\mathrm{DH}}^{-1} = 161$ nm for polystyrene sulfate spheres of radius $\sigma_0 = 32$ nm and charge $Q = 1991\mathrm{e}$. Assuming $\sigma_2 = 0.1$ nm and $q = -\mathrm{e}$, one can

calculate that $\beta c_1 \simeq 13$ and $\beta c_2 \simeq 10^{13}$ for $T = 298$ K. This is in agreement with our expectation that $c_i \gg k_B T$.

In conclusion, our model based on the formula (41) proves to be equivalent to the DLVO potential, which has been shown to accurately describe screening effects for the charged spheres in colloidal solution [22].

D. Yukawa particles

As discussed in the preceding section, the Yukawa potential is an accurate model for charged particles in solution. Since this potential is also tractable in terms of its Fourier transform, analyzing the binary mixture of Yukawa particles is another interesting example for our theory. For $D = 3$, the Yukawa potential $Y(r)$ and its Fourier transform read

$$Y(r) = \epsilon\sigma \frac{e^{-\kappa(r-\sigma)}}{r}, \quad \mathcal{Y}(k) = \frac{4\pi\epsilon\sigma e^{\kappa\sigma}}{k^2+\kappa^2}. \tag{86}$$

Let us consider a system composed of Yukawa particles, where $\sigma_1,\epsilon_1,\kappa_1$ describe particle-depletant interaction $Y_1(r)$, and depletant-depletant interaction $Y_2(r)$ depends on $\sigma_2,\epsilon_2,\kappa_2$. Then, the effective interaction can be calculated analytically from (41), namely

$$\begin{aligned} U_{\text{eff}}(\Delta R) &= -\frac{1}{(2\pi)^3}\int_{\tilde{\Omega}} d\mathbf{k}\, e^{i\mathbf{k}\cdot\Delta\mathbf{R}} \frac{|\mathcal{Y}_1(k)|^2}{\mathcal{Y}_2(k)} \\ &= -\frac{\epsilon_1^2\sigma_1^2}{\epsilon_2\sigma_2} e^{-\kappa_1(\Delta R-2\sigma_1)-\kappa_2\sigma_2}\left(\frac{1}{\Delta R} - \frac{\kappa_1^2-\kappa_2^2}{2\kappa_1}\right). \end{aligned} \tag{87}$$

A graphical representation of (87) for various parameters is shown in Fig. 3. In general, for $\epsilon_2 > 0$ the particular profiles of effective interaction are strongly dependent on parameters and can vary from purely attractive to strongly repulsive. When the range of interaction is of the order of particle radius ($\kappa_i \simeq \sigma_i^{-1}$), the effective interaction is attractive (curves 1–3 in Fig. 3) and its range increases with the downturn in the depletant radius. In fact, this range is surprisingly long, namely for $\sigma_2/\sigma_1 = 0.25$ the interaction is significant over a range of $5\sigma_1$ (curve 1, Fig. 3). This is in stark contrast with the

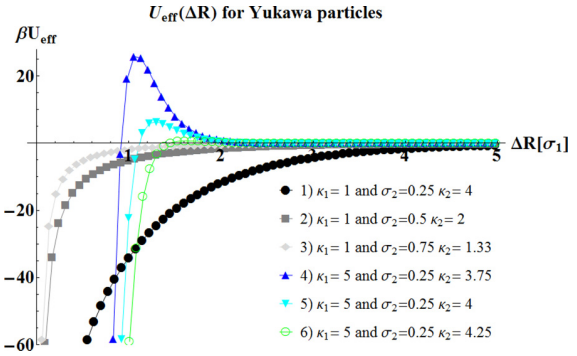

FIG. 3. (Color online) Effective potential for a binary mixture of Yukawa particles, according to formula (87), for which $\beta\epsilon_1^2/\epsilon_2 = 1$, and σ_2 and κ_i are given in units $[\sigma_1]$ and $[\sigma_1^{-1}]$, respectively. Curves 1–3: growing depletion attraction for decreasing size of depletant particles, $\kappa_i = \sigma_i^{-1}$, to match the size of the particle. Curves 4–6: for higher values of κ_1, a κ_2-dependent energy barrier appears.

Asakura-Oosawa model for HS of radii σ_1 and σ_2, where the interaction would cease over a range of $\sigma_1 + \sigma_2$ [16]. Another interesting characteristic of U_{eff} for Yukawa particles appears when κ_1 is increased, in which case a repulsive barrier emerges. This barrier grows as the range of depletant-depletant interaction increases (curves 4–6, Fig. 3). Apparently, possible energetic advantages of lower $Y_1(r)$ cannot dominate the depletant-depletant repulsion. Finally, if we assume $\epsilon_2 < 0$, the global sign of $U_{\text{eff}}(\Delta R)$ is inversed, leading to repulsion-through-attraction effects.

Summarizing, this relatively simple model indicates possible self-organization of Yukawa particles, although analytical calculations analogous to Gaussian particles cannot be easily completed here. Nevertheless, phase separation in binary Yukawa systems has been encountered in simulations [41] and also in the context of plasma research, e.g., [42,43].

E. Particles with a repulsive core and a Yukawa interaction tail

The pure Yukawa potential suffers from the lack of a repulsive core independent from the interaction tail, so a realistic description of colloid particles requires a more complicated potential. In [25], Louis *et al.* simulated a binary system consisting of HS particles with Yukawa interaction tails, both as depletant and colloid particles. The potential applied in [25] reads

$$\begin{aligned} &+\infty \quad \text{if} \quad r < \sigma_i, \\ &\frac{\epsilon_i\sigma_i}{r} e^{-\kappa_i(r-\sigma_i)} \quad \text{if} \quad r \geqslant \sigma_i, \end{aligned} \tag{88}$$

where index i denotes big-small or small-small potential, σ_i is the size of the particle core, and ϵ_i is the energy scale. Reference [25] reports that the sign of the big-small interaction tail is decisive for the effective interaction being attractive or repulsive. In particular, the repulsive tail results in effective attraction in the system, while the attractive tail induces "repulsion-through-attraction." Within our framework, we are able to qualitatively reproduce these two effects with an analytical formula.

We propose to model both the hard core and interaction tail of a single particle with two Yukawa potentials, namely

$$Y_i^{\text{HS}}(r) = \frac{c_i\sigma_i}{r} e^{-\lambda_i(r-\sigma_i)} + \frac{t_i\sigma_i}{r} e^{-\kappa_i(r-\sigma_i)}, \tag{89}$$

where index $i = 1$ denotes particle-depletant interaction and $i = 2$ denotes depletant-depletant interaction. For $\lambda_i > \kappa_i$, the first term becomes a repulsive core, while the second term can now be either repulsive or attractive, depending on t_i. To allow a direct comparison between our results and [25], we would like to control the attractive tail of $Y_i^{\text{HS}}(r)$ with the depth of its minimum ϵ_i. Thus, for $\epsilon_i < 0$ we have determined t_i numerically from the following equations:

$$\begin{aligned} \tfrac{d}{dr} Y_i^{\text{HS}}(r)\big|_{r=r_0} &= 0, \\ Y_i^{\text{HS}}(r_0) &= \epsilon_i. \end{aligned} \tag{90}$$

In the case of a repulsive tail, we have assumed $t_i = \epsilon_i \geqslant 0$.

The Fourier transform of $Y_i^{\text{HS}}(r)$ is simply a sum of two $\mathcal{Y}(k)$ for relevant parameters. Therefore, the effective interaction

reads

$$U_{\mathrm{eff}}(\Delta R) = -\frac{1}{(2\pi)^3}\int_{\tilde{\Omega}} d\mathbf{k}\, e^{i\mathbf{k}\cdot\Delta\mathbf{R}}\frac{|\mathcal{Y}_1^{\mathrm{HS}}(k)|^2}{\mathcal{Y}_2^{\mathrm{HS}}(k)}$$
$$= -\frac{2}{\pi}\frac{\sigma_1^2}{\sigma_2}\int_0^{+\infty} dk \frac{k\sin\Delta Rk}{\Delta R}\frac{\left(k^2+\kappa_2^2\right)\left(k^2+\lambda_2^2\right)}{\left(k^2+\lambda_1^2\right)^2\left(k^2+\kappa_1^2\right)^2}$$
$$\times\frac{\left[c_1 e^{\sigma_1\lambda_1}\left(k^2+\kappa_1^2\right)+t_1 e^{\kappa_1\sigma_1}\left(k^2+\lambda_1^2\right)\right]^2}{\left[c_2 e^{\sigma_2\lambda_2}\left(k^2+\kappa_2^2\right)+t_2 e^{\kappa_2\sigma_2}\left(k^2+\lambda_2^2\right)\right]}. \quad (91)$$

The integrand in the above expression is an even function, and the degree of polynomial expression in the denominator is higher than that in the numerator, so this integral can be calculated analytically, thanks to the residue theorem. Due to its length and complexity, we discuss the full formula in the Appendix.

The core parameters c_i and λ_i cannot be determined from first principles, and our initial experience with (91) has shown that the exact shape of interactions obtained from our model is very sensitive to these parameters. It is also usually possible to find the parameters that differ by many orders of magnitude but lead to similar results. Therefore, in order to determine the physically reasonable range of core parameters, we have fitted our model to the simulation data from [25]. In [25], the values of potential parameters read $\sigma_1 = 0.6\sigma_0$, $\sigma_2 = 0.2\sigma_0$, $\kappa_1 = 6/\sigma_0$, and $\kappa_2 = 15/\sigma_0$, where σ_0 is the radius of the bigger particle. The simulations have been performed for nine combinations of tail parameters, namely for $\beta\epsilon_1$ equal to -0.82, 0, and 0.82, and for $\beta\epsilon_2$ set to 0, 2.99, and -0.996. We read the data from Fig. 6 in [25] with the resolution of 25 points per curve and fit them using the quasi-Newton algorithm with a constraint $c_i > 0$. The constraint is applied to prevent the tendency of the algorithm to find the unphysical values of parameters.

To fit the data, we should find four core parameters c_i and λ_i for each choice of ϵ_1 and ϵ_2. However, the algorithm usually could not achieve convergence if λ_1 and λ_2 have been varied. Therefore, we have chosen $\lambda_1 = 3\kappa_1$ and $\lambda_2 = 2.4\kappa_2$ and kept these values constant for all curves, fitting solely c_1 and c_2. For such a choice of λ_i, the microscopic potentials $Y_i^{\mathrm{HS}}(\Delta R)$ are relatively soft-core, but this choice improved the quality of fits for all $\epsilon_2 \neq 0$ cases, with the error of c_1 up to 15% (except for case 3, which was 44%) and the errors of c_2 lower than 0.0002%. However, extreme errors (higher than 500%) are encountered for all $\epsilon_2 = 0$ cases (plots 1, 4, and 7, Fig. 4), though the algorithm achieved convergence even in this situation. These errors might arise from the fact that we fit the

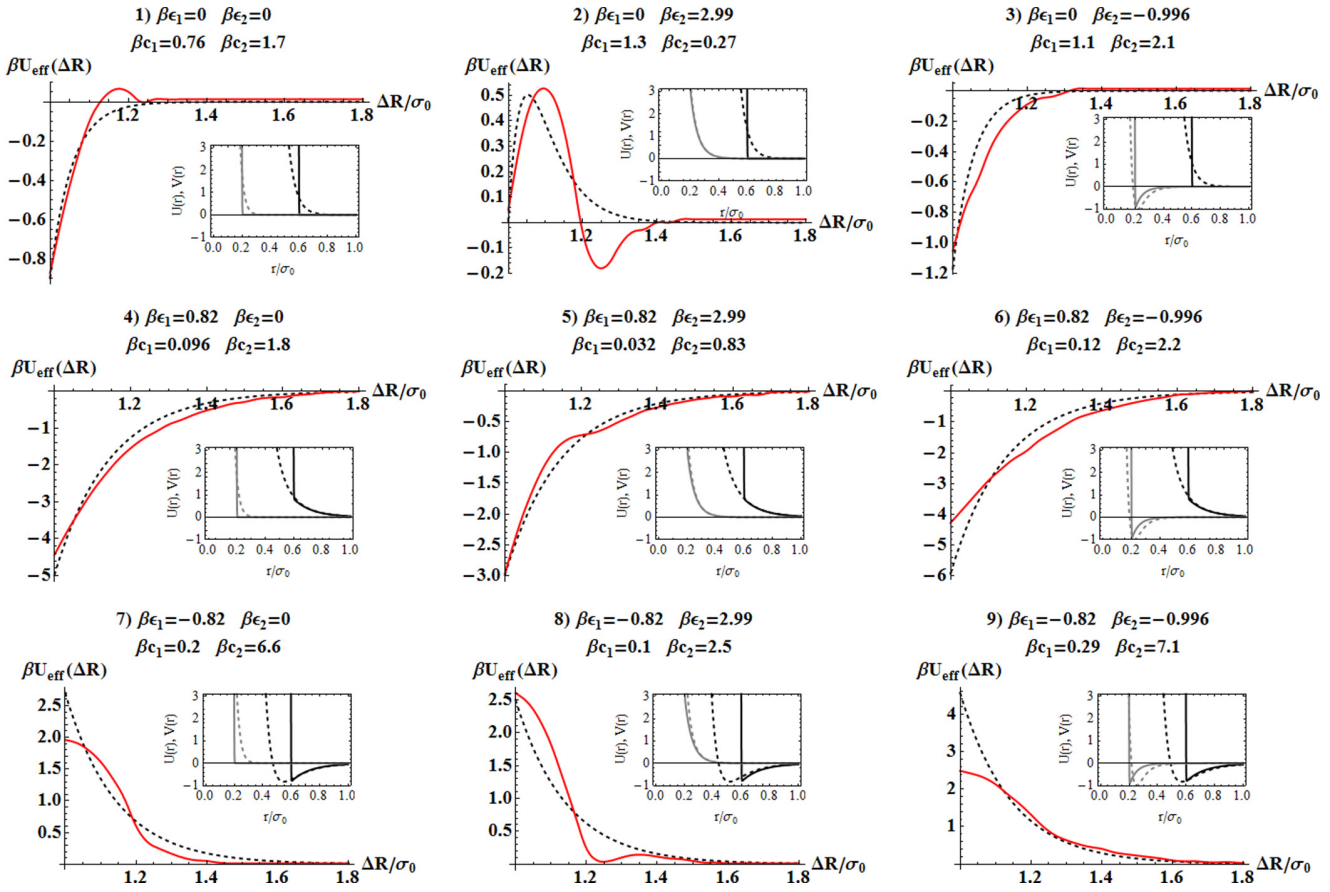

FIG. 4. (Color online) Model (91) (dashed black line) fitted to simulation data (red solid line) from [25]. In all cases, core exponents read $\lambda_1 = 3\kappa_1$ and $\lambda_2 = 2.4\kappa_2$; c_i are determined from the fitting procedure. Insets: a comparison between potential wells resulting from the fitting procedure and the hard-core potentials applied in [25]; gray, small-small interaction; black, big-small interaction; dashed lines, soft-core potential generated with λ_i and c_i; solid lines, referential hard-core potential from [25].

essentially soft-core model to the data that are directly affected by the hard-core potential. In the absence of mitigating effects from the tail, our model becomes highly sensitive to λ_i, though no such problem is encountered for $\epsilon_1 = 0$. While increasing λ_i might improve those three fits, we have decided to keep common λ_i for all examples, to allow as much comparison between them as possible.

The data from simulations and our fits are presented in Fig. 4. In general, our model is capable of reproducing all types of effective interactions found in [25] in terms of their sign and range. In particular, our model reproduces the "attraction-though-repulsion" effect for $\epsilon_1 > 0$ (plots 4–6, Fig. 4) and the "repulsion-through-attraction" effect for $\epsilon_1 < 0$ (plots 7–9, Fig. 4). In the former case, our model exhibits a general tendency to predict a shallower effective potential than in the simulations. However, in the latter case of $\epsilon_1 < 0$ our model evidently lacks the oscillatory behavior which is manifested in the simulations. This is also a problem for the $\epsilon_1 = 0$, $\epsilon_2 = 2.99$ case (plot 2, Fig. 4), which is entirely dominated by the oscillations, and, to a lesser extent, for the pure hard-sphere case ($\epsilon_1 = 0$, $\epsilon_2 = 0$, plot 1, Fig. 4). In all of these examples, our model can be applied only qualitatively, whenever the oscillations can be treated as a higher-order effect. In the insets of Fig. 4, there are also microscopic potential wells presented, generated according to fitted parameters, and compared to the HS potentials applied in the simulations. As expected, the highest discrepancies occur for $\epsilon_1 < 0$, most likely due to the lack of oscillations. The other examples show agreement in the shape of the interaction tail, though for $\epsilon_i = 0$ a compensating softening of the core occurs.

In principle, varying solely ϵ_1 and ϵ_2 should be enough to explain the differences in effective interaction for a common set of core parameters. Taking the suggestion from the previously fitted parameters, we have chosen $\lambda_1 = \frac{5}{3}\kappa_1$, $\lambda_2 = \frac{32}{15}\kappa_2$, $\beta c_1 = 1$, and $\beta c_2 = 2.2$. The results are shown in Fig. 5. For such a choice of parameters, the core part of the microscopic potential is even softer than before, but now our model simultaneously reproduces eight out of nine types of simulated effective interactions, in terms of their energy scale, range, and sign. As before, our predictions lack the oscillations for $\epsilon_1 < 0$, which is one group of results (curves 7–9, Fig. 5). In this case, our predictions might be treated only as a crude approximation. Another group is the effective attraction for $\epsilon_1 > 0$ (curves 4–6, Fig. 5). In this group, our predictions vary more uniformly with changing ϵ_2 than in the simulations, and our effective potential is usually stronger for $\Delta R/\sigma_0$ close to 1, but sooner becomes flat. Yet another group is formed by $\epsilon_1 = 0$ results. The sole qualitative disagreement occurs for the $\epsilon_1 = 0$, $\epsilon_2 = 2.99$ case (curve 2, Fig. 5), which is predicted as attractive, but the simulations show its mainly oscillatory behavior. In the remaining cases of $\epsilon_1 = 0$, $\epsilon_2 = 0$ and $\epsilon_1 = 0$, $\epsilon_2 = -0.996$ (curves 1 and 2, Fig. 5), the predicted range of interaction is slightly longer than in simulations.

In summary, (91) qualitatively reproduces most of the expected effective interaction characteristics. The discrepancies between our model and simulations might originate from both the application of soft-core potentials and the fact that Φ is only a part of the total effective interaction. In the Appendix, we comment briefly on the possibility of generating oscillatory behavior from (91).

IV. FINAL REMARKS

In this paper, we have proposed an occupation number functional as a tool to describe binary colloidal systems. This functional is an alternative to the Asakura-Oosawa approach, density functional theory, and closure relations. In Sec. III, we have shown that with the aid of our formalism, we are able to reproduce analytically the important features of systems ranging from Gaussian particle mixtures to Yukawa particle mixtures. Our theory proved to be a versatile qualitative tool, which supports our proposition that $U_{\text{eff}}(\mathbf{R}_i - \mathbf{R}_j)$ can be the dominant source of effective interactions. While the

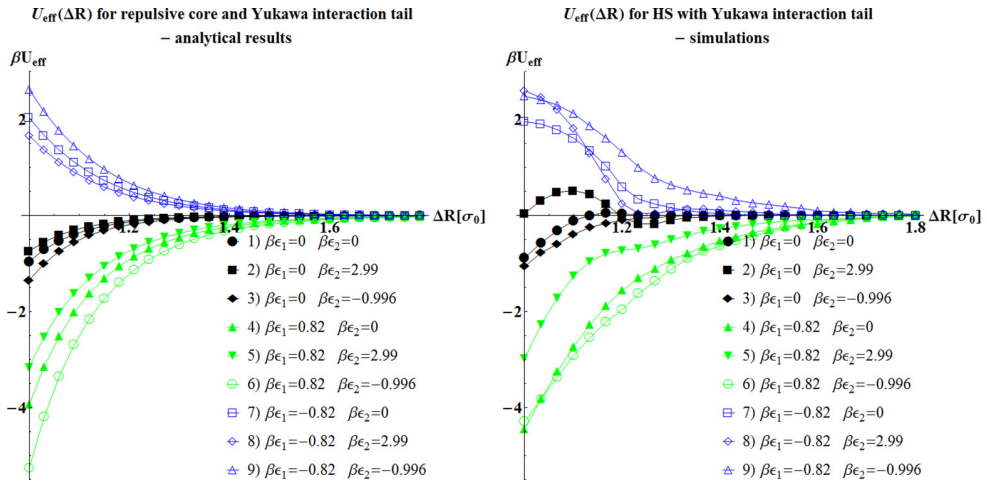

FIG. 5. (Color online) Effective interaction in the binary mixture of particles consisting of a repulsive core and a Yukawa interaction tail. Left: effective interaction generated from formula (91) for soft-core particles. Right: effective interaction measured in the simulations of hard-core particles, reprinted from [25]. σ_0 is the radius of bigger particles, $\sigma_1 = 0.6\sigma_0$, $\sigma_2 = 0.2\sigma_0$, $\kappa_1 = 6/\sigma_0$, and $\kappa_2 = 15/\sigma_0$. Core parameters for all curves: $\lambda_1 = \frac{5}{3}\kappa_1$, $\lambda_2 = \frac{32}{15}\kappa_2$, $\beta c_1 = 1$, and $\beta c_2 = 2.2$. Curves 1–3: for $\epsilon_1 = 0$, the behavior of U_{eff} depends on the sign of ϵ_2. Curves 4–6: for $\epsilon_1 > 0$, U_{eff} is attractive. Curves 7–9: for $\epsilon_1 < 0$, U_{eff} is repulsive.

framework we propose is currently far less developed and not as accurate as other approaches in the field, it provides a more direct insight into how effective interactions arise from microscopic potentials. We have provided a discussion on the assumptions and approximations that determine the limits of applicability for our theory. Further development of the occupation number functional approach might include reproducing thermodynamics of binary systems or relating this model to spatiotemporal correlations in noise in a Langevin-like description.

ACKNOWLEDGMENTS

M.M. acknowledges the support of the M. Smoluchowski KRAKOW SCIENTIFIC CONSORTIUM, in the framework of the KNOW scholarship.

APPENDIX: FULL FORMULA FOR THE EFFECTIVE INTERACTION OF PARTICLES WITH A REPULSIVE CORE AND A YUKAWA INTERACTION TAIL

In this appendix, we present the full analytic formula for effective interaction given by (91):

$$\begin{aligned} U_{\text{eff}}(\Delta R) &= -\frac{1}{(2\pi)^3}\int_{\tilde{\Omega}} d\mathbf{k}\, e^{i\mathbf{k}\cdot\Delta\mathbf{R}}\frac{\left|\mathcal{Y}_1^{\text{HS}}(k)\right|^2}{\mathcal{Y}_2^{\text{HS}}(k)} \\ &= -\frac{2}{\pi}\frac{\sigma_1^2}{\sigma_2}\int_0^{+\infty} dk \frac{k\sin\Delta R k}{\Delta R}\frac{\left(k^2+\kappa_2^2\right)\left(k^2+\lambda_2^2\right)}{\left(k^2+\lambda_1^2\right)^2\left(k^2+\kappa_1^2\right)^2}\frac{\left[c_1 e^{\sigma_1\lambda_1}\left(k^2+\kappa_1^2\right)+t_1 e^{\kappa_1\sigma_1}\left(k^2+\lambda_1^2\right)\right]^2}{\left[c_2 e^{\sigma_2\lambda_2}\left(k^2+\kappa_2^2\right)+t_2 e^{\kappa_2\sigma_2}\left(k^2+\lambda_2^2\right)\right]}. \end{aligned} \tag{A1}$$

The integrand is the even function of k, and the nominator has lower order than the denominator, so this integral can be calculated via residue theorem. The integrand has four poles:

$$k_1 = i\lambda_1, \tag{A2}$$

$$k_2 = i\kappa_1, \tag{A3}$$

$$k_{3,\pm} = \pm i\sqrt{\frac{c_2\kappa_2^2 e^{\sigma_2\lambda_2}+t_2\lambda_2^2 e^{\sigma_2\kappa_2}}{c_2 e^{\lambda_2\sigma_2}+t_2 e^{\kappa_2\sigma_2}}}. \tag{A4}$$

k_1 and k_2 lie in the upper complex half-plane. $k_{3,\pm}$ can be either purely imaginary, in which case only $k_{3,+}$ lies in the upper complex half-plane, or purely real, in which case both $k_{3,+}$ and $k_{3,-}$ lie on the real axis. For three imaginary poles, the result of integration reads

$$U_{\text{eff}}(\Delta R) = 2\pi i[\text{Res}(k_1)+\text{Res}(k_2)+\text{Res}(k_{3,+})], \tag{A5}$$

where

$$\begin{aligned} 2\pi i\,\text{Res}(k_1) = {}& \frac{\sigma_1^2}{\sigma_2}c_1 e^{\lambda_1(\sigma_1-\Delta R)}\left\{4t_1\lambda_1 e^{\kappa_1\sigma_1}\left(\kappa_2^2-\lambda_1^2\right)\left(\lambda_2^2-\lambda_1^2\right)\left[c_2 e^{\lambda_2\sigma_2}\left(\kappa_2^2-\lambda_1^2\right)-t_2 e^{\kappa_2\sigma_2}\left(\lambda_1^2-\lambda_2^2\right)\right]\right. \\ & -c_1 e^{\lambda_1\sigma_1}\left(\kappa_1^2-\lambda_1^2\right)\left[t_2 e^{\kappa_2\sigma_2}\left[\Delta R\left(\lambda_1^2-\kappa_2^2\right)-2\lambda_1\right]\left(\lambda_1^2-\lambda_2^2\right)^2+c_2 e^{\lambda_2\sigma_2}\left(\kappa_2^2-\lambda_1^2\right)^2\left[\Delta R\left(\lambda_1^2-\lambda_2^2\right)-2\lambda_1\right]\right]\} \\ & \left./\left\{\lambda_1\Delta R\left(\lambda_1^2-\kappa_1^2\right)\left[c_2 e^{\lambda_2\sigma_2}\left(\kappa_2^2-\lambda_1^2\right)-t_2 e^{\kappa_2\sigma_2}\left(\lambda_1^2-\lambda_2^2\right)\right]^2\right\}, \end{aligned} \tag{A6}$$

$$\begin{aligned} 2\pi i\,\text{Res}(k_2) = {}& \frac{\sigma_1^2}{\sigma_2}t_1 e^{\kappa_1(\sigma_1-\Delta R)}\left\{4c_1\kappa_1 e^{\lambda_1\sigma_1}\left(\kappa_1^2-\kappa_2^2\right)\left(\lambda_2^2-\kappa_1^2\right)\left[c_2 e^{\lambda_2\sigma_2}\left(\kappa_1^2-\kappa_2^2\right)+t_2 e^{\kappa_2\sigma_2}\left(\kappa_1^2-\lambda_2^2\right)\right]\right. \\ & +t_1 e^{\kappa_1\sigma_1}\left(\kappa_1^2-\lambda_1^2\right)\left[t_2 e^{\kappa_2\sigma_2}\left(\kappa_1^2-\lambda_2^2\right)^2\left[\Delta R\left(\kappa_1^2-\kappa_2^2\right)-2\kappa_1\right]+c_2 e^{\lambda_2\sigma_2}\left(\kappa_1^2-\kappa_2^2\right)^2\left[\Delta R\left(\kappa_1^2-\lambda_2^2\right)-2\kappa_1\right]\right]\} \\ & \left./\left\{\kappa_1\Delta R\left(\kappa_1^2-\lambda_1^2\right)\left[c_2 e^{\lambda_2\sigma_2}\left(\kappa_1^2-\kappa_2^2\right)+t_2 e^{\kappa_2\sigma_2}\left(\kappa_1^2-\lambda_2^2\right)\right]^2\right\}, \end{aligned} \tag{A7}$$

$$\begin{aligned} 2\pi\, i\text{Res}(k_{3,+}) = {}& 2\frac{\sigma_1^2}{\sigma_2}c_2 t_2\left(\kappa_2^2-\lambda_2^2\right)^2\exp\left(\sigma_2(\kappa_2+\lambda_2)-\Delta R\sqrt{\frac{c_2\kappa_2^2 e^{\lambda_2\sigma_2}+t_2\lambda_2^2 e^{\kappa_2\sigma_2}}{c_2 e^{\lambda_2\sigma_2}+t_2 e^{\kappa_2\sigma_2}}}\right) \\ & \times\left\{c_1 e^{\lambda_1\sigma_1}\left[c_2 e^{\lambda_2\sigma_2}\left(\kappa_1^2-\kappa_2^2\right)+t_2 e^{\kappa_2\sigma_2}\left(\kappa_1^2-\lambda_2^2\right)\right]-t_1 e^{\kappa_1\sigma_1}\left[c_2 e^{\lambda_2\sigma_2}\left(\kappa_2^2-\lambda_1^2\right)-t_2 e^{\kappa_2\sigma_2}\left(\lambda_1^2-\lambda_2^2\right)\right]\right\}^2 \\ & \left./\left\{\Delta R\left(c_2 e^{\lambda_2\sigma_2}+t_2 e^{\kappa_2\sigma_2}\right)\left[c_2 e^{\lambda_2\sigma_2}\left(\kappa_1^2-\kappa_2^2\right)+t_2 e^{\kappa_2\sigma_2}\left(\kappa_1^2-\lambda_2^2\right)\right]^2\left[c_2 e^{\lambda_2\sigma_2}\left(\kappa_2^2-\lambda_1^2\right)-t_2 e^{\kappa_2\sigma_2}\left(\lambda_1^2-\lambda_2^2\right)\right]^2\right\}. \end{aligned} \tag{A8}$$

In the case of real $k_{3,\pm}$, the contribution $2\pi i\,\mathrm{Res}(k_{3,+})$ must be replaced with

$$\pi i[\mathrm{Res}(k_{3,+})+\mathrm{Res}(k_{3,-})] = 4\frac{\sigma_1^2}{\sigma_2}c_2t_2\left(\kappa_2^2-\lambda_2^2\right)^2 e^{\sigma_2(\kappa_2+\lambda_2)}\cos\left(\Delta R\sqrt{\left|\frac{c_2\kappa_2^2e^{\lambda_2\sigma_2}+t_2\lambda_2^2e^{\kappa_2\sigma_2}}{c_2e^{\lambda_2\sigma_2}+t_2e^{\kappa_2\sigma_2}}\right|}\right)$$
$$\times\left\{c_1e^{\lambda_1\sigma_1}\left[c_2e^{\lambda_2\sigma_2}\left(\kappa_1^2-\kappa_2^2\right)+t_2e^{\kappa_2\sigma_2}\left(\kappa_1^2-\lambda_2^2\right)\right]-t_1e^{\kappa_1\sigma_1}\left[c_2e^{\lambda_2\sigma_2}\left(\kappa_2^2-\lambda_1^2\right)-t_2e^{\kappa_2\sigma_2}\left(\lambda_1^2-\lambda_2^2\right)\right]\right\}^2$$
$$\Big/\left\{\Delta R\left(c_2e^{\lambda_2\sigma_2}+t_2e^{\kappa_2\sigma_2}\right)\left[c_2e^{\lambda_2\sigma_2}\left(\kappa_1^2-\kappa_2^2\right)+t_2e^{\kappa_2\sigma_2}\left(\kappa_1^2-\lambda_2^2\right)\right]^2\left[c_2e^{\lambda_2\sigma_2}\left(\kappa_2^2-\lambda_1^2\right)\right.\right.$$
$$\left.\left.-t_2e^{\kappa_2\sigma_2}\left(\lambda_1^2-\lambda_2^2\right)\right]^2\right\}. \tag{A9}$$

In general, the obtained formula for (A5) is a combination of Yukawa-like and exponential functions. Looking at the final expressions from the perspective of λ_1 and λ_2, one can see that there are several exponent terms that differ in their characteristic "length scale," some of them even divergent for growing λ_i. This explains the sensitivity of the model to core parameters, and it is probably the reason for the numerical difficulties encountered in the fitting procedure when λ_i are varied.

Interestingly, the contribution (A9) might introduce oscillatory behavior, which is apparently missing in Sec. III E. However, this contribution appears for $-\frac{\kappa_2^2}{\lambda_2^2}c_2e^{\sigma_2(\kappa_2-\lambda_2)} > t_2 > -c_2e^{\sigma_2(\kappa_2-\lambda_2)}$, which means that t_2 must be negative. In our model, $t_2 < 0$ requires $\epsilon_2 < 0$ [by (90)], so only cases 3, 6, and 9 from Fig. 4 could be affected by oscillations from (A9). This means that in the discussed model, it is not possible to choose the core parameters that provide oscillations in cases 2, 7, and 8 from Fig. 4. Therefore, this effect is most likely embedded in the neglected part of the effective interaction.

[1] C. N. Likos, Phys. Rep. **348**, 267 (2001).
[2] A. Strander, H. Sedgwick, F. Cardinaux, W. C. K. Poon, S. U. Egelhaaf, and P. Schurtenberger, Nature (London) **432**, 492 (2004).
[3] E. R. Weeks, J. C. Crocker, and D. A. Weitz, J. Phys.: Condens. Matter **19**, 205131 (2007).
[4] D. Marenduzzo, K. Finan, and P. R. Cook, J. Cell. Biol. **175**, 5 (2006).
[5] H. Dietsch, V. Malik, M. Reufer, C. Dagallier, A. Shalkevich, M. Saric, T. Gibaud, F. Cardinaux, F. Scheffold, A. Stradner, and P. Schurtenberger, Chimia **62**, 805 (2008).
[6] A. Kudrolli, Rep. Prog. Phys. **67**, 209 (2004).
[7] S. Aumaitre, C. A. Kruelle, and I. Rehberg, Phys. Rev. E **64**, 041305 (2001).
[8] J. P. Hansen and I. R. McDonald, *Theory of Simple Liquids* (Elsevier Academic, London, 2006).
[9] H. N. W. Lekkerkerker and R. Tuinier, *Colloids and the Depletion Interaction* (Springer, London, 2011).
[10] S. Asakura and F. Oosawa, J. Polym. Sci. **33**, 183 (1958).
[11] S. Asakura and F. Oosawa, J. Chem. Phys. **22**, 1255 (1954).
[12] A. Vrij, Pure Appl. Chem. **48**, 471 (1976).
[13] K. Yaman, C. Jeppesen, and C. M. Marques, Europhys. Lett. **42**, 221 (1998).
[14] P. R. Lang, J. Chem. Phys. **127**, 124906 (2007).
[15] D. G. Grier, Nature (London) **424**, 810 (2003).
[16] A. G. Yodh, K. Lin, J. C. Crocker, A. D. Dinsmore, R. Verma, and P. D. Kaplan, Phil. Trans. R. Soc. Lond. A **359**, 921 (2001).
[17] E. Donth, H. Huth, and M. Beiner, J. Phys.: Condens. Matter **13**, L451 (2001).
[18] C. Dalle-Ferrier, C. Thibierge, C. Alba-Simionesco, L. Berthier, G. Biroli, J. P. Bouchaud, F. Ladieu, D. L'Hôte, and G. Tarjus, Phys. Rev. E **76**, 041510 (2007).
[19] C. Donati, S. C. Glotzer, P. H. Poole, W. Kob, and S. J. Plimpton, Phys. Rev. E **60**, 3107 (1999).
[20] B. Doliwa and A. Heuer, Phys. Rev. E **61**, 6898 (2000).
[21] A. C. Mitus, A. Z. Patashinski, A. Patrykiejew, and S. Sokolowski, Phys. Rev. B **66**, 184202 (2002).
[22] J. C. Crocker and D. G. Grier, Phys. Rev. Lett. **73**, 352 (1994).
[23] K. Kegler, M. Salomo, and F. Kremer, Phys. Rev. Lett. **98**, 058304 (2007).
[24] P. G. Bolhuis, A. A. Louis, J. P. Hansen, and E. J. Meijer, J. Chem. Phys. **114**, 4296 (2001).
[25] A. A. Louis, E. Allahyarov, H. Löwen, and R. Roth, Phys. Rev. E **65**, 061407 (2002).
[26] M. Dijkstra, R. van Roij, and R. Evans, Phys. Rev. E **59**, 5744 (1999).
[27] M. Dijkstra and J. M. Brader, J. Phys.: Condens. Matter **11**, 10079 (1999).
[28] V. Heinonen, A. Mijailovi, C. V. Achim, T. Ala-Nissila, R. E. Rozas, J. Horbach, and H. Löwen, J. Chem. Phys. **138**, 044705 (2013).
[29] G. Yatsenko, E. J. Sambriski, M. A. Nemirovskaya, and M. Guenza, Phys. Rev. Lett. **93**, 257803 (2004).
[30] J. McCarty, I. Y. Lyubimov, and M. G. Guenza, Macromolecules **43**, 3964 (2010).
[31] F. Sagués, J. M. Sancho, and J. García-Ojalvo, Rev. Mod. Phys. **79**, 829 (2007).
[32] M. Majka and P. F. Góra, Acta Phys. Pol. B **43**, 1133 (2012).
[33] M. Majka and P. F. Góra, Phys. Rev. E **86**, 051122 (2012).
[34] M. Majka and P. F. Góra, Acta Phys. Pol. B **44**, 1099 (2013).
[35] M. Chaichian and A. Demichev, *Path Integrals in Physics* (IOP, London, 2001), Vol. I.
[36] J. Dautenhahn and C. K. Hall, Macromolecules **27**, 5399 (1994).
[37] A. A. Louis, P. G. Bolhuis, and J. P. Hansen, Phys. Rev. E **62**, 7961 (2000).

[38] R. Finken, J. P. Hansen, and A. A. Louis, J. Stat. Phys. **110**, 1015 (2003).
[39] R. Kubo, M. Toda, and N. Hashitsume, *Statistical Mechanics I* (Springer, Berlin, 1985).
[40] K. Huang, *Statistical Mechanics* (Wiley, New York, 1987).
[41] C. Hoheisel and R. Zhang, Phys. Rev. A **43**, 5332 (1991).
[42] K. R. Sütterlin, A. Wysocki, A. V. Ivlev, C. Räth, H. M. Thomas, M. Rubin-Zuzic, W. J. Goedheer, V. E. Fortov, A. M. Lipaev, V. I. Molotkov, O. F. Petrov, G. E. Morfill, and H. Löwen, Phys. Rev. Lett. **102**, 085003 (2009).
[43] A. V. Ivlev, S. K. Zhdanov, H. M. Thomas, and G. E. Morfill, Europhys. Lett. **85**, 45001 (2009).

Polymer unfolding and motion synchronization induced by spatially correlated noise

M. Majka* and P. F. Góra
Marian Smoluchowski Institute of Physics, Jagiellonian University, Reymonta 4, 30-059 Kraków, Poland
(Received 14 August 2012; published 19 November 2012)

The problem of a spatially correlated noise affecting a complex system is studied in this paper. We present a comprehensive analysis of a two-dimensional model polymer chain, driven by the spatially correlated Gaussian noise, for which we have varied the amplitude and the correlation length. The chain model is based on a bead-spring approach, enriched with a global Lennard-Jones potential and angular interactions. We show that spatial correlations in the noise inhibit the chain geometry dynamics, enhancing the preservation of the polymer shape. This is supported by the analysis of correlation functions of both the module length and angles between neighboring modules, which have been measured for the noise amplitude ranging over three orders of magnitude. Moreover, we have observed the correlation length dependent bead motion synchronization and the spontaneous polymer unfolding, resulting from an interplay between chain potentials and the spatially structured noise.

DOI: 10.1103/PhysRevE.86.051122 PACS number(s): 05.40.Ca, 36.20.−r, 61.43.Fs, 87.15.A−

I. INTRODUCTION

The understanding of diffusion in complex media is crucial for both modeling conformation transitions in biomolecules and intracellular transport. It is also well known that various systems organize spontaneously in response to random forcing [1] and that the introduction of temporal correlations into the noise can lead to synchronization effects [2]. A well-established framework to simulate these phenomena is provided by Langevin equations, which introduce the concept of stochastic force mimicking the molecular collisions [3]. An important advance in this formalism has been the introduction of the generalized Langevin equation (GLE), which reproduces the anomalous diffusion thanks to the time-correlated stochastic force and the corresponding integral memory kernel, which represents the friction [4]. Recently, Kou [4] derived the GLE from a microscopic model of a particle coupled to a large number of oscillators, thus showing that the particle-environment interaction is essential for the occurrence of temporal correlations in thermal noise. However, it is remarkable that this theory explains solely the temporal aspect of diffusion, while little work has been done to understand its spatial counterpart. This has led us to investigate the problem of a spatially correlated noise affecting a complex system.

The collective media behavior, which is random but characterized by a certain correlation length λ, occurs at a length scale of micrometers in the context of hydrodynamic interactions, e.g., in colloid sedimentation [5,6] or in the study of active particle motion [7]. However, the spatial correlations at the lower length scale play a fundamental role in the theory of phase transitions [8], among which the liquid-glass transition is of special interest. During this transition, the particles suffer a dramatic drop of mobility without the emergence of structural ordering [9]. This phenomenon has been intensively researched for the past two decades, and according to extensive simulations [10,11], it is characterized by the occurrence of spatial correlations in the particles' motion [11], which is recognized as the formation of different-sized clusters [10,12]. Choosing a single moment in time, one could interpret these clusters as a source of a disturbance which is random at the large length scale ($\gg\lambda$) but ordered at the length scale of λ. Figure 1 illustrates this idea. The temporal evolution of this system is still indeterministic, as it "randomly reorders." We propose that this behavior could be imitated by the spatially correlated noise, which is affecting a subsystem, in our case, a model two-dimensional polymeric chain.

We have simulated the chain based on the bead-spring approach under the forcing of spatially correlated Gaussian noise (SCGN) for which we have varied the correlation length and the amplitude. Our previous findings regarding the stiffening of the chain under the SCGN, shown with the aid of the reduced dynamics, have been published in [13]. However, our further investigation into this system, which involves the extension of the parameters' range and the measurements of chain characteristics, has revealed several new effects, namely, bead motion synchronization, increased time correlation of both module length and angles between modules, the inhibition of the average module length growth, and, most notably, the chain unfolding induced by the increased correlation length.

Our simulations are related to the actual physical situation by the choice of λ. Unfortunately, currently, there are few experimentally accessible quantities that describe the collective molecular behavior in the vicinity of the glass transition and can be measured for the variety of temperatures [14]. One of these parameters is the number of cooperatively rearranging molecules [15], which has been reported to increase from 1 in the liquid phase to approximately 10 in the glass phase [15]. Additionally, these results are qualitatively similar for the different chemical compounds [15]. On the other hand, the direct measurements of the correlation length are scarce and limited to a specific experimental setup, as, e.g. in [16], which reports λ to be of the order of two to four molecule diameters. These measurements suggest that λ covering up to five chain nodes is physically meaningful.

This paper has following structure: in Sec. II the methods of the SCGN generation are introduced, and in Sec. III we propose the equations of motion and the correlation function. In Sec. IV we present our polymer model, and Sec. V briefly discusses simulation methods. Sections VI to IX present the

*maciej.majka@uj.edu.pl

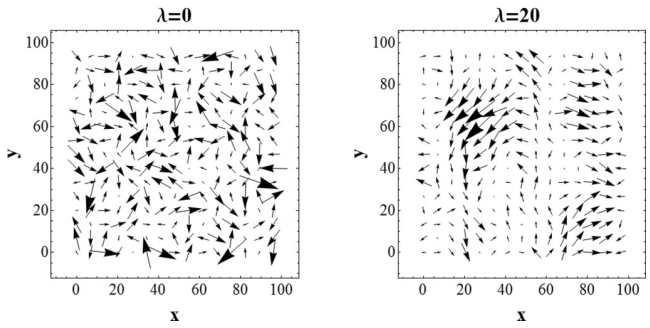

FIG. 1. Spatially correlated random vectors with correlation length λ, generated on a regular network. For $\lambda = 0$ the pattern is entirely random, but for $\lambda = 20$ the ordered clusters can be noticed.

results regarding each effect with an interpretation, and in Sec. X we summarize our findings.

II. MULTIPLE CORRELATED GAUSSIAN VARIABLES

The generation of multiple correlated Gaussian variables is a central problem in the simulation of SCGN driven systems; therefore we shall outline here the basic algorithm. Let's assume that we have two real vectors of random, zero-mean Gaussian variables, namely, $\vec{\xi}^T = (\xi_1, \ldots, \xi_N)$ and $\vec{\eta}^T = (\eta_1, \ldots, \eta_N)$, whose components satisfy the following correlation relations:

$$\langle \xi_i \xi_j \rangle = S_{ij}, \tag{1}$$

$$\langle \eta_i \eta_j \rangle = \delta_{ij}. \tag{2}$$

Here, δ_{ij} denotes the Kronecker delta, and S_{ij} are elements of the correlation matrix, defined as

$$\langle \vec{\xi} \vec{\xi}^T \rangle = \hat{S}. \tag{3}$$

The matrix $\hat{S}$ is symmetric and positively definite [17], so it is suitable for Cholesky decomposition [18], which factorizes $\hat{S}$ into a lower triangular matrix $\hat{L}$ and its transposition:

$$\hat{S} = \hat{L}\hat{L}^T. \tag{4}$$

The vector of correlated variables $\vec{\xi}$ is related to the uncorrelated vector $\vec{\eta}$ via a linear transformation [19]:

$$\vec{\xi} = \hat{L}\vec{\eta}. \tag{5}$$

This means that, given a correlation matrix, one can generate the correlated Gaussian vector $\vec{\xi}$ simply by sampling N times the normal distribution to obtain the components of $\vec{\eta}$ and then performing the transformation (5).

III. EQUATIONS OF MOTION AND CORRELATION FUNCTION

Our system is equivalent to an ordered set of N interacting material points on a plane, enumerated by the index i. The position of the ith point (or bead, as we will refer to it in the following) is $\vec{r}_i^{\,T} = (x_i, y_i)$. In order to simulate the trajectory $\{\vec{r}_i(t)\}_N$ of the whole system, we have to solve numerically a set of $2N$ stochastic equations of motion:

$$\begin{aligned} m\ddot{x}_i + \gamma \dot{x}_i + \partial_{x_i} U &= \xi_x(\vec{r}_i), \\ m\ddot{y}_i + \gamma \dot{y}_i + \partial_{y_i} U &= \xi_y(\vec{r}_i). \end{aligned} \tag{6}$$

Here, U is the potential energy of the system, which we will discuss in detail in the next section. $\vec{\xi}(\vec{r}_i)^T = [\xi_x(\vec{r}_i), \xi_y(\vec{r}_i)]$ is the two-dimensional SCGN, m is a bead mass, and γ is a friction constant. In the absence of a more relevant theory, we have applied the simplest friction model and have chosen γ to be constant. The differential equations (6) are, in principle, of second order, which we preserve for generality, but in the course of our simulations we have overdamped the system by choosing γ to be large enough.

We assume that the correlation function S_{ij} of stochastic forces acting on beads i and j should depend only on a relative distance between these beads, which is $r_{ij} = |\vec{r}_i - \vec{r}_j|$. Additionally, we assume that there are no cross correlations between the x and y components, which allows us to reduce the correlation relations to the form

$$\begin{aligned} \langle \xi_x(\vec{r}_i)\xi_x(\vec{r}_j)\rangle &= \langle \xi_y(\vec{r}_i)\xi_y(\vec{r}_j)\rangle = S(r_{ij}), \\ \langle \xi_x(\vec{r}_i)\xi_y(\vec{r}_j)\rangle &= 0. \end{aligned} \tag{7}$$

It should be emphasized that the correlation matrix $\hat{S}$ is a dynamical object and evolves in t as the relative distances $r_{ij}(t)$ do. The conditions (7) suggest the following procedure to integrate Eqs. (6): once all beads' positions $\{\vec{r}_i(t)\}_N$ at some moment t are determined, we can calculate the $N \times N$ correlation matrix and its Cholesky decomposition $\hat{L}$; next, according to (5), we shall use $\hat{L}$ and two different $\vec{\eta}$ to obtain $\{\xi_x(\vec{r}_i)\}_N$ and $\{\xi_y(\vec{r}_i)\}_N$. Finally, we can use them to perform an integration step, which gives $\{\vec{r}_i(t + \Delta t)\}_N$. The repeated Cholesky decompositions are the most computationally expansive part of our simulations, as the computational complexity of this decomposition is $O(N^3)$ [18].

Along with conditions (7), we assume that the correlation function S_{ij} is characterized by the correlation length λ, and it reproduces the standard Brownian diffusion for $\lambda \to 0$ [20], so

$$S(r_i(t), r_j(t')) \overset{\lambda \to 0}{=} \frac{2k_B T \gamma}{m} \delta(t - t'). \tag{8}$$

In the above formula k_B denotes the Boltzmann constant and T is temperature. Taking into account (7) and (8), we chose the exponentially decaying spatial correlation function, which resembles the displacement correlation function from [11] and [16]. We also neglect the temporal correlations, as we are interested in the effects of the purely spatially structured noise. Finally, the spatiotemporal correlation function reads

$$S(r_i(t), r_j(t')) = \sigma \frac{\gamma}{m} e^{-\frac{|\vec{r}_i - \vec{r}_j|}{\lambda}} \delta(t - t'), \tag{9}$$

where $\sigma = 2k_B T$ denotes the noise amplitude and we will refer to it as temperature, as it is proportional to the actual physical temperature.

In order to illustrate how the spatial correlations affect the noise pattern, we have applied (5) and (9) to generate the random vectors on a regular network. A snapshot of this simulation is presented in Fig. 1. One can easily notice

clusters of correlated vectors; however, this pattern changes dramatically for every new generation.

IV. THE MODEL OF A POLYMER CHAIN

The polymeric chain is an archetype of many biomolecules; thus we have chosen it as a test object for our simulation. Our model is based on the bead-spring approach, in which i and $i+1$ beads interact with a harmonic potential:

$$U_R = \sum_{i=1}^{N-1} \frac{1}{2} k_1 (|\vec{r}_{i+1} - \vec{r}_i| - d_0)^2. \tag{10}$$

Every bead is also the source of the Lennard-Jones type interaction, which provides the excluded volume effect and

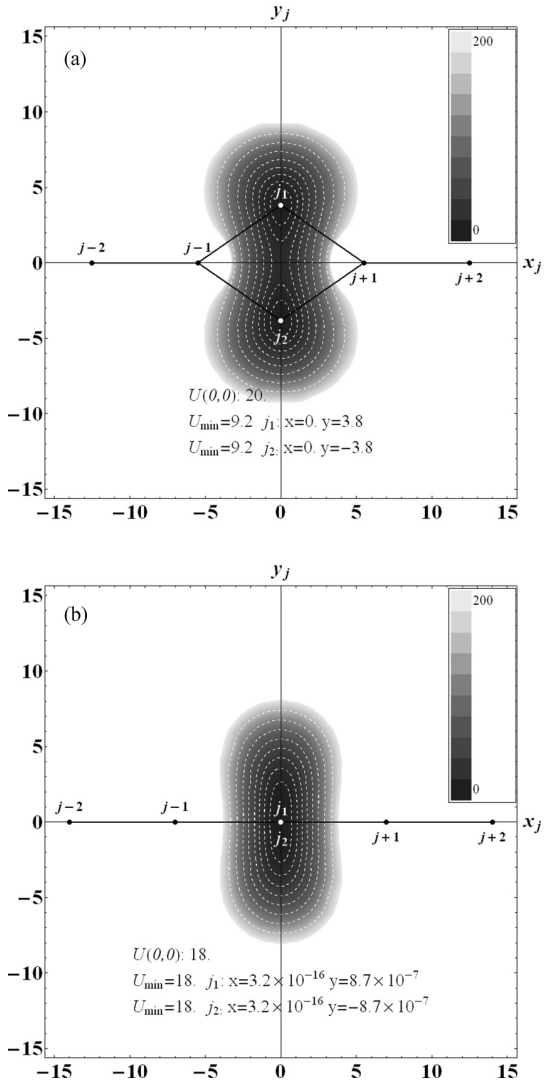

FIG. 2. The energetic landscape for a single bead interacting with its four nearest neighbors. The potential parameters are chosen according to Table I. (a) The distance $|\vec{r}_{j+1} - \vec{r}_{j-1}| = l_0$, and j_1 and j_2 enumerate two possible positions of the jth bead that minimize the potential energy. $U(0,0)$ is the height of the energy barrier, and $U_{\min}$ is the depth of the minimum. (b) The distance $|\vec{r}_{j+1} - \vec{r}_{j-1}| = 1.25 l_0$, and j_1 and j_2 merge into a single minimum as the energy barrier disappears.

TABLE I. The parameters of the system chosen for simulation.

N	k_1	d_0	k_2	l_0	ϵ	σ_{LJ}	γ	m
128	7	7	2	11	1	3	20	1

an interaction between the distant tails of the chain:

$$U_{LJ} = \sum_{i,j}^{N} \epsilon \left(\frac{\sigma_{LJ}^{12}}{|\vec{r}_i - \vec{r}_j|^{12}} - \frac{\sigma_{LJ}^{6}}{|\vec{r}_i - \vec{r}_j|^{6}} \right). \tag{11}$$

Finally, we introduce a harmonic interaction between beads i and $i+2$ which resembles angular interactions:

$$U_\psi = \sum_{i=1}^{N-2} \frac{1}{2} k_2 (|\vec{r}_{i+2} - \vec{r}_i| - l_0)^2. \tag{12}$$

The total potential energy U is equal to

$$U = U_R + U_\psi + U_{LJ}. \tag{13}$$

For $\epsilon = 0$ (no U_{LJ} contribution) the potential energy is minimized when the beads' positions satisfy

$$|\vec{r}_{i+1} - \vec{r}_i| = d_0, \quad |\vec{r}_{i+2} - \vec{r}_i| = l_0. \tag{14}$$

In this case, all of the minimum energy conformations are equienergetic. In fact, unless $l_0 > 2d_0$, once $\vec{r}_1$ and $\vec{r}_2$ are chosen to satisfy $|\vec{r}_2 - \vec{r}_1| = d_0$, the third bead can be positioned in two ways, so the relation $|\vec{r}_3 - \vec{r}_1| = l_0$ is also fulfilled. Successively applying the conditions (14) to the following beads, one can build numerous minimum energy geometries. When $U_{LJ} \neq 0$, the energetic structure of the chain becomes more complex, but if $d_0 > \sigma_{LJ}$ and $\epsilon \simeq k_1$, the Lennard-Jones contribution becomes a perturbation. However, the U_{LJ} influence makes the structures no longer equienergetic.

When the chain's energy is not minimized, the dynamical topography of the potential energy surface depends on both potentials' parameters and the local geometry of the chain. An effective way to represent snapshots of this energy landscape for a single bead is to take into account its four nearest neighbors. An example of such a landscape is reproduced in Fig. 2(a). We have chosen the values of potential energy parameters (Table I) such that the double-minimum structure is distinct and holds for a wide range of local conformations. However, this structure is extremely sensitive to a single parameter, which is the distance $l_j = |\vec{r}_{j+1} - \vec{r}_{j-1}|$. Whenever $l_j > 2d_0$, the two minima tend to merge rapidly into a single one, positioned in line with beads $j-1$ and $j+1$. This is reproduced in Fig. 2(b). This fact significantly affects the high temperature dynamics of the chain, as is show in Sec. IX.

V. SIMULATION

Applying the classical Runge-Kutta method modified for stochastic differential equations [21], we have simulated the system described by Eqs. (6) with the potential (13) and the parameters from Table I. The number of beads has been set to $N = 128$, the bead's mass has been chosen as $m = 1$, and the friction coefficient γ has been set to 20, which overdamped the system.

In our research, we have explored three regimes of temperature. First, we have varied the noise amplitude σ from 0 to 20 units with an interval of 1 unit, and we have increased the correlation length λ from 0 to 20 with an interval of 5 units. In the second regime, we have increased σ from 25 to 250 with an interval of 25 units, and in the third regime we have explored the region from 300 to 1000 units with an interval of 100 units. For the second and the third regimes we have varied λ from 0 to 50 with an interval of 10 units. For each pair of λ and σ we have performed 64 runs, starting from different initial positions. The initial coordinates have been chosen so that the distance between nearest neighbors is equal to d_0, but the angle between modules has been chosen randomly from $\pi/2$ to $3\pi/2$.

The integration step has been set to $1/128$ time unit, and each simulation lasted 2148 time units. The data for the first 100 units have been rejected due to system thermalization. If not stated otherwise, the data have been collected once per time unit. We have gathered the data regarding bead synchronization, module length, and the angle between modules.

VI. THE BEAD MOTION SYNCHRONIZATION

The introduction of the spatial correlations into the noise implies that, at a length scale comparable to the correlation length λ, the stochastic force vectors have similar direction and value. Therefore, one could expect that the motion of beads with a relative distance lower than λ will synchronize. This prediction has been fully confirmed.

As the measure of synchronization at a particular moment t, we have chosen the normalized product of two beads' velocities, distanced by n nodes, which has been averaged along the chain:

$$K_n(t) = \frac{1}{(N-n)} \sum_{i=1}^{N-n} \frac{\vec{v}_i \cdot \vec{v}_{i+n}}{v_i v_{i+n}} = \langle \cos \theta_{i,i+n} \rangle. \qquad (15)$$

Here $\theta_{i,i+n}$ is an angle between velocity vectors of the ith and $(i+n)$th beads. For each run, we have gathered $K_n(t)$, which was time averaged to obtain the synchronization factor K_n. The maximal value of $K_n = 1$ indicates a fully synchronized motion, while $K_n = 0$ implies the opposite.

We have gathered the data for n ranging from 1 to 9. A representative sample of our results is show in Fig. 3. The rise in the synchronization factor K_n along with increasing λ and $\sigma = \text{const}$ is evident. Conversely, the level of synchronization is almost constant for $\lambda = \text{const}$ and varying amplitude, which is valid even for temperatures below $\sigma = 5$. For every n, the factor K_n grows from 0 for $\lambda = 0$ to the maximal observed value for $\lambda = 50$, which is approximately 0.8 for $n = 1$ and 0.3 for $n = 9$.

A further insight into the synchronization comes from the rearrangement of data, so K_n is represented as a function of n, with λ and T being parameters. Figure 4 shows the qualitative similarity between these data for two extreme temperatures ($\sigma = 1$ and $\sigma = 1000$). To obtain a quantitative measure of the decrease in synchronization with the rise in n, we have fitted our data with the exponential decay model:

$$K_n = A_\lambda e^{-B_\lambda n}. \qquad (16)$$

This model proved to be an accurate description of data, as the coefficient of determination R^2 exceeded 0.99 for all fits, except those with $\lambda = 0$, for which $B_{\lambda=0}$ has no physical meaning.

In Fig. 5, we have juxtaposed the values of B_λ for $\sigma \geqslant 25$, at which temperature the behavior of the chain is noise

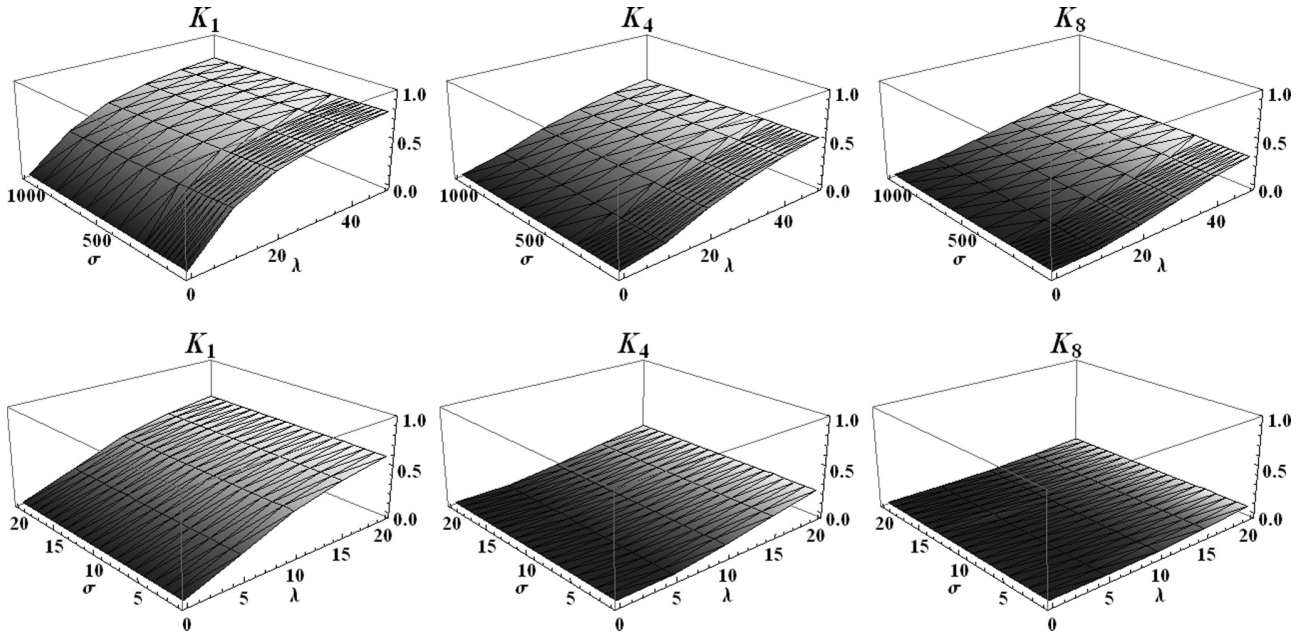

FIG. 3. The synchronization factor K_n for $n = 1,4,8$ as a function of the correlation length λ and the noise amplitude σ. Each column contains the data for the same n in (top) the high temperature regime and (bottom) the low temperature regime.

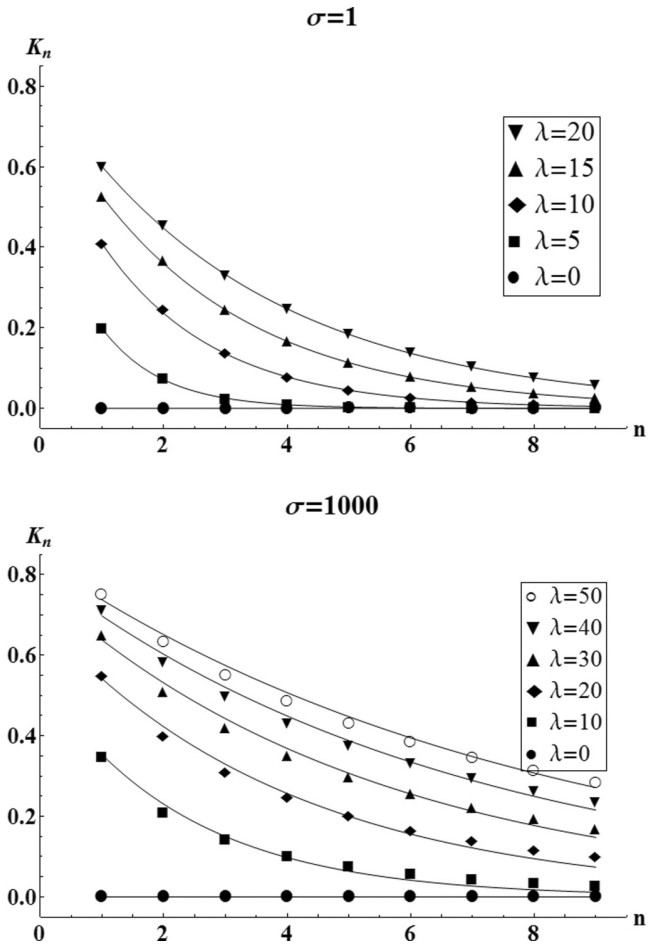

FIG. 4. The synchronization factor K_n for two extreme values of temperature as a function of the beads' distance n. The data have been fitted with the model: $K_n = A_\lambda e^{-B_\lambda n}$.

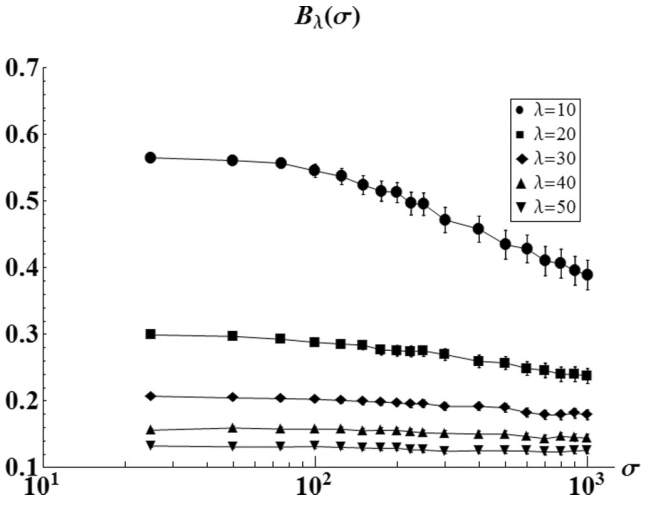

FIG. 5. The synchronization decay factor B_λ as a function of temperature for $\sigma \geqslant 25$.

dominated. According to Fig. 5, the value of B_λ is mainly determined by λ and decreases when the temperature grows by two orders of magnitude. However, for $\lambda \geqslant 30$ this fall is rather insignificant; thus, we conclude that the noise correlation length is the primary factor that influences the effective range of synchronization along the chain.

VII. BEAD MOTION CORRELATION

The other quantities that are also affected by the presence of spatial correlations in noise are the time correlation of the module length and the time correlation of the angles between neighboring modules. These two characteristics describe the time evolution of the chain geometry.

By a module we understand two neighboring beads, so the length of the jth module, at certain moment t, is defined as

$$d_j(t) = |\vec{r}_j(t) - \vec{r}_{j-1}(t)|. \tag{17}$$

The angle between two neighboring modules is defined by the positions of the three following beads:

$$\psi_j(t) = \angle[\vec{r}_{j-1}(t), \vec{r}_j(t), \vec{r}_{j+1}(t)]. \tag{18}$$

With the beginning at the center of the coordinate system, vectors $\vec{r}_i$ are equivalent to the coordinates on a plane; thus they are applied in the above definition. Additionally, one has to remember that the angle ψ_j is directed and varies from 0° to 360° (with 180° indicating that three beads are exactly in line), so the angles have to be measured in a unified way along the whole chain, conserving the initial numeration of beads.

The time correlation function of angles has been calculated in a following way:

$$C_\psi(\tau) = \frac{1}{C_\psi} \sum_{k=0}^{T} \sum_{j=2}^{N-1} [\psi_j(t_k + \tau) - \langle\psi\rangle][\psi_j(t_k) - \langle\psi\rangle]. \tag{19}$$

Here, we introduce the additional summation over j due to the fact that we have $N - 2$ angles for a single moment t, which allows us to increase statistics and obtain a correlation measure for a whole chain, rather than a single site. The normalization factor C_ψ has been chosen as

$$C_\psi = \sum_{k=0}^{T} \sum_{j=2}^{N-1} [\psi_j(t_k) - \langle\psi\rangle]^2, \tag{20}$$

which means that $C_\psi(0) = 1$. Finally, $\langle\psi\rangle$ reads

$$\langle\psi\rangle = \frac{1}{T(N-2)} \sum_{k=0}^{T} \sum_{j=2}^{N-1} \psi_j(t_k). \tag{21}$$

In a strict analogy to the angle correlation function $C_\psi(\tau)$, we can define the module length correlation function $C_d(\tau)$:

$$C_d(\tau) = \frac{1}{C_d} \sum_{k=0}^{T} \sum_{j=2}^{N} [d_j(t_k + \tau) - \langle d\rangle][d_j(t_k) - \langle d\rangle]. \tag{22}$$

C_d and $\langle d\rangle$ are defined similarly to their angle counterparts.

An example of collected data is presented in Fig. 6. In the high temperature regime (approximately for $\sigma > 200$), both $C_\psi(\tau)$ and $C_d(\tau)$ are positive functions, asymptotically falling from 1 to 0, which is typical of stochastic motion. However, they differ significantly in the low temperature regime. While $C_\psi(\tau)$ preserves its high temperature profile (but with values much closer to 1), $C_d(\tau)$ resembles a linear function, falling

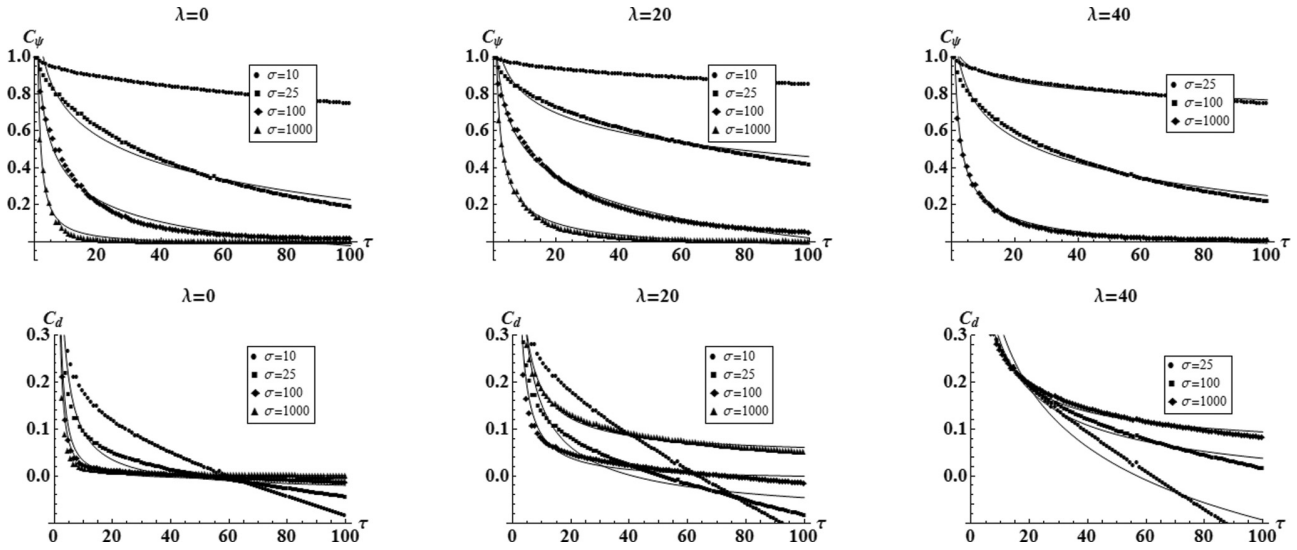

FIG. 6. A representative selection of the module length correlation functions $C_d(\tau)$ and the correlation functions of the angles between neighboring modules $C_\psi(\tau)$. Profiles have been fitted with the function $a\tau^\alpha + c$.

below 0 with the increase in τ. This long-term behavior of the low-temperature $C_d(\tau)$ indicates the domination of the deterministic motion in this temperature regime. In the context of the energetic landscape, introduced in Sec. IV, we can suppose that the beads are trapped at the bottom of their potential energy wells and perform the damped oscillations, slightly perturbed by the noise. Apparently, while the bead motion makes d_j oscillate, it barely affects the angles, so the values of $C_\psi(\tau)$ are relatively close to 1. Additionally, the comparison between $C_\psi(\tau)$ and $C_d(\tau)$ suggests that the module length behavior evolves from deterministic into purely stochastic as the temperature grows, while $\psi_j(t)$ is of a stochastic nature for all σ.

In order to measure the influence of σ and the noise correlation length λ on $C_\psi(\tau)$ and $C_d(\tau)$, we have fitted the profile functions with the following model:

$$C(\tau) = a\tau^\alpha + c. \tag{23}$$

Despite the inaccuracy for $\tau \to 0$ and a divergence in the low-temperature regime, the power function model provides quantitative information on the σ and λ dependencies, thanks to the α parameter. The values of α_d and α_ψ plotted against σ and λ are shown in Fig. 7. As expected, for all values of σ and λ, α is negative and tends to 0 with the decrease in temperature. However, for constant λ, α_ψ decreases at a similar pace with the growth of σ, while α_d varies slowly for most of the temperature range but jumps rapidly below $\sigma = 100$.

The increase in the noise correlation length λ affects both α_d and α_ψ in a similar way, namely, the larger λ is, the lower the $|\alpha|$ obtained is. This means that the correlation functions $C_\psi(\tau)$ and $C_d(\tau)$ decrease at a slower rate, so $d_j(t)$ and $\psi_j(t)$ vary less rapidly over time. Therefore, the dynamics of the chain's shape becomes attenuated, and a current conformation is preserved longer.

VIII. MODULE LENGTH DISTRIBUTION

We have also investigated the marginal distribution $\Gamma(d)$ of the module length d and its temperature evolution, with and without spatial correlations in noise. Taking into account that $d_j(t)$ may express an oscillatory behavior, we have reduced the time interval between data acquisitions to 1/4 of a time unit to avoid synchronization effects. The spatial resolution of histograms has been set to 0.21 length unit.

The profile of $\Gamma(d)$ proved to be a single peaked distribution, concentrated in the vicinity of its mean, with slight, but noticeable, asymmetry. Therefore, in order to describe $\Gamma(d)$ we have calculated its first moment, second central moment (presented in Fig. 8), and the skewness.

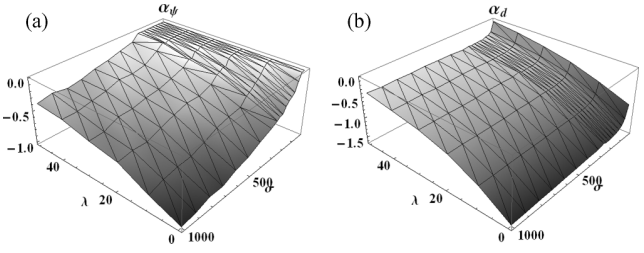

FIG. 7. The exponents (a) α_d and (b) α_ψ resulting from fitting the power function to correlation profiles $C_d(\tau)$ and $C_\psi(\tau)$.

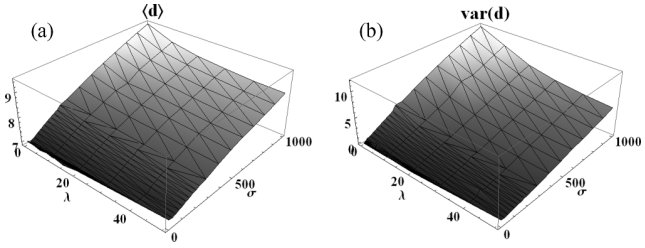

FIG. 8. Statistical characteristics of the module length distribution $\Gamma(d)$ as functions of the noise correlation length λ and the temperature σ: (a) the mean module length $\langle d \rangle$ and (b) the variance of $\Gamma(d)$.

The skewness grows with σ from 0 to approximately 0.6 and saturates at this value. Fortunately, the asymmetry proved to be small enough, so the other parameters are still physically meaningful. The dispersion of distribution $\Gamma(d)$ grows with increasing σ [Fig. 8(b)], which is expected diffusive behavior, but the mean distance $\langle d \rangle$ also tends to grow [Fig. 8(a)], starting from $\langle d \rangle \approx d_0$. This fact, along with the nonzero skewness, indicates that the underlying potential is asymmetric, and, indeed, the presence of the repulsive Lennard-Jones core provides the reflective barrier preventing two neighboring beads from closing up. Conversely, the lengthening of d_j is still possible as the energy well is not as steep for $d_j > d_0$ as in the opposite situation.

The spatial correlations in noise play an inhibitory role for the process of the temperature dependent broadening of $\Gamma(d)$. Here $\lambda \neq 0$ slows down the growth of both $\langle d \rangle$ and the dispersion of $\Gamma(d)$. This effect can be explained by the following reasoning. When a thermal bath imposes noncorrelated, stochastic forces on beads j and $j+1$, this commonly results in a nonzero relative force stretching (or shrinking) the module. However, when the noise is spatially correlated, stochastic forces applied to beads become similar at the length scale of λ, which significantly reduces the relative forcing, and in turn, d is less affected by the noise.

IX. POLYMER UNFOLDING

The most unexpected effect that stems from the presence of the spatial correlations in the noise is the spontaneous linearization of the chain. Having defined angles $\psi_j(t)$ in (18), we have been able to obtain a marginal distribution of angles $\Phi(\psi)$ depending on temperature σ and correlation length λ. Similar to the previous section, the data have been collected every $1/4$ of a time unit, with the resolution of the histogram set to 1°. The representative selection covering the entire range of tested parameters is presented in Fig. 9.

The temperature evolution of distribution $\Phi(\psi)$ gives an insight into how the angular degrees of freedom are freed with the rise in temperature. Let us analyze the $\lambda = 0$ case first. For low temperatures ($\sigma < 10$) we obtain a symmetric bimodal distribution, which is in accordance with the predictions of the double-minimum energetic landscape. However, for extremely low temperatures ($\sigma < 3$) one can see four distinct peaks, which indicates that, probably, there are two additional minima. We can suppose that they are shallow, as they disappear quickly with the rise in σ. For temperatures from $\sigma = 5$ to $\sigma = 13$ the increased penetration of the energy barrier region is noticeable, and the third peak appears exactly at $\psi = 180^\circ$. At $\sigma = 13$ the two peaks indicating energy minimums can no longer be distinguished, and from then on, the shape of the distribution gradually transforms from a bell-like curve into a triangle profile, which is completed approximately for $\sigma = 100$. After that, the distribution broadens systematically with the increase in temperature.

The introduction of $\lambda \neq 0$ affects $\Phi(\psi)$ in a subtle, but remarkable, way. In the low noise regime ($\sigma < 25$) the increase in λ retards the temperature evolution of $\Phi(\psi)$, so the bimodal profile is preserved in a wider interval of σ. However, when σ exceeds 50, the profile transforms into a heavy-tailed peaked

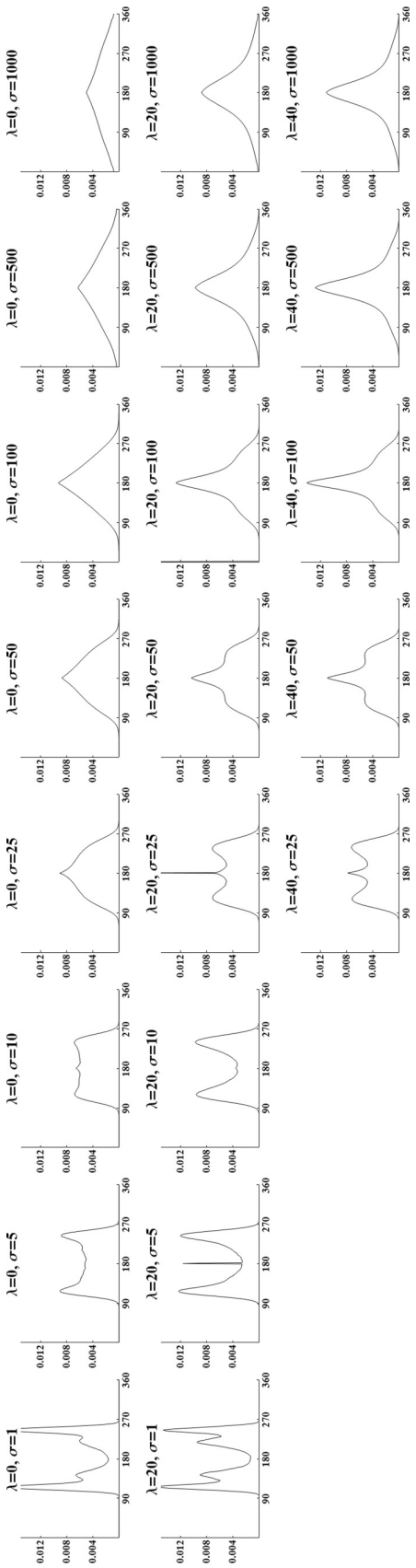

FIG. 9. The temperature evolution of angle distribution $\Phi(\psi)$ for noise correlation length $\lambda = 0$, $\lambda = 20$, and $\lambda = 40$.

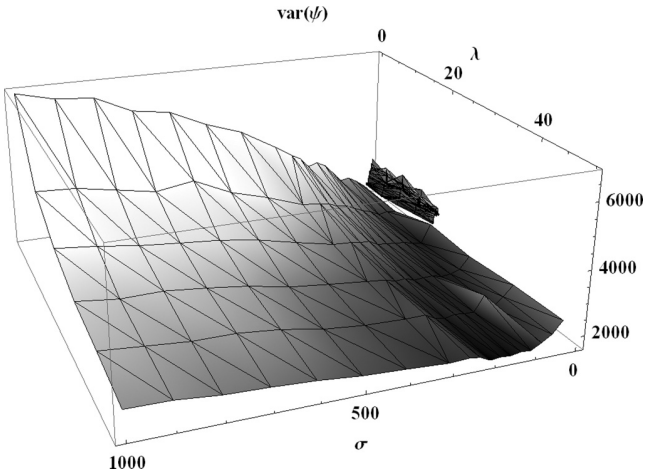

FIG. 10. The dispersion of distribution $\Phi(\psi)$ as a function of the noise correlation length λ and the temperature σ.

distribution, much more concentrated in the vicinity of $\psi = 180^\circ$ than in the case of $\lambda = 0$. The dispersion of $\Phi(\psi)$ is a measure of this effect, which shows that the higher λ is, the lower the value of $\Phi(\psi)$'s second central moment is. This indicates the linearization of the chain and thus its unfolding. This is illustrated in Fig. 10.

The single-peaked distribution with $\langle\psi\rangle = 180^\circ$ indirectly suggests that for high temperatures the system selects the single-minimum energetic configuration similar to the one shown in Fig. 2(b) rather than the double-minimum landscape in Fig. 2(a). Knowing that the growth of the distance $l_j = |\vec{r}_{j+1} - \vec{r}_{j-1}|$ is a crucial factor in the merging of energetic minima, we can suppose that l_j is subject to interplay similar to d_j, namely, the repulsive cores do not allow beads $j-1$ and $j+1$ to close up, while the stretching of l_j is still possible. With sufficiently high noise, this asymmetry could lead to the rise in $\langle l\rangle$ and the domination of the single-minimum potential topology. This transition seems inherent to the system, and it is present regardless of the spatial correlations in noise. Nevertheless, once the single-minimum state prevails, the bead can explore the well, provided there is enough relative forcing, and for $\lambda \neq 0$ this forcing drops dramatically. As a result, despite the high noise amplitude, the bead is trapped near the minimum, so the angles between modules cannot vary as much as in the noncorrelated case. This leads to a narrowing of $\Phi(\psi)$ around $\psi_j = 180^\circ$.

X. SUMMARY

Summarizing our research, the most salient conclusion one can draw is that spatial correlations in thermal noise have an overall inhibitory effect on the system. This manifests in the general attenuation of the chain geometry dynamics both in the time domain, where the polymer tends to preserve its current shape, and in the temperature domain, where the evolution of the statistical chain properties is retarded. It is also in agreement with our previous findings that the presence of nonzero correlations reduced the ability of the chain to transfer between different conformations [13].

Such a behavior is not a surprise, as we can perceive the introduction of the spatial correlations into the thermal bath as a freezing of environment, and in the limit $\lambda \to +\infty$, this should also lead to the complete attenuation of the system dynamics. In this context, it is not solely the temperature of the thermal bath that influences the system behavior but also the structure of the environment. Our approach, which decouples the temperature from the environmental correlation length, allows for more plasticity than the explicit simulation of thermal bath particles but requires proper scaling to avoid unphysical situations.

[1] F. Sagués, J. M. Sancho, and J. García-Ojalvo, Rev. Mod. Phys. **79**, 829 (2007).
[2] R. Morgado, M. Cieśla, L. Longa, and F. A. Oliveira, Europhys. Lett. **79**, 10002 (2007).
[3] C. W. Gradiner, *A Handbook of Stochastic Processes*, 3rd ed. (Springer, Berlin, 2004).
[4] S. C. Kou, Ann. Appl. Stat. **2**, 501 (2008).
[5] P. N. Segrè, E. Herbolzheimer, and P. M. Chaikin, Phys. Rev. Lett. **79**, 2574 (1997).
[6] E. Guazzelli, Phys. Fluids **13**, 1537 (2001).
[7] P. T. Underhill, J. P. Hernandez-Ortiz, and M. D. Graham, Phys. Rev. Lett. **100**, 248101 (2008).
[8] J. J. Binney *et al.*, *The Theory of Critical Phenomena* (Oxford University Press, Oxford, 1992).
[9] M. Mosayebi, E. Del Gado, P. Ilg, and H. C. Öttinger, Phys. Rev. Lett. **104**, 205704 (2010).
[10] C. Donati, S. C. Glotzer, P. H. Poole, W. Kob, and S. J. Plimpton, Phys. Rev. E **60**, 3107 (1999).
[11] B. Doliwa and A. Heuer, Phys. Rev. E **61**, 6898 (2000).
[12] A. C. Mitus, A. Z. Patashinski, A. Patrykiejew, and S. Sokolowski, Phys. Rev. B **66**, 184202 (2002).
[13] M. Majka, P. F. Góra, Acta Phys. Pol. B **43**, 1133 (2012).
[14] E. Donth, H. Huth, and M. Beiner, J. Phys. Condens. Matter **13**, L451 (2001).
[15] C. Dalle-Ferrier, C. Thibierge, C. Alba-Simionesco, L. Berthier, G. Biroli, J. P. Bouchaud, F. Ladieu, D. L'Hôte, and G. Tarjus, Phys. Rev. E **76**, 041510 (2007).
[16] E. R. Weeks, J. C. Crocker, and D. A. Weitz, J. Phys. Condens. Matter **19**, 205131 (2007).
[17] R. Kubo, M. Toda, and N. Hashitsume, *Statistical Mechanics II* (Springer, Berlin, 1985).
[18] G. H. Golub and C. F. Van Loan, *Matrix Computations* (Johns Hopkins University Press, Baltimore, 1996).
[19] R. Wieczorkowski and R. Zieliński, *Komputerowe generatory liczb losowych* (WNT, Warsaw, 1997).
[20] N. G. van Kampen, *Stochastic Processes in Physics and Chemistry* (Elsevier, Amsterdam, 1987).
[21] P. E. Kloeden and E. Platen, *Numerical Solutions of Stochastic Differential Equations*, 3rd ed. (Springer, Berlin, 1999).

REINTERPRETING POLYMER UNFOLDING EFFECT INDUCED BY A SPATIALLY CORRELATED NOISE*

M. Majka, P.F. Góra

The M. Smoluchowski Institute of Physics, Jagiellonian University
Reymonta 4, 30-059 Kraków, Poland

(Received May 10, 2013)

This paper provides additional insight into the effect of spontaneous unfolding of the model polymeric chain driven by spatially correlated noise, described in M. Majka, P.F. Góra, *Phys. Rev.* **E86**, 051122 (2012). We examine the statistical data on the linearized chain substructures to find that the global unfolding effect arises mainly from the cumulation of short, 2-segment-long fragments, scattered along the chain. This supports an alternative view of spatially correlated noise as both the source of disturbance and the conformation preserving factor.

DOI:10.5506/APhysPolB.44.1099
PACS numbers: 05.40.Ca, 36.20.–r, 61.43.Fs, 87.15.A–

1. Introduction

Noise induced phenomena *e.g.* spontaneous ordering induced by white noise [1] or the system synchronization induced by colored noise [2] are of great concern for contemporary research. However, while the white noise and Langevin dynamics are standard tools in complex system simulations [1] and also the time-correlated noise combined with Generalized Langevin Equations becomes increasingly popular in applications [3], little research has been devoted to the spatially correlated noise.

The spatially correlated noise is a disturbance which is random at large length-scale, but ordered at the length-scale of correlation length λ. This kind of disturbance forms a space pattern which can evolve over time in a completely random or temporally correlated manner, tough preserving a certain ordering below the length λ. Such noise is designed to resemble

* Presented at the XXV Marian Smoluchowski Symposium on Statistical Physics, "Fluctuation Relations in Nonequilibrium Regime", Kraków, Poland, September 10–13, 2012.

a collectively acting heat-bath affecting a sub-system of interest with possible application to soft matter simulations. Random, yet spatially correlated phenomena are encountered especially in the research on glass-forming [4–6], active particles swimming [7, 8] and sedimentation in crowded solutions [9, 10].

Our main results regarding the influence of spatially correlated noise on the model two dimensional polymeric chain has been already published in [11] and [12]. The paper [11] is a primary reading which provides the most complete introduction to the topic as well as full support for our findings, and we shall relate to this article repeatedly in the present work. Thus, it is preferable that the Reader will familiarize himself with [11] before proceeding. Nevertheless, we should present here a brief summarization of the most important notions from [11] to facilitate the reading.

We have examined a two dimensional polymer chain model based on the bead-spring approach with the nearest neighbor, angular and excluded volume interactions. The position of ith bead has been simulated according to the equations of motion

$$\begin{cases} m\ddot{x}_i + \gamma\dot{x} + \partial_{x_i}U = \xi_x\left(\vec{r}_i, t\right) , \\ m\ddot{y}_i + \gamma\dot{y} + \partial_{y_i}U = \xi_y\left(\vec{r}_i, t\right) . \end{cases} \tag{1}$$

Here m is a bead mass, γ is a friction constant and U is total potential energy (to be specified in Section 2). While we have kept inertial terms in (1) for the sake of numerical accuracy, the constants were chosen so $\gamma/m = 20$, which was enough to over-damp the system. $\vec{\xi}(\vec{r}, t)$ denotes the spatially correlated Gaussian noise, whose correlation function reads

$$\left\langle \xi_x\left(\vec{r_i}, t_2\right) \xi_x\left(\vec{r_j}, t_1\right) \right\rangle = \left\langle \xi_y\left(\vec{r_i}, t_2\right) \xi_y\left(\vec{r_j}, t_1\right) \right\rangle = \sigma \frac{\gamma}{m} e^{-\frac{\left|\vec{r}_i - \vec{r}_j\right|}{\lambda}} \delta(t_2 - t_1) , \tag{2}$$

$$\left\langle \xi_x\left(\vec{r_i}, t_2\right) \xi_y\left(\vec{r_j}, t_1\right) \right\rangle = 0 . \tag{3}$$

Here, σ is temperature and λ is a correlation length.

We have found that the presence of spatial correlations in the noise results in several measurable effects, which are: chain stiffening (discussed comprehensively in [12]), the synchronization of beads motion, increased time correlation of segments lengths and angles between segments, and the spontaneous unfolding of the chain [11].

The effect of spontaneous unfolding is of special interest in this paper, and we would like to discuss it now in a greater detail. In [11], we have presented the distribution of angles between neighboring polymer segments (defined by equation (10), Section 2) for a range of temperatures and correlation lengths. For sufficiently high temperatures, these data proved to be single peaked distributions, symmetric around their mean values. The peak

in probability is associated with neighboring segments lying exactly in line, yet these distributions are broad and, especially for the uncorrelated noise, the raise in σ increases the variance of distribution. Having introduced spatial correlations into noise, the distributions become remarkably narrower and, for constant temperature, the longer correlation length is, the lower is the variance. In the range of correlation lengths which we have tested (approximately from 1 to 7 segment equilibrium lengths), this fall of variance seems to asymptotically approach certain minimal, yet non-zero, value. Additionally, for constant and non-zero correlation length, the temperature dependent growth of variance is significantly mitigated in comparison to the uncorrelated case.

From the preceding description, one can conclude that neighboring segments tends to linearize, yet the distribution of angles gives no information what structures prevail in the chain geometry to give rise to this effect, and, especially, how long those linearized fragments are. We will elaborate on this in Section 3. In Section 4, we will outline a new interpretation of the unfolding effect, alternative to one given in [11]. However, first, we would like to present our polymer model in Section 2.

2. Polymer chain model

Our polymer chain model consists of N interacting material points (beads) for which we have applied the Langevin dynamics. The beads interact via three kinds of potential that form a bead-spring model enriched with angular and excluded volume interactions. The total potential energy of the system reads

$$U = U_R + U_\psi + U_{\mathrm{LJ}} \,. \tag{4}$$

U_R is the nearest neighbor interaction, which resembles bonds, and it is defined by

$$U_R = \sum_{i=1}^{N-1} \tfrac{1}{2} k_1 \left(|\vec{r}_{i+1} - \vec{r}_i| - d_0 \right)^2 \,. \tag{5}$$

Here, $\vec{r}_i$ is a position of the ith bead and d_0 is an equilibrium segment length. The angular interaction U_ψ is modeled with the second nearest neighbor interaction, which is

$$U_\psi = \sum_{i=1}^{N-2} \tfrac{1}{2} k_2 \left(|\vec{r}_{i+2} - \vec{r}_i| - l_0 \right)^2 \,. \tag{6}$$

In this case, l_0 defines the preferable distance between ith and $i+2$nd bead, and to ensure a saw-like chain conformation, it should be satisfied that [11]

$$l_0 < 2d_0 \,. \tag{7}$$

Finally, we introduce the global Lennard–Jones interaction U_{LJ}

$$U_{\mathrm{LJ}} = \sum_{i,j}^{N} \epsilon \left(\frac{\sigma_{\mathrm{LJ}}^{12}}{|\vec{r}_i - \vec{r}_j|^{12}} - \frac{\sigma_{\mathrm{LJ}}^{6}}{|\vec{r}_i - \vec{r}_j|^{6}} \right) . \tag{8}$$

This interaction brings in the effect of excluded volume thanks to its repulsive core (its diameter is proportional to σ_{LJ}) and provides the attraction whenever the distant parts of chain close up. Parameters k_1, k_2 and ϵ are scaling constants and their exact values used in simulations are gathered in Table I.

TABLE I

The parameters of the system chosen for simulations. These parameters provided the saw-like chain conformation, presence of repulsive core for each bead and the over-damping of beads' motion.

N	k_1	d_0	k_2	l_0	ϵ	σ_{LJ}	γ	m
128	7	7	2	11	1	3	20	1

For the detailed discussion of the minimal energy structures, a single bead energy landscape and a chain geometry dynamics, please see [11], but here we would like to outline only the most important facts. A single bead moves in a potential well determined by the positions of its neighboring beads. For parameters chosen according to Table I, this well has most often a double minimum, so there are two possible positions of a bead relative to the rest of the chain that minimize the bead's energy. Both, the depth of each minimum and their exact positions change as the local geometry evolves, yet the double-well landscape is predominant and fairly invulnerable to changing angles between segments. However, this double-well structure is extremely sensitive to the increase in distance between the nearest neighbors of the bead. Such stretching causes the two minima to merge rapidly into one, which is positioned in line with the nearest neighbors. This is seen as a local frustration of the chain, because the minimal energy structures never tend to linearize.

In [11], the conformational dynamics of chain is examined primarily with two parameters, namely the length of the segment

$$d_j(t) = |\vec{r}_j(t) - \vec{r}_{j-1}(t)| \tag{9}$$

and the angle between neighboring segments, which has been obtained from positions $\vec{r}_j$ of the three following beads

$$\psi_j = \angle(\vec{r}_{j-1}, \vec{r}_j, \vec{r}_{j+1}) . \tag{10}$$

This angle is directed, varies from 0 to 360° and it is always measured with respect to certain initial numeration of beads. It is also scaled, so $\psi_j = 180°$ indicates three beads being exactly in-line. We have found that for parameters from Table I and low ($3 < \sigma < 12$) uncorrelated noise, the system prefers the saw-like conformation, with $d_j \approx d_0$. For such σ, the distribution of angles ψ_j is symmetric, double peaked, with one peak approximately at 110° and the other at 250°. This is consistent with the double-well picture, described in the previous paragraph. With the rise in temperature above $\sigma = 13$, the two peaks melt down and the third peak appears exactly at $\psi_j = 180°$. This process is gradually retarded with the rise in noise's spatial correlation length, *e.g.* for $\lambda = 50$ the single peaked distribution appears as late as for $\sigma > 25$. From now on, the distribution of ψ_j evolves as described in the introductory section, giving rise to the effect of unfolding.

In general, the prevalence of mono-peaked ψ_j distributions can be explained by the presence of repulsive Lennard–Jones cores. The rise in temperature increases the mobility of beads, but such cores prevent beads from closing up. Effectively, average distances between beads tend to grow and many sites along the chain suffer frustration, which means that these sites are govern by the single-minimum energy landscape. In other words, the random disturbance can much easier stretch the system than squeeze it. While such mechanism could be accepted for the uncorrelated noise, which provides relative forcing at all length-scales, it is not clear why it should be also valid for the spatially correlated noise, which introduces low relative forcing below correlation length. Namely, the ability of noise to compress or extend the system at the length-scale of λ is remarkably reduced, and, in fact, in [11], it has been shown that spatial correlations mitigate the growth in average distances. Therefore, for $\lambda \neq 0$ the chain should be less affected by the noise, but ψ_j indicates the opposite. In order to explain this contradiction, we would like to provide another data, regarding the length of linearized fragments and their distribution along the chain.

3. Chain substructures

Having determined ψ_j angles in one particular moment, it is also possible to count the lengths of linearized fragments of the chain. Two neighboring segments are treated as linearized if the angle between them satisfies $\psi_j \in [160°, 200°]$. The length of a linearized fragment is defined as the number n of following beads that sequentially fulfill the given criterion. Scanning along the chain, a single segment is assigned to the longest linearized fragment it belongs to. Repeating the scans for different moments leads to the statistics of such fragments' lengths. A single, non-linearized segment is taken as the fragment with $n = 1$, so only fragments with $n \geq 2$ are truly indicating linearization.

We have conducted simulations for σ ranging from 1 to 1000 and λ from 0 to 50. In the range $1 \leq \sigma \leq 20$, with the temperature increment equal 1, we have varied λ from 0 to 20 by 5 units. For $25 \leq \sigma \leq 250$, the σ increment was 25 and in the interval $300 \leq \sigma \leq 1000$ the increment was equal 100. For these two temperature ranges, the correlation length has been varied by 10 from 0 to 50. For each pair of σ and λ, we have performed 64 runs, from which the statistics has been averaged out. During each run, which lasted 2^{18} steps, we have measured statistics every 32 steps. There have been also 100×2^7 initial steps for system thermalization, during which there has been no acquisition of data.

We have collected data regarding the abundance of n-segment-long linearized fragments in the form of a histogram. The value P_n of the nth bin estimates the probability that a single segment belongs to an n-segment-long linearized fragment, with P_1 occupied by non-linearized segments. For

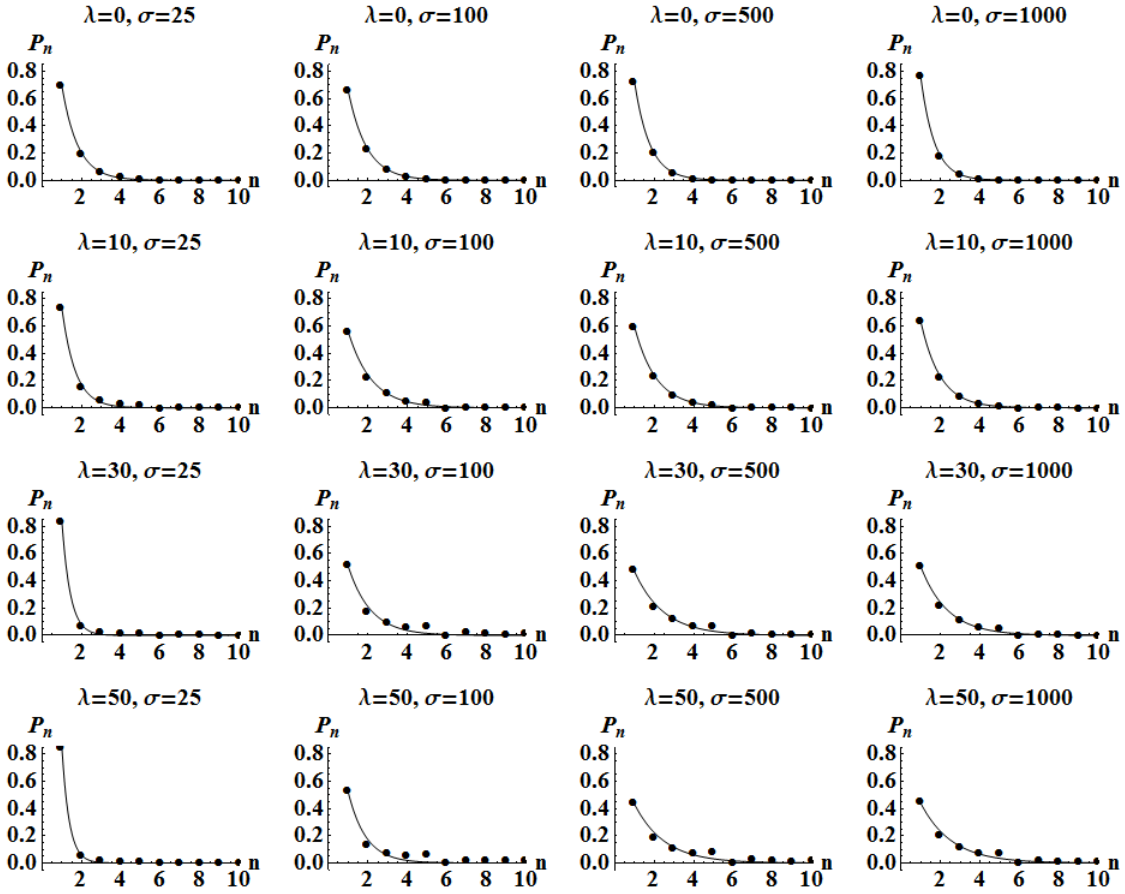

Fig. 1. The comparison of histograms P_n for temperatures $25 \leq \sigma \leq 1000$ and correlation lengths $0 \leq \lambda \leq 50$. Data from simulations (black dots) has been fitted with exponential decay function (solid line). With increasing σ histograms approach exponential distribution.

selected temperatures, these data are presented in Fig. 1. Histograms have been fitted with an exponential decay function

$$p(n) = A \exp\left(-\frac{n-1}{\kappa}\right) . \tag{11}$$

This model proved to fit the data exceptionally well for $\lambda = 0$ and $\lambda = 10$ with $\sigma > 75$, but for lower temperatures fits became inaccurate. This is also the problem for larger λ, for which fits seem to gradually improve with the rise in σ, yet this process is spanned over even larger temperature interval (see Fig. 1). The general trend of P_n is to exceed the values predicted with $p(n)$, thus the exponential decay model is a lower boundary approximation at best. Nevertheless, Fig. 1 suggests that exponential distribution is correct at least in the large temperature limit. The retardation of the temperature dependent evolution has been also described in [11], regarding the angles distributions, thus it is no surprise to encounter it in the current dataset.

Despite discussed limitations, the model (11) provides a reasonable approximation for $n = 1, 2, 3$-long fragments, which are the most abundant. Parameter κ from equation (11) indicates overall trend in the linearization effect, and its relative error has been lower that 5% for all fitted curves. In Fig. 2, we have visualized κ with respect to the correlation length and temperature. In general, the behavior of κ is complicated, yet for $\sigma > 300$, it is evidently growing with the rise in λ from approximately 0.7 to 1.6. This is clear indication that the participation of short, linearized structures is λ dependent and increases with the growing correlation length.

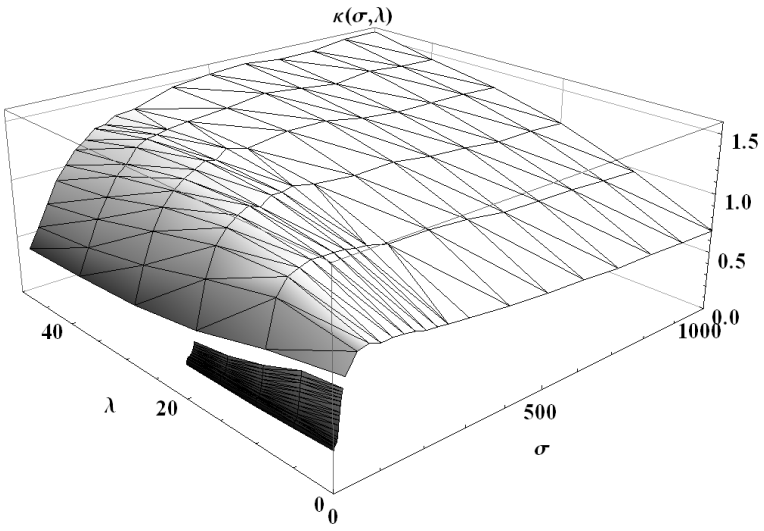

Fig. 2. Decay constant κ (see equation (11)) as a function of temperature σ and correlation length λ. For $\sigma > 300$, the κ is growing with λ, which reflects the increasing linearization of the chain.

We have also compared P_n for $n = 2, 3, 4$ in relation to λ and σ (Fig. 3). Typically, for $\sigma > 300$ and $\lambda \geq 10$, P_2 exceeds 0.16, P_3 is approximately equal to 0.1 and P_4 reaches 0.06, which means that 2 to 4 long fragments are dominant structures and usually contain around 30% of segment population. In general, from 15% to 45% of segments form linearized structures, so fragments which are even longer than 4 are also present, yet significantly less abundant (*e.g.* P_6 is always smaller than 0.01) and they are not vital for the unfolding effect. Additionally, knowing that two linear fragments are separated by at least one non-linearized segment, we can suppose that the linearized fragments are distributed along the chain more or less uniformly. This means that the unfolding effect is a global process occurring parallel at multiple sites and based mainly on the short linear substructures.

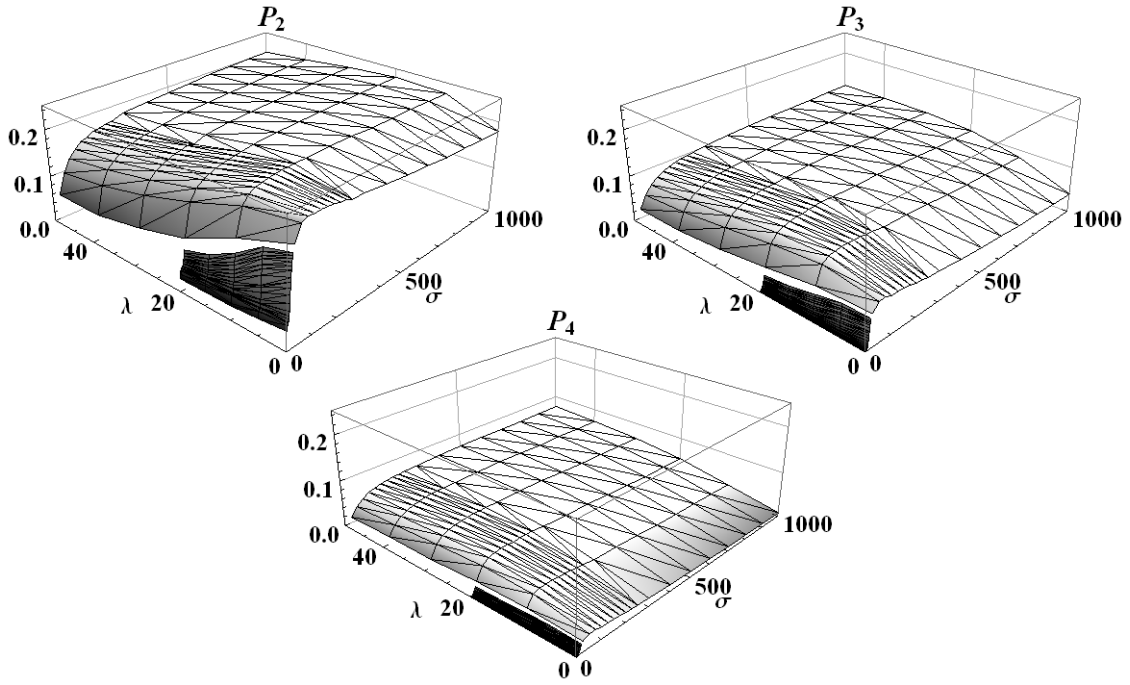

Fig. 3. P_n is a probability that a given chain segment belongs to an n-long linearized segment. Above, a comparison between P_2, P_3 and P_4 showing the abundance of these structures and their dependence on temperature σ and correlation length λ.

4. Reinterpretation of chain unfolding

Now, we would like to propose a reinterpretation of the chain unfolding process. As it has been stated in Section 2, local linearization indicates the single minimum energy landscape and can be interpreted as a frustration. The spatially correlated noise provides low relative forcing at the distances below λ, and, indeed, it does not directly affect the low-level structure itself.

However, the fragments of chain which are larger than λ can move in an uncorrelated manner. As a result of this incoherent motion, there appear frustrated sites, and they should occur randomly and uniformly along the chain. The exact positions of these frustrated sites depend only on the random realization of spatial noise pattern at certain time moment. Yet, this pattern evolves rapidly, so a single site that has been once frustrated can found itself in the middle of region which is not affected by the noise, because of spatial correlations. In this case, the lack of relative forcing hinders a local relaxation process, and so frustration is stabilized. In turn, frustrated sites are accumulated along the chain, which is manifested as the unfolding effect. Therefore, the interplay between frustrated sites production and the shape preserving influence of spatially correlated noise could be a main source of the unfolding effect. Such notion is in agreement with our data, both those presented in [11] and those discussed in previous section.

REFERENCES

[1] F. Sagués, J.M. Sancho, J. García-Ojalvo, *Rev. Mod. Phys.* **79**, 829 (2007).

[2] R. Morgado, M. Cieśla, L. Longa, F.A. Oliveira, *Eur. Phys. Lett.* **79**, 10002 (2007).

[3] S.C. Kou, *Ann. Appl. Stat.* **2**, 501 (2008).

[4] C. Donati *et al.*, *Phys. Rev.* **E60**, 3107 (1999).

[5] B. Doliwa, A. Heuer, *Phys. Rev.* **E61**, 6898 (2000).

[6] A.C. Mitus, A.Z. Patashinski, A. Patrykiejew, A. Sokolowski, *Phys. Rev.* **B66**, 184202 (2002).

[7] P.T. Underhill, J.P. Hernandez-Ortiz, M.D. Graham, *Phys. Rev. Lett.* **100**, 248101 (2008).

[8] P. Romanczuk *et al.*, *Eur. Phys. J. Special Topics* **202**, 1 (2012).

[9] P.N. Segré, E. Herbolzheimer, P.M. Chaikin, *Phys. Rev. Lett.* **79**, 2574 (1997).

[10] E. Guazzelli, *Phys. Fluids* **13**, 1537 (2001).

[11] M. Majka, P.F. Góra, *Phys. Rev.* **E86**, 051122 (2012).

[12] M. Majka, P.F. Góra, *Acta Phys. Pol. B* **43**, 1133 (2012).

Non-Gaussian polymers described by alpha-stable chain statistics: Model, effective interactions in binary mixtures, and application to on-surface separation

M. Majka* and P. F. Góra

Marian Smoluchowski Institute of Physics, Jagiellonian University, ul. prof. Stanisława Łojasiewicza 11, 30-348 Kraków, Poland

(Received 22 January 2015; published 13 May 2015)

The Gaussian chain model is the classical description of a polymeric chain, which provides analytical results regarding end-to-end distance, the distribution of segments around the mass center of a chain, coarse-grained interactions between two chains and effective interactions in binary mixtures. This hierarchy of results can be calculated thanks to the α stability of the Gaussian distribution. In this paper we show that it is possible to generalize the model of Gaussian chain to the entire class of α-stable distributions, obtaining the analogous hierarchy of results expressed by the analytical closed-form formulas in the Fourier space. This allows us to establish the α-stable chain model. We begin with reviewing the applications of Levy flights in the context of polymer sciences, which include: chains described by the heavy-tailed distributions of persistence length; polymers adsorbed to the surface; and the chains driven by a noise with power-law spatial correlations. Further, we derive the distribution of segments around the mass center of the α-stable chain and construct the coarse-grained interaction potential between two chains. These results are employed to discuss the model of binary mixture consisting of the α-stable chains. In what follows, we establish the spinodal decomposition condition generalized to the mixtures of the α-stable polymers. This condition is further applied to compare the on-surface phase separation of adsorbed polymers (which are known to be described with heavy-tailed statistics) with the phase separation condition in the bulk. Finally, we predict the four different scenarios of simultaneous mixing and demixing in the two- and three-dimensional systems.

DOI: 10.1103/PhysRevE.91.052602 PACS number(s): 36.20.−r, 05.40.Fb, 68.35.Dv, 82.35.Gh

I. INTRODUCTION

While the theory of Flory provides an accurate description of the ideal polymeric chains [1], factors such as complex environment interactions, adsorption, or designed chemical composition can lead to significant deviations from this model. The Flory approach is based on the Gaussian chain model, in which the conformation of a chain is equivalent to the trajectory of a particle undergoing the thermal Brownian motion [1]. In this model the chain is characterized by the Gaussian distribution of the nearest-neighbor distances, a fact that leads to the entire hierarchy of analytical results. In particular, the Gaussian shape propagates to such characteristics as end-to-end distance distribution [1], distribution of segments around the mass center of the chain [2], and the coarse-grained interaction potential between two chains in terms of the distance between their mass centers [3]. Deriving all of these characteristics is possible due to a single fact: the Gaussian distribution is α stable. Since there exists the entire class of α-stable, heavy-tailed distributions [4], this suggests that a natural and equally prolific generalization of the Gaussian chain model can be based on the α-stable distributions. Indeed, in this paper we discuss the α-stable chain model and calculate all of the characteristics analogous to the Gaussian model.

The first goal of this paper is to establish the physical context in which the α-stable distributions are relevant for the polymer sciences. Since the application of α-stable distributions (or Levy walks and Levy flights) in this context is not an entirely new concept, in Sec. II we review the relevant literature. In addition, we provide our own simulations of a model polymeric chain under the spatially correlated noise, which establish another context for our considerations.

The main part of this paper is focused on deriving and analyzing the different aspects of the α-stable chain model. In Sec. III we introduce the model itself. The distribution of nodes around the mass center of a chain is calculated in Appendix. In Sec. IV the coarse-grained model of interaction between two chains is established. All of these results are analytical and closed form in the Fourier space.

Another goal of this paper is to analyze the stability of binary mixtures composed of the α-stable chains. Understanding the behavior of binary mixtures is a vital problem in industry, medicine, wet nanotechnology, and biophysics. Usually, this problem is considered in the framework of spinodal decomposition. In this approach the local extremes of the free-energy functional are identified with respect to the thermodynamical parameters. While the local minima are associated with stable thermodynamic phases, which are insensitive to the fluctuations of parameters, the local maxima indicate the phase transitions. This method was successfully applied to find the decomposition condition in the mixtures of Gaussian particles [5,6], namely, there exists a well defined region of mixing and demixing, dependent on the proportion of gyration radii.

From the microscopic perspective, the stability of solution is governed by effective interactions [7], whose prediction is a classical problem of soft matter physics [8]. In the context of binary mixtures of Gaussian particles, Bolhuis *et al.* found via simulations that the interaction between particles of one species has also a Gaussian profile, but with an addition of a shallow attractive tail [9]. Similar results were predicted half analytically via closure-relations techniques in Refs. [10,11]. On the other hand, a simpler, but entirely analytical method has been recently proposed in Ref. [12] by the authors of

*maciej.majka@uj.edu.pl

this paper. Therein, we have studied the stability of Gaussian particles mixtures and our results proved similar to the spinodal decomposition analysis [5,6]. Since our methodology from Ref. [12] can be conveniently extended to the particles described with the α-stable profiles, we apply this approach in the current paper. As the main result of Sec. V, we generalize the spinodal decomposition condition for Gaussian particles to the entire class of particles based on the α-stable distributions. We discuss the validity of our methodology in Sec. VI.

Finally, in Sec. VII we employ the results regarding phase separation in binary mixtures to analyze the phase separation of adsorbed polymers versus their behavior in the bulk. As a result we predict the parameters for which the different combinations of simultaneous mixing or demixing on the surface and in the bulk can be achieved.

II. LEVY FLIGHTS IN POLYMER SCIENCES

Except for the Gaussian case, the asymptotic behavior of the α-stable distributions is of the power-law type $\propto 1/r^{\alpha+1}$ [4], where $\alpha \in [0,2]$ is the characteristic exponent of the distribution. A random walk characterized by such a heavy-tailed distribution of steps is known as a Levy flight. It is usually difficult to interpret Levy flights in physical terms, therefore let us discuss three situations justifying such statistics in the context of polymers.

The first scenario can be related to the non-Gaussian distribution of segment persistence lengths. The Gaussian chain model is usually derived from a discrete model, in which all segments have the same persistence length [1]. However, it can be also seen as the model for a chain made of unequal segments, whose persistence lengths follow the Gaussian distribution. This can be further generalized to the α-stable distribution, the idea suggested by Moon and Nakanishi in Ref. [13]. They proposed the Levy walk chain model, based on the formalism of turbulent flows [14] and calculated Flory exponents for this model. While no direct experimental confirmation of this idea is known to the present authors, non-Gaussian persistence length distribution might be the result of the varying chemical composition of a chain. For example, the DNA double strand is characterized by the persistence length much greater than a single base pair [15], but also certain sequences of chemical monomers can assemble into relatively long and stable structures of significant persistence length, such as protein domains [16]. A possible realization of such Levy flights could be the intrinsically disordered proteins, in which second-order structural motifs such as α helices coexist with disordered loops [17,18]. However, it should be mentioned that some numerical experiments on the structure of partially unfolded proteins indicate that Gaussian statistics is rather robust [19].

Another scenario is similar to the problem of a tracer, which mixes one- and three-dimensional diffusion. Such motion has been observed experimentally in DNA-binding proteins [20] and its simulations revealed the heavy-tailed distributions of steps along the polymer in certain configurations [21]. This behavior can be efficiently modeled with Levy flights [22]. In the context of polymers, we consider the adsorption of a chain to the surface. This problem was first analyzed by de Gennes from the scaling perspective in Refs. [23,24].

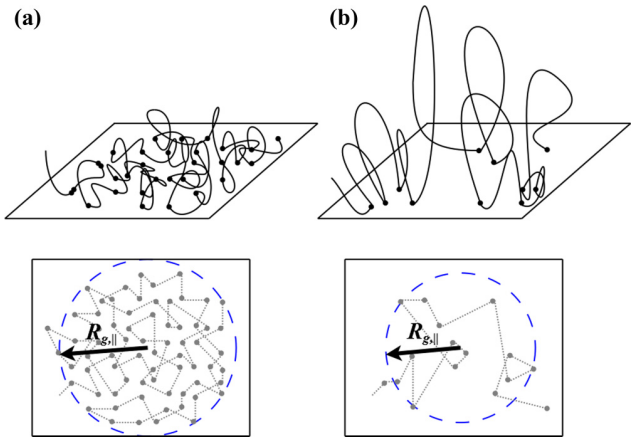

FIG. 1. (Color online) Top: schematic representation of a polymer adsorbed to the surface, dots indicate the adsorbed segments. Bottom: planar trajectories connecting the subsequent adsorbed segments. (a) In the strong adsorption regime freely-diffusing loops are short and subsequent adsorbed nodes are found close to each other. The radius of gyration parallel to the surface scale as $R_{g,||} \propto N^{3/4}$ [25]. (b) In the weak adsorption limit the long, freely diffusing loops are numerous and introduce Levy flights into the planar trajectory. $R_{g,||}$ scales as $\propto N^{3/5}$ [25].

For the intermediate attraction strength, only some fraction of segments is attached to the surface, while the loops that connect those segments diffuse into the bulk. Considering the projection of the chain on the surface, it has been argued by Bouchaud and Daoud [25] that the planar trajectory connecting adsorbed nodes can be modeled as Levy flights, since the subsequent adsorbed segments connected by a loop can be found at abnormally long distances. The schematic representation of a polymer in the strong versus the weak adsorption limit is shown in Fig. 1. Bouchaud and Daoud predict that for an adsorbed polymer its gyration radius parallel to the surface scales as $R_{g,||} \propto N^{3/4}$ for the strong adsorption and $R_{g,||} \propto N^{3/5}$ for the weak adsorption [25]. Within the Flory-type theory for Levy flights discussed in Ref. [25], the latter translates into the characteristic exponent of the distribution $\alpha = 1$ and the former demands $\alpha = 2$. This means that while in the strong adsorption regime the Levy flights and the Gaussian statistics are equivalent, for the weak adsorption limit $R_{g,||}$ should be modeled with power-law distributions.

One final interpretation can be related to the situation in which a polymer experiences a random, though spatially correlated, behavior of surrounding environment. Such conditions occur in the glassy state, in which the correlations are exponential [26–28], or near crystallization, in which case the scale-free behavior results in the power-law correlations [29]. In Ref. [30] we have simulated a two-dimensional model polymeric chain driven by the spatially correlated noise and observed the effect of spontaneous chain unfolding, i.e., a significant number of segments tends to form linearized structures, scattered along the chain. As we have shown in Ref. [31], this effect was mainly due to the short (2–3 segments) structures, but structures up to 50 segments were also observed. Such elongated fragments may act as Levy flights, provided that their distribution is wide enough.

The model from Ref. [30] consisted of a bead-spring chain with a global Lennard-Jones potential assigned to each bead and a second-nearest-neighbor harmonic interaction to induce nonlinear conformations. The system was driven by the noise $\boldsymbol{\xi}$, whose spatial correlation function read:

$$\langle \boldsymbol{\xi}(\mathbf{r})\boldsymbol{\xi}(\mathbf{r}+\Delta\mathbf{r})\rangle \propto \exp(-|\Delta\mathbf{r}|/\lambda). \tag{1}$$

For the purpose of the current paper we have repeated the simulations from Ref. [30], replacing the exponential correlations in the noise with a heavy-tailed function, based on the Cauchy distribution, namely:

$$\langle \boldsymbol{\xi}(\mathbf{r})\boldsymbol{\xi}(\mathbf{r}+\Delta\mathbf{r})\rangle \propto 1/[1+(|\Delta\mathbf{r}|/\lambda)^2]. \tag{2}$$

The data regarding the linearized fragments has been gather in the same fashion as in Ref. [31]. To improve statistics, the single set of parameters was simulated 128 times, otherwise, the details of the simulations remained the same as in Refs. [30] and [31]. In Fig. 2, we include the representative probability distributions S_n of finding the n-segments-long structure in the chain geometry. The data has been gathered from the regime of noise-dominated dynamics. With the growing correlation length λ the distribution S_n gradually develops a linear region in the log-log plot. For $\lambda \geqslant 40$, where relevant, we have fitted S_n for $n > 17$ with a power-law model $S_n = cn^{-(\alpha+1)}$. We obtain α ranging from 1.18 ± 0.39 to 2.44 ± 0.54, with the relative error typically at the level of 20–30 %. The uncertainty intervals for these values of α overlap with the interval $\alpha \in [0,2]$, which is expected for the asymptotic behavior of the α-stable distributions [4]. For comparison, the data have been also fitted with the exponential decay model $S_n = ae^{-n/b}$. While both the linear and exponential fit describe the tail part of S_n similarly well (in both cases $R^2 \simeq 0.8$) and, most probably, even for $\lambda = 50$ the distribution S_n eventually develops the exponential decay for $n \gg 50$, a power-law-like region suggests that in the special conditions of long-range spatial correlations the α-stable distributions might be a more relevant description of the chain statistics than the Gaussian distribution. For comparison we also include in Fig. 2 the data from Ref. [30], which preserve the exponential form in the entire range of parameters.

III. α-STABLE CHAIN MODEL

In the Gaussian chain model, the geometry of a chain is described as a random walk trajectory, in which the distribution of the distances between nearest neighbors is Gaussian, namely [1]:

$$G(|\mathbf{r}_{i+1}-\mathbf{r}_i|) = \left(\frac{2\pi b^2}{D}\right)^{-D/2} \exp\left(-\frac{D(\mathbf{r}_{i+1}-\mathbf{r}_i)^2}{2b^2}\right). \tag{3}$$

Here, D is the dimension of the system, b is usually interpreted as the length of a segment and $\mathbf{r}_i$ is the vector position of ith node. The characteristic function of G reads:

$$\phi_G(k) = \exp\left(-\frac{2b^2}{D}k^2\right). \tag{4}$$

Let us now consider the generalization of $G(|\mathbf{r}_{i+1}-\mathbf{r}_i|)$ to the α-stable distribution $P(|\mathbf{r}_{i+1}-\mathbf{r}_i|)$. The multivariate α-stable distributions are defined in terms of their characteristic functions, which can be written in the following parametrization [4]:

$$\phi(\mathbf{k}) = \begin{cases} \exp\left(-\int_{S_D} |\mathbf{k}\cdot\mathbf{s}|^\alpha \left(1 - i\,\mathrm{sgn}(\mathbf{k}\cdot\mathbf{s})\tan\frac{\pi\alpha}{2}\right)\Gamma(d\mathbf{s}) + i\mathbf{k}\cdot\boldsymbol{\mu}\right) & \text{for} \quad \alpha \neq 1 \\ \exp\left(-\int_{S_D} |\mathbf{k}\cdot\mathbf{s}| \left(1 + i\,\mathrm{sgn}(\mathbf{k}\cdot\mathbf{s})\frac{2\ln\mathbf{k}\cdot\mathbf{s}}{\pi}\right)\Gamma(d\mathbf{s}) + i\mathbf{k}\cdot\boldsymbol{\mu}\right) & \text{for} \quad \alpha = 1. \end{cases} \tag{5}$$

In the above definition $\Gamma(d\mathbf{s})$ stands for the spectral measure defined on the D-dimensional unit sphere S_D, $\mathbf{k}\cdot\mathbf{s}$ denotes the scalar product, and $\boldsymbol{\mu}$ is the vector of mean values. Since we are interested in the spherically symmetric distributions, we choose the uniform spectral measure $\Gamma(d\mathbf{s}) =$ const. [32]. Under such choice, and assuming $\boldsymbol{\mu} = 0$, the general parametrization can be simplified to the following form:

$$\phi(k) = \exp(-ck^\alpha), \tag{6}$$

where $k = |\mathbf{k}|$ and c is a constant. Eq. (4) is a special case of $\phi(k)$, and our choice of c should agree with $\phi_G(k)$ for $\alpha = 2$. Therefore, we postulate that c reads:

$$c = \frac{2b^\alpha}{D} \tag{7}$$

and, finally, the nearest-neighbor spatial distribution in the α-stable chain model reads:

$$P(|\mathbf{r}_{i+1}-\mathbf{r}_i|) = \frac{1}{(2\pi)^D}\int d\mathbf{k}\exp\left(i\mathbf{k}\cdot(\mathbf{r}_{i+1}-\mathbf{r}_i) - \frac{2}{D}b^\alpha k^\alpha\right). \tag{8}$$

Having established the nearest-neighbor spatial distribution $P(|\mathbf{r}_{i+1}-\mathbf{r}_i|)$, we can calculate such distribution for any pair of segments, namely:

$$\begin{aligned} P(|\mathbf{r}_i - \mathbf{r}_j|) &= \int d\mathbf{r}_{i+1}\ldots\int d\mathbf{r}_{j-1}\prod_{n=i+1}^{j} P(|\mathbf{r}_n - \mathbf{r}_{n-1}|) \\ &= \frac{1}{(2\pi)^D}\int d\mathbf{k}\exp\left(i\mathbf{k}\cdot(\mathbf{r}_i-\mathbf{r}_j) - \frac{2}{D}|i-j|b^\alpha k^\alpha\right), \end{aligned} \tag{9}$$

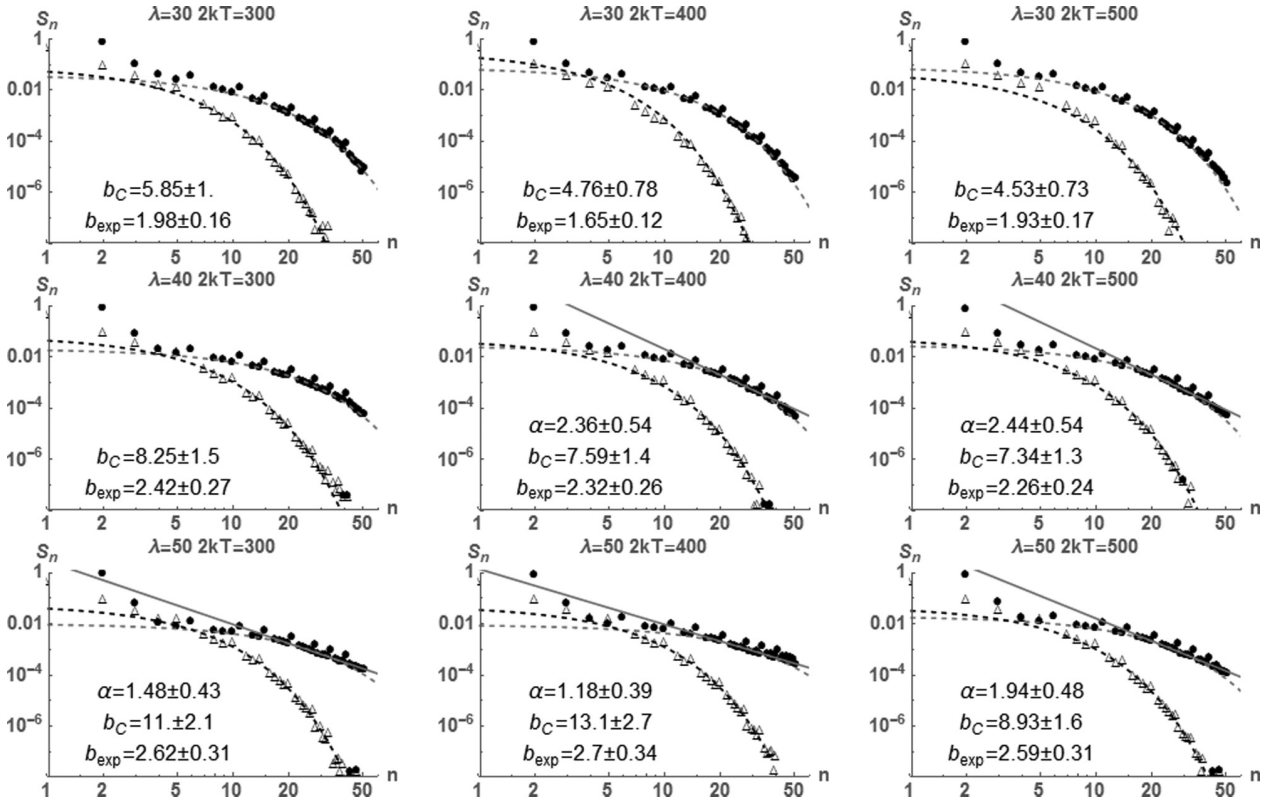

FIG. 2. The probability distribution S_n of finding the n-segment-long linearized fragment in a chain driven by the spatially correlated noise. Each plot represents the results for noise amplitude $2kT$ and correlation length λ. Triangles: exponential noise correlation function $\langle \boldsymbol{\xi}(\mathbf{r})\boldsymbol{\xi}(\mathbf{r}+\Delta\mathbf{r})\rangle \propto \exp(-|\Delta\mathbf{r}|/\lambda)$; dots: Cauchy noise correlation function $\langle \boldsymbol{\xi}(\mathbf{r})\boldsymbol{\xi}(\mathbf{r}+\Delta\mathbf{r})\rangle \propto 1/[1+(|\Delta\mathbf{r}|/\lambda)^2]$. The tail behavior ($n \geqslant 17$) has been fitted with exponential decay model $S_n = ce^{-n/b_i}$ (dashed lines) with b_i given on the plot. For $\lambda \geqslant 40$ the data has been also fitted with power law $S_n = cn^{-(\alpha+1)}$ for $n \geqslant 17$, indicating the power-law asymptotic behavior.

where we made use of α stability. For $\alpha = 2$ this formula comes down to the well known result for Gaussian chain [1]:

$$G(|\mathbf{r}_i - \mathbf{r}_j|) = \left(\frac{2\pi|i-j|b^2}{D}\right)^{-D/2} \exp\left(-\frac{D(\mathbf{r}_i-\mathbf{r}_j)^2}{2|i-j|b^2}\right). \tag{10}$$

It is also possible to calculate $\alpha = 1$ case explicitly:

$$P_{\alpha=1,D=3}(|\mathbf{r}_i - \mathbf{r}_j|) = \frac{16\pi|i-j|}{3} \frac{1}{\left(\frac{4|i-j|^2}{9} + r^2\right)^2}. \tag{11}$$

In particular, taking as i and j the first and the last segment respectively, we obtain the end-to-end distance distribution.

A classical problem in polymer physics is to predict the scaling behavior of radius of gyration R_g with the growing N. In order to do so, we will calculate R_g using a method mentioned in Ref. [13], namely $R_g = \langle r^\alpha \rangle^{1/\alpha}$, where $\langle . \rangle$ denotes the average:

$$\begin{aligned} R_g &= \left[\frac{1}{(2\pi)^D}\int d\mathbf{r} r^\alpha \int d\mathbf{k} \exp\left(i\mathbf{k}\cdot\mathbf{r} - \frac{2N}{D}b^\alpha k^\alpha\right)\right]^{1/\alpha} \\ &= b\left(\frac{2N}{D}\right)^{1/\alpha} \\ &\quad \times \left(\frac{1}{(2\pi)^D}\int d\mathbf{r}' r'^\alpha \int d\mathbf{k}' \exp(i\mathbf{k}'\cdot\mathbf{r}' - k'^\alpha)\right)^{1/\alpha}. \end{aligned} \tag{12}$$

This result is obtained via the change of variables $\mathbf{k}' = b(2N/D)^{1/\alpha}\mathbf{k}$ and $\mathbf{r}' = b^{-1}(2N/D)^{-1/\alpha}\mathbf{r}$, which completely factors the dependence on b and N out of the integral. Therefore, the scaling reads $R_g \propto bN^{1/\alpha}$.

While this scaling seems reasonable for $\alpha \geqslant 1$, it becomes questionable for $0 < \alpha < 1$, for which the scaling exponent of N becomes greater than 1. On the one hand, the examples from Sec. II use $\alpha \geqslant 1$ almost exclusively. In particular, Moon and Nakanishi in Ref. [13] introduce their more complicated Levy walk model to avoid $\alpha < 1$ problem and, in their approach, the scaling exponent of N is always lower than 1. On the other hand, Bouchaud and Daoud in Ref. [25] systematically discuss every possible value of α, pointing out that for $\alpha < 1$ the Flory correction from the self-avoiding nodes becomes irrelevant. In

conclusion, while $\alpha < 1$ seems physically unlikely, with so little literature on the subject it cannot be rejected at this point.

Finally, with $P(|\mathbf{r}_{i+1} - \mathbf{r}_i|)$ at our disposal, we can calculate the distribution of nodes around the mass center of the chain. This derivation is highly technical, so we include it in Appendix and here we discuss the final result only. In the limit of huge number of nodes N, the sought distribution reads:

$$P_{\mathrm{CM}}(|\mathbf{r}-\mathbf{R}|) = \frac{1}{(2\pi)^D}\int_0^1 dq \int d\mathbf{k} \exp\left[i\mathbf{k}\cdot(\mathbf{r}-\mathbf{R}) - \frac{2Nb^\alpha k^\alpha}{D(\alpha+1)}\left((1-q)^{\alpha+1} + q^{\alpha+1}\right)\right], \quad (13)$$

where $\mathbf{R}$ is the mass center. While this expression is exact, the integral with respect to q makes it unwieldy. We can simplify it by resorting to the integral mean value theorem. Namely, there exists such $q_0 \in [0,1]$, that:

$$P_{\mathrm{CM}}(|\mathbf{r}-\mathbf{R}|) = \frac{1}{(2\pi)^D}\int d\mathbf{k} \exp\left[i\mathbf{k}_0\cdot(\mathbf{r}-\mathbf{R}) - \frac{2Nb^\alpha k^\alpha}{D(\alpha+1)}\left((1-q_0)^{\alpha+1} + q_0^{\alpha+1}\right)\right]. \quad (14)$$

On the other hand, since the integrand of (13) is a peak function of q with maximum at $q = 1/2$, this value contributes the most to the integral. For this reason, we will approximate (14) by imposing $q_0 = 1/2$. This results in the characteristic function of $P_{\mathrm{CM}}(|\mathbf{r}-\mathbf{R}|)$ in a form $\exp(-c(\alpha)k^\alpha)$, where:

$$c(\alpha) = \frac{2N}{D(\alpha+1)}\left(\frac{b}{2}\right)^\alpha. \quad (15)$$

IV. COARSE-GRAINED INTERACTION BETWEEN TWO NON-GAUSSIAN POLYMERS

Having established $P_{\mathrm{CM}}(|\mathbf{r}-\mathbf{R}|)$ for a single chain, we can calculate the coarse-grained interaction between two chains in terms of the distance between their mass centers. From now on, the lower index numerates the type of particle, so $P_{\mathrm{CM},i}(|\mathbf{r}-\mathbf{R}_i|)$ describes an ith type of chain characterized by N_i segments, constant b_i and exponent α_i. We can follow the reasoning of Flory and Krigbaum [3] and assume that the systems suffers an energetic penalty ϵ_{ij} if a segment belonging to one chain invades a small volume in the vicinity of a segment belonging to the other chain. For a single site $\mathbf{r}$, the probability of such event is proportional to $P_{\mathrm{CM},i}(|\mathbf{r}-\mathbf{R}_i|)P_{\mathrm{CM},j}(|\mathbf{r}-\mathbf{R}_j|)d\mathbf{r}$. Therefore, the entire interaction reads:

$$\begin{aligned} V_{ij}(|\mathbf{R}_i-\mathbf{R}_j|) &= \epsilon_{ij}\tilde{c}_{ij}\int d\mathbf{r}\, P_{\mathrm{CM},i}(|\mathbf{r}-\mathbf{R}_i|)P_{\mathrm{CM},j}(|\mathbf{r}-\mathbf{R}_j|) \\ &= \frac{\epsilon_{ij}\tilde{c}_{ij}}{(2\pi)^D}\int d\mathbf{k}\exp[i\mathbf{k}\cdot(\mathbf{R}_i-\mathbf{R}_j) \\ &\quad - c_i(\alpha_i)k^{\alpha_i} - c_j(\alpha_j)k^{\alpha_j}]. \end{aligned} \quad (16)$$

Assuming that ϵ_{ij} has a dimension of energy, it is necessary to introduce an additional constant $\tilde{c}_{ij}$, which has a dimension of volume. We can deduce this constant from the case of $\alpha_i = \alpha_j = 2$, for which we obtain the following universal Gaussian potential [8] and its Fourier transform:

$$V(r) = \epsilon\exp\left(-\frac{r^2}{4c}\right) \qquad \mathcal{V}(k) = \epsilon\,(4\pi c)^{D/2}\,e^{-ck^2}. \quad (17)$$

When ϵ is independent from N, this potential is perceived as an accurate and reliable model for interaction of identical chains [8,9]. Comparing (17) to (16), one can see that $c = c_i(2) + c_j(2)$ and hence $\tilde{c}_{ij} = (4\pi c)^{D/2}$. This can be generalized for $\alpha_i = \alpha_j = \alpha$ by:

$$\tilde{c}_{ij} = \{4\pi[c_i(\alpha) + c_j(\alpha)]\}^{D/\alpha}. \quad (18)$$

For the case of $\alpha_i \neq \alpha_j$ the constant $\tilde{c}_{ij}$ cannot be uniquely deduced from the dimensional analysis, thus we will restrict our further considerations to the potentials with common α.

V. EFFECTIVE INTERACTIONS AND MIXTURE STABILITY

Once V_{ij} has been found, we can analyze the interactions in binary mixtures. The system is described by three microscopic potentials in the form (16), where V_{11} and V_{22} are the internal interactions of each species and V_{12} is the cross-species interaction. When the behavior of one species in a mixture is considered, the presence of the other species modifies the microscopic interaction [7,8]. The additional potential, known as the effective interaction, is of entropic origin [7,8] and it is a key factor in controlling mixture stability and demixing. The prediction of effective interactions from arbitrary microscopic potentials is usually a challenging numerical task, but in our previous work [12] we have proposed a simple analytical method, suitable for soft interactions. According to Ref. [12], the effective interaction can be estimated by:

$$U_{\mathrm{eff}}(\Delta R) = -\frac{1}{(2\pi)^D}\int_{\tilde{\Omega}} d\mathbf{k} e^{i\mathbf{k}\cdot\Delta\mathbf{R}}\frac{|\mathcal{V}_{12}(k)|^2}{\mathcal{V}_{22}(k)}, \quad (19)$$

where $\mathcal{V}_{ij}(k) = \int d\mathbf{r}\exp(i\mathbf{k}\cdot\mathbf{r})V_{ij}(r)$ is a Fourier transform of relevant $V_{ij}(r)$ and $\tilde{\Omega}$ is the volume in the reciprocal space. Substituting (16) with relevant constants given by (18) into the expression for effective interactions, one obtains:

$$U_{\mathrm{eff}}(\Delta R) = -\frac{1}{(2\pi)^D}\frac{\epsilon_{12}^2}{\epsilon_{22}}\frac{(4\pi)^{D/\alpha}[c_1(\alpha)+c_2(\alpha)]^{2D/\alpha}}{[2c_2(\alpha)]^{D/\alpha}} \times \int_{\tilde{\Omega}} d\mathbf{k} e^{i\mathbf{k}\cdot\Delta\mathbf{R} - 2c_1(\alpha)k^\alpha}. \quad (20)$$

The total interaction for the first species in the mixture reads:

$$U_{\mathrm{tot}}(\Delta R) = V_{11}(\Delta R) + U_{\mathrm{eff}}(\Delta R) \quad (21)$$

or explicitly:

$$\begin{aligned} U_{\mathrm{tot}}(r) &= \left(\epsilon_{11}\,[8\pi c_1(\alpha)]^{D/\alpha} - \frac{\epsilon_{12}^2}{\epsilon_{22}}\frac{(4\pi)^{D/\alpha}[c_1(\alpha)+c_2(\alpha)]^{2D/\alpha}}{[2c_2(\alpha)]^{D/\alpha}}\right) \\ &\quad \times\frac{1}{(2\pi)^D}\int_{\tilde{\Omega}} d\mathbf{k} e^{i\mathbf{k}\cdot\Delta\mathbf{R} - 2c_1(\alpha)k^\alpha}. \end{aligned} \quad (22)$$

One can see that $U_{\rm tot}(\Delta R)$ and $V_{11}(\Delta R)$ have the same shape, up to the scaling factor S:

$$S = \epsilon_{11}\,[8\pi c_1(\alpha)]^{D/\alpha} - \frac{\epsilon_{12}^2}{\epsilon_{22}}\frac{(4\pi)^{D/\alpha}[c_1(\alpha)+c_2(\alpha)]^{2D/\alpha}}{[2c_2(\alpha)]^{D/\alpha}}. \tag{23}$$

S has a complicated form and it can take both the negative and positive values, depending on the parameters. The change in the sign of the total interaction indicates a remarkable change in the behavior of the system. Namely, for $S > 0$ the total interaction between the particles of the first species is purely repulsive, which means that these particles will disperse in the volume. Conversely, for $S < 0$, the first species of particles interacts via attractive potential, which results in the clustering of these particles and demixing in the system. Equating S to 0, the condition for demixing reads:

$$\frac{\epsilon_{11}\epsilon_{22}}{\epsilon_{21}^2} < \left(\frac{[c_1(\alpha)+c_2(\alpha)]^2}{4c_1(\alpha)c_2(\alpha)}\right)^{D/\alpha}. \tag{24}$$

Let us now analyze the condition (24) and introduce a common energy scale:

$$\tilde{\epsilon} = \frac{\epsilon_{12}}{\sqrt{\epsilon_{11}\epsilon_{22}}} \tag{25}$$

and:

$$g = \left(\frac{c_1(\alpha)}{c_2(\alpha)}\right)^{1/\alpha} = \frac{b_1}{b_2}\left(\frac{N_1}{N_2}\right)^{1/\alpha} \tag{26}$$

for which condition (24) can be reduced to:

$$\tilde{\epsilon} > \left(\frac{4g^\alpha}{(1+g^\alpha)^2}\right)^{D/(2\alpha)}. \tag{27}$$

Recalling the equation (12) for the radius of gyration R_g, one can see that for the chains characterized by the distributions sharing the same α, the parameter g becomes the ratio of R_g:

$$g = \frac{R_{g,1}}{R_{g,2}}. \tag{28}$$

For $\alpha = 2$ and $D = 3$ the condition (24) becomes exactly the spinodal decomposition condition for Gaussian particles, as given in Ref. [5] and [6], namely:

$$\tilde{\epsilon} > \left(\frac{2g}{1+g^2}\right)^{3/2}. \tag{29}$$

Therefore, the condition (27) is a direct generalization of the spinodal decomposition to the systems of particles described with α-stable distributions.

The condition (27) is plotted in Fig. 3. For every pair of g and α its value varies from 0 to 1. In the entire range of α, the region of mixing (below the surface) preserves the features of the Gaussian case, namely it falls rapidly to 0 for $g \ll 1$, reaches the single maximum at $g = 1$, and asymptotically decreases to 0 for $g \gg 1$. However, as α decreases to 0 the mixing region for $g \gg 1$ becomes wider, asymptotically reaching the region defined by $\tilde{\epsilon} > 1$. This means that the gyration radius ratio g becomes less and less relevant for the mixing of chains characterized by very wide distributions. The changes in the mixing region shape are much more pronounced for $\alpha < 1$.

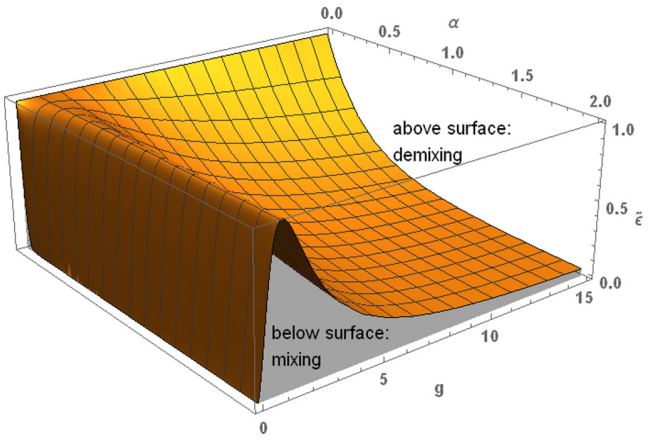

FIG. 3. (Color online) The spinodal decomposition condition (27) for the binary systems of particles described with the α-stable statistics as a function of gyration radii ratio $g = R_{g,1}/R_{g,2}$ and the distribution exponent α for $D = 3$ dimensional system. $\tilde{\epsilon} = \epsilon_{12}/\sqrt{\epsilon_{11}\epsilon_{22}}$ is the common energy scale. In the region above the plotted surface the binary system undergoes demixing due to the prevalence of the attractive effective interactions, in the region below the surface the effective interaction is repulsive and the system is homogeneous.

VI. DISCUSSION

It is known that the spinodal decomposition condition for Gaussian particles leads to the predictions on mixture separation, which are qualitatively and quantitatively comparable to the more advanced methods [6]. Thus, a similar efficiency can be expected from (27), at least for α mildly deviating from 2. However, some possible issues should be mentioned.

The fact that the total interaction (21) can become entirely negative is unrealistic. This evident problem is mitigated by the fact that the energy density of a pair interaction behaves as $U_{\rm tot}(r)r^{D-1}dr$. Therefore, r^{D-1} factor suppresses the lack of repulsive core at short distances and amplifies the influence of the attractive tail. The unrealistic shape of $U_{\rm tot}$ is also a consequence of the way the potential $V_{ij}(r)$ given by (16) is constructed. This potential is mean field in its nature and its width is governed by the constant $c_i(\alpha) + c_j(\alpha)$. In the context of Gaussian particles, while the dominant shape of the interaction between two separate chains is agreed to be Gaussian [9,33], there is an open problem of whether there are additional components [33] or how the width of such Gaussian is related to the gyration radii of the component chains [5]. A similar problem is relevant in our case and the choice of the width constant different from $c_i(\alpha) + c_j(\alpha)$ might result in a more realistic shape of $U_{\rm tot}$

VII. PHASE SEPARATION IN THE ADSORPTION OF GAUSSIAN PARTICLES TO THE SURFACE

The result (27) is particularly interesting in the context of the already mentioned work of Bouchaud and Daoud [25], where the gyration radius parallel to the surface is calculated for an adsorbed polymer. As mentioned in Sec. II, the characteristic exponent for the distribution on the surface reads $\alpha_{ss} = 2$ in the strong adsorption limit and $\alpha_{ws} = 1$ in the weak

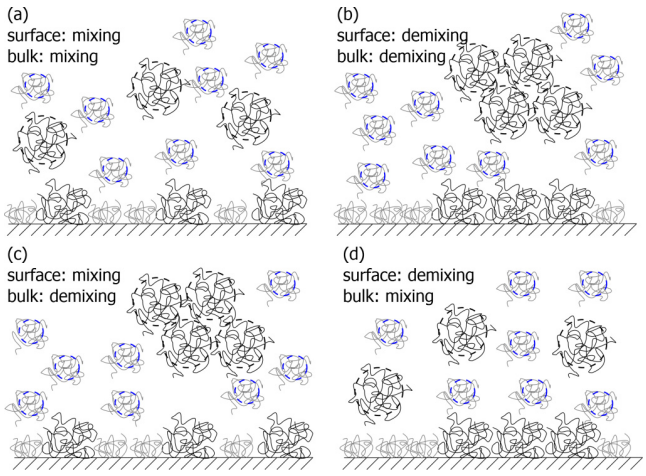

FIG. 4. (Color online) Schematic representation of four mixing and demixing scenarios in the binary system consisting of a solution and an adsorbing surface. In the bulk polymers follow the Gaussian statistics ($\alpha_b = 2$, $D_b = 3$). On the surface ($D_s = 2$) polymers are described either by $\alpha_{ss} = 2$ in the strong adsorption limit or $\alpha_{ws} = 1$ for the weak adsorption.

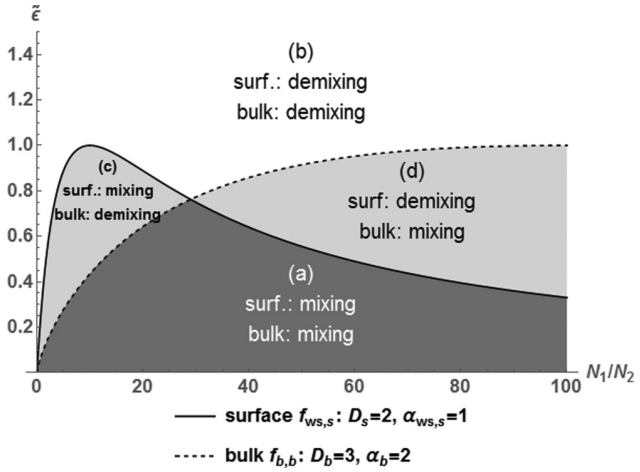

FIG. 5. The exemplary comparison of the phase separation conditions on the surface in the weak adsorption limit ($f_{ws,s}$, solid line) and in the bulk ($f_{b,b}$, dashed line) for the binary system of Gaussian polymers characterized by the persistence length ratio $b_1/b_2 = 0.1$. $f_{ws,s}$ and $f_{b,b}$ are defined by (30). $f_{ws,s}$ and $f_{b,b}$ divide the plot into four regions: (a) simultaneous mixing on the surface and in the bulk, (b) simultaneous demixing on the surface and in the bulk, (c) mixing on the surface, demixing in the bulk, (d) demixing on the surface, mixing in the bulk.

adsorption limit [25]. Considering the adsorption from the binary mixture, (27) provides the condition for homogeneous versus inhomogeneous adsorption, i.e., the ratio of gyration radii parallel to the surface ($R_{g,||}$) decides whether both species cover the surface in a homogeneous manner or they separate into the islands consisting of the particles of the same type. On the other hand (27) allows us to compare for which parameters the separation on the surface and in the bulk coappear.

Let us consider a simple binary system in which the behavior of chains in the bulk ($D_b = 3$, $\alpha_b = 2$) is Gaussian, but on the surface it is characterized by $D_s = 2$ and α_{ss} or α_{ws}. The types of particles differ by the number of monomers N_i and their persistence length b_i. The condition (27) reads:

$$\tilde{\epsilon} > \left(\frac{4 \left(\frac{b_1}{b_2}\right)^{\alpha_x} \frac{N_1}{N_2}}{\left[1 + \left(\frac{b_1}{b_2}\right)^{\alpha_x} \frac{N_1}{N_2}\right]^2} \right)^{\frac{D_y}{2\alpha_x}} = f_{x,y}. \qquad (30)$$

In the strong adsorption limit it is always true that $f_{ss,s} \geqslant f_{b,b}$ for any b_1/b_2 and N_1/N_2. Therefore, assuming that in this system $\tilde{\epsilon}$ is the same on the surface and in the bulk, three scenarios of mixing or demixing are allowed. First, for (a) [Fig. 4(a)] $f_{ss,s} \geqslant f_{b,b} \geqslant \tilde{\epsilon}$ the solution in the bulk is homogeneous and so is the coverage of the surface. Conversely, for (b) [Fig. 4(b)] $\tilde{\epsilon} \geqslant f_{ss,s} \geqslant f_{b,b}$ the separation is simultaneous on the surface and in the bulk. Finally, for (c) [Fig. 4(c)] $f_{ss,s} \geqslant \tilde{\epsilon} \geqslant f_{b,b}$ demixing in the bulk occurs, but the surface coverage is still homogeneous. The schematic representation of scenarios (a)–(c) is shown in Fig. 4.

In the weak adsorption limit ($\alpha_{ws} = 1$), the situation is more complicated because both $f_{ws,s} \geqslant f_{b,b}$ and $f_{ws,s} \leqslant f_{b,b}$ are possible, depending on b_1/b_2 and N_1/N_2. Replacing $f_{ss,s}$ by $f_{ws,s}$ in the inequalities from the previous paragraph one obtains the conditions for separation scenarios (a)–(c) in the weak adsorption limit. However, there exists the additional region in which it is possible that (d) [Fig. 4(d)] $f_{b,b} \geqslant \tilde{\epsilon} \geqslant f_{ws,s}$. In this region the separation on the surface occurs, while the solution in the bulk is still homogeneous (see Fig. 4). In Fig. 5 the exemplary phase separation diagram for the weak adsorption limit and $b_1/b_2 = 0.1$ is presented, which contains all of the phase separation scenarios (a)–(d). Figure 6 shows the difference $f_{ws,s} - f_{b,b}$, which indicates where scenarios (c) and (d) are allowed. In particular, for $b_1/b_2 \to 0$ and $b_1/b_2 \gg 1$ the scenario (d) becomes almost inaccessible, while it is allowed in the vicinity of $b_1/b_2 \simeq 1$.

These considerations show that the behavior of a mixture can be designed by the choice of b_1/b_2 (which is dependent on the chemical composition) and N_1/N_2. However, our predictions can be affected by a few additional effects. In general, there are two main factors that determine the behavior of the system as a whole. On the one hand, the system tends to minimize its energy, so the details of adsorption mechanism (e.g., binding energy, a preference for a certain type of particles, adsorption rate, etc.) are important. Since our model is valid for thermodynamic equilibrium, the surface binding should not be significantly stronger than other interactions, to allow equilibration. On the other hand, the system globally maximizes its entropy, which includes the on-surface and in-the-bulk contributions. However, there is also the bulk-surface component, i.e., the bigger particles can decrease their excluded volume in the vicinity of a wall, hence they experience the entropy-driven affinity to the flat surface [7,34]. This effect is not included in our model. One would generally expect the increased concentration of bigger particles in the near-surface region and a reduced availability of smaller particles. Indeed, for the hard-sphere mixtures this effect depends on the concentration of smaller particles and it precedes the in-bulk clustering [34], which can be also expected for polymers. It is not clear, however, whether this

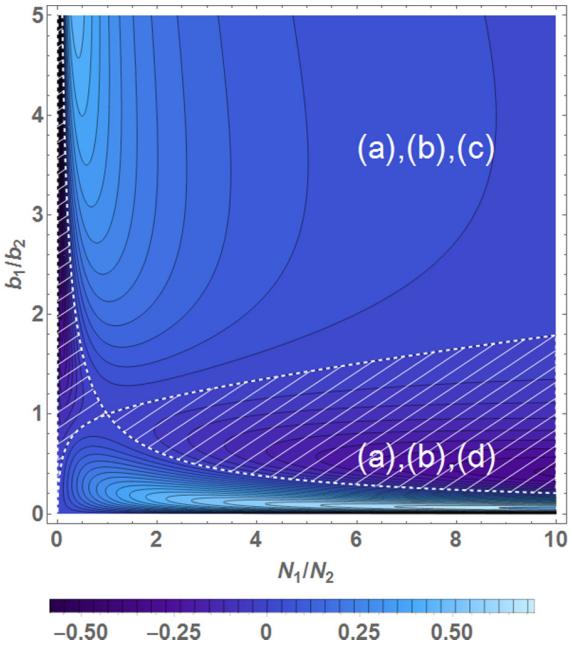

FIG. 6. (Color online) The density plot of the difference $f_{ws,s} - f_{b,b}$ as a function of persistence length ratio b_1/b_2 and the ratio of monomer numbers N_1/N_2. $f_{ws,s} - f_{b,b}$ indicates which surface/bulk demixing scenarios are allowed (see Sec. VII and Fig. 5 for explanation). White meshed region: $f_{ws,s} - f_{b,b} < 0$ indicates scenario (d) allowed (demixing on the surface, mixing in the bulk), complement region: $f_{ws,s-} f_{b,b} > 0$ scenario (c) allowed (mixing on the surface, demixing in the bulk).

effect can be strong enough to result in the complete coating of the surface with bigger particles.

In conclusion, the full theory should also include both the detailed adsorption mechanism and the surface affinity. However, our model is potentially valid in the semidilute regime for adsorption strength comparable to entropic interactions and in the systems in which the surface effects are a significant contribution to the entropy of the entire system.

VIII. SUMMARY

In summary, in this paper we have presented the generalization of the results known from the Gaussian chain theory to the particles described with the α-stable distributions. As expected, it is possible to obtain a similar hierarchy of analytical results ranging from end-to-end distribution up to the effective interactions in binary mixtures. Typically for α-stable distributions, we obtained the closed-form formulas in the Fourier space. Our theory also allows us to generalize the spinodal decomposition condition from Gaussian particles to the α-stable particles. This can be readily applied to the problem of mixing or demixing of adsorbed polymers, as we also show. Our results might be further utilized in the context of Levy flights applications reviewed in Sec. II.

APPENDIX: DISTRIBUTION OF SEGMENTS AROUND THE CENTER OF MASS

In this Appendix we derive the distribution of segments around the mass center of a chain. Let us consider an N-segments-long chain, described by the nearest-neighbor probability given by (8). The position of the mass center reads:

$$\mathbf{R} = \frac{1}{N}\sum_{i=1}^{N}\mathbf{r}_i. \tag{A1}$$

The probability that each segment occupies its position $\mathbf{r}_i$ under condition that the mass center is positioned at $\mathbf{R}$ reads:

$$P(\mathbf{r}_1,\ldots,\mathbf{r}_N|\mathbf{R}) = \prod_{i=1}^{N-1} P(|\mathbf{r}_{i+1}-\mathbf{r}_i|)\delta\left(\mathbf{R}-\frac{1}{N}\sum_{i=1}^{N}\mathbf{r}_i\right). \tag{A2}$$

From this expression we can calculate the probability of finding jth segment at some position relative to the mass center:

$$P(|\mathbf{r}_j-\mathbf{R}|) = \int d\mathbf{r}_1\ldots\int d\mathbf{r}_{j-1}\int d\mathbf{r}_{j+1}\ldots\int d\mathbf{r}_N \times\prod_{i=1}^{N-1} P(|\mathbf{r}_{i+1}-\mathbf{r}_i|)\delta\left(\mathbf{R}-\frac{1}{N}\sum_{i=1}^{N}\mathbf{r}_i\right). \tag{A3}$$

The integrals in the above expression can be done particularly easily, if we switch to relative variables:

$$\begin{aligned}\Delta\mathbf{r}_{i-j} &= \mathbf{r}_i-\mathbf{r}_{i-1} \quad \text{for} \quad i>j\\ \Delta\mathbf{r}_{i-j} &= \mathbf{r}_{i-1}-\mathbf{r}_i \quad \text{for} \quad i<j,\end{aligned} \tag{A4}$$

which allows us to express $\mathbf{r}_i$ as:

$$\begin{aligned}\mathbf{r}_i &= \mathbf{r}_j+\sum_{n=1}^{N-i}\Delta\mathbf{r}_{+n} \quad \text{for} \quad N\geqslant i>j\\ \mathbf{r}_i &= \mathbf{r}_j+\sum_{n=1}^{j-i}\Delta\mathbf{r}_{-n} \quad \text{for} \quad 1\leqslant i<j.\end{aligned} \tag{A5}$$

In these coordinates the position of mass center reads:

$$\frac{1}{N}\sum_{i=1}^{N}\mathbf{r}_i = \mathbf{r}_j+\sum_{n=1}^{N-j}\frac{N-j-n+1}{N}\Delta\mathbf{r}_{+n} + \sum_{n=1}^{j-1}\frac{j-n}{N}\Delta\mathbf{r}_{-n}. \tag{A6}$$

The change of variables (A4) is linear and its Jacobian is equal to 1, so applying the new coordinates to (A3), we obtain:

$$P(|\mathbf{r}_j-\mathbf{R}|) = \prod_{\substack{n=-j\\ n\neq 0}}^{N-j}\int d\Delta\mathbf{r}_n P(\Delta r_n) \times\delta\left(\mathbf{R}-\mathbf{r}_j+\sum_{n=1}^{N-j}\frac{N-j-n+1}{N}\Delta\mathbf{r}_{+n} + \sum_{n=1}^{j-1}\frac{j-n}{N}\Delta\mathbf{r}_{-n}\right). \tag{A7}$$

The following step is to express $P(\Delta r_n)$ in (A7) in terms of its characteristic function (8):

$$P(|\mathbf{r}_j-\mathbf{R}|)=\frac{1}{(2\pi)^{ND}}\prod_{\substack{n=-j\\ n\neq 0}}^{N-j}\int d\Delta\mathbf{r}_n\int d\mathbf{k}_n e^{i\mathbf{k}_n\cdot\Delta\mathbf{r}_n}\phi(k_n)\times\int d\mathbf{k}_0\exp\left(i\mathbf{k}_0\cdot(\mathbf{R}-\mathbf{r}_j)+i\sum_{n=1}^{N-j}\frac{N-j-n+1}{N}\mathbf{k}_0\cdot\Delta\mathbf{r}_{+n}+i\sum_{n=1}^{j-1}\frac{j-n}{N}\mathbf{k}_0\cdot\Delta\mathbf{r}_{-n}\right). \tag{A8}$$

Further, we integrate out every component of $\Delta\mathbf{r}_{\pm n}$, which introduces multiple Dirac-δ functions:

$$\begin{aligned}P(|\mathbf{r}_j-\mathbf{R}|)&=\frac{1}{(2\pi)^D}\\&=\int d\mathbf{k}_0\left[\prod_{n=1}^{N-j}\int d\mathbf{k}_{+n}\phi(k_{+n})\times\delta\left(\mathbf{k}_{+n}-\frac{N-j-n+1}{N}\mathbf{k}_0\right)\right]\\&\quad\times\left[\prod_{n=1}^{j-1}\int d\mathbf{k}_{-n}\phi(k_{-n})\delta\left(\mathbf{k}_{-n}-\frac{j-n}{N}\mathbf{k}_0\right)\right]e^{i\mathbf{k}_0\cdot(\mathbf{R}-\mathbf{r}_j)}\\&=\frac{1}{(2\pi)^D}\int d\mathbf{k}_0\left[\prod_{n=1}^{N-j}\phi\left(\frac{N-j-n+1}{N}k_0\right)\right]\\&\quad\times\left[\prod_{n=1}^{j-1}\phi\left(\frac{j-n}{N}k_0\right)\right]e^{i\mathbf{k}_0\cdot(\mathbf{R}-\mathbf{r}_j)}.\end{aligned} \tag{A9}$$

At this point we apply the explicit form of $\phi(k)$, so the final expression for $P(|\mathbf{r}_j-\mathbf{R}|)$ reads:

$$P(|\mathbf{r}_j-\mathbf{R}|)=\frac{1}{(2\pi)^D}\int d\mathbf{k}_0\exp\left\{i\mathbf{k}_0\cdot(\mathbf{R}-\mathbf{r}_j)-\frac{2b^\alpha}{D}\left[\sum_{n=1}^{N-j}\left(\frac{N-j-n+1}{N}\right)^\alpha+\sum_{n=1}^{j-1}\left(\frac{j-n}{N}\right)^\alpha\right]k_0^\alpha\right\}. \tag{A10}$$

Expression (A10) gives the probability of finding jth segment in the vicinity of mass center, so the probability of finding any segment reads:

$$P_{\mathrm{CM}}(|\mathbf{r}-\mathbf{R}|)=\frac{1}{N}\sum_{j=1}^{N}P(|\mathbf{r}_j-\mathbf{R}|), \tag{A11}$$

where the factor $1/N$ provides normalization. Let us assume now that N is a large number, so both $n/N=q$ and $j/N=q'$ can be treated as continuous variables, hence we can simplify:

$$\sum_{n=1}^{N-j}\left(\frac{N-j-n+1}{N}\right)^\alpha\to N\int_0^{1-q'}dq(1-q'-q)^\alpha=\frac{N}{\alpha+1}(1-q')^{\alpha+1} \tag{A12}$$

$$\sum_{n=1}^{j-1}\left(\frac{j-n}{N}\right)^\alpha\to N\int_0^{q'}dq(q'-q)^\alpha=\frac{N}{\alpha+1}q'^{\alpha+1}. \tag{A13}$$

The final expression for the distribution of any segment around the mass center reads:

$$P_{\mathrm{CM}}(|\mathbf{r}-\mathbf{R}|)=\frac{1}{(2\pi)^D}\int_0^1 dq'\int d\mathbf{k}_0\exp\left[i\mathbf{k}_0\cdot(\mathbf{r}-\mathbf{R})-\frac{2Nb^\alpha k_0^\alpha}{D(\alpha+1)}((1-q')^{\alpha+1}+q'^{\alpha+1})\right]. \tag{A14}$$

[1] I. Teraoka, *Polymer solutions: an Introduction to Physical Properties* (Wiley, New York, 2002).
[2] P. Debye and F. Bueche, J. Chem. Phys. **20**, 1337 (1952).
[3] P. J. Flory and W. R. Krigbaum, J. Chem. Phys. **18**, 1086 (1950).
[4] G. Samorodnitsky and M. S. Taqqu, *Stable Non-Gaussian Random Processes: Stochastic Models with Infinite Variance* (Chapman and Hall, New York, 1994).
[5] A. A. Louis, P. G. Bolhuis, and J. P. Hansen, Phys. Rev. E **62**, 7961 (2000).
[6] R. Finken, J. P. Hansen, and A. A. Louis, J. Stat. Phys. **110**, 1015 (2003).
[7] H. N. W. Lekkerkerker and R. Tuinier, *Colloids and the Depletion Interaction* (Springer, London, 2011).
[8] C. N. Likos, Phys. Rep. **348**, 267 (2001).
[9] P. G. Bolhuis, A. A. Louis, J. P. Hansen, and E. J. Meijer, J. Chem. Phys. **114**, 4296 (2001).
[10] G. Yatsenko, E. J. Sambriski, M. A. Nemirovskaya, and M. Guenza, Phys. Rev. Lett. **93**, 257803 (2004).
[11] J. McCarty, I. Y. Lyubimov, and M. G. Guenza, Macromolecules **43**, 3964 (2010).
[12] M. Majka and P. F. Góra, Phys. Rev. E **90**, 032303 (2014).
[13] J. Moon and H. Nakanishi, Phys. Rev. A **42**, 3221 (1990).
[14] M. F. Shlesinger, B. J. West, and J. Klafter, Phys. Rev. Lett. **58**, 1100 (1987).
[15] F. Valle, M. Favre, P. De Los Rios, A. Rosa, and G. Dietler, Phys. Rev. Lett. **95**, 158105 (2005).
[16] T. E. Fisher, A. F. Oberhauser, M. Carrion-Vazquez, P. E. Marszalek, and J. M. Fernandez, Trends Biochem. Sci. **24**, 379 (1999).

[17] G. W. Daughdrill, G. J. Pielak, V. N. Uversky, M. S. Cortese, and A. K. Dunker, *Natively Disordered Proteins, in Protein Folding Handbook*, edited by J. Buchner and T. Kiefhaber (Wiley-VCH Verlag GmbH, Weinheim, 2005).
[18] V. N. Uversky and A. K. Dunker, BBA-Proteins Proteom **1804**, 1231 (2010).
[19] N. C. Fitzkee and G. D. Rose, Proc. Natl. Acad. Sci. USA **101**, 12497 (2004).
[20] J. Elf, G. W. Li, and X. S. Xie, Science **316**, 1191 (2007).
[21] L. Mirny, M. Slutsky, Z. Wunderlich, A. Tafvizi, J. Leith, and A. Kosmrlj, J. Phys. A: Math. Theor. **42**, 434013 (2009).
[22] M. A. Lomholt, T. Ambjörnsson, and R. Metzler, Phys. Rev. Lett. **95**, 260603 (2005).
[23] P. G. de Gennes, J. Phys. France **37**, 1445 (1976).
[24] P. G. de Gennes and P. Pincus, J. Physique Lett. **44**, 241 (1983).
[25] E. Bouchaud and M. Daoud, J. Phys. A: Math. Gen. **20**, 1463 (1987).
[26] C. Donati, S. C. Glotzer, P. H. Poole, W. Kob, and S. J. Plimpton, Phys. Rev. E **60**, 3107 (1999).
[27] B. Doliwa and A. Heuer, Phys. Rev. E **61**, 6898 (2000).
[28] A. C. Mitus, A. Z. Patashinski, A. Patrykiejew, and S. Sokolowski, Phys. Rev. B **66**, 184202 (2002).
[29] J. J. Binney *et al.*, *The Theory of Critical Phenomena* (Oxford University Press, Oxford, 1992).
[30] M. Majka and P. F. Góra, Phys. Rev. E **86**, 051122 (2012).
[31] M. Majka and P. F. Góra, Acta Phys. Pol. B **44**, 1099 (2013).
[32] K. Szczepaniec and B. Dybiec, Phys. Rev. E **90**, 032128 (2014).
[33] J. Dautenhahn and C. K. Hall, Macromolecules **27**, 5399 (1994).
[34] A. G. Yodh, K. Lin, J. C. Crocker, A. D. Dinsmore, R. Verma, and P. D. Kaplan, Phil. Trans. R. Soc. Lond. A **359**, 921 (2001).